AN ABSTRACT OF THE THESIS OF

Kenneth Melvin Evenson (Name) for the Ph. D. (Degree) in Physics (Major)

Date thesis is presented April 18, 1964

Title ATOMIC NITROGEN RECOMBINATION STUDIED BY ELECTRON PARAMAGNETIC RESONANCE

Abstract approved Redacted for Privacy (Major professor)

Three-body and wall recombination coefficients of atomic nitrogen were measured using an electron paramagnetic resonance spectrometer to determine the atomic nitrogen concentrations. Studies of nitrogen gas at pressures from 3 to 35 torr flowing in a cylindrical tube and of non-flowing nitrogen gas at pressures from 0.3 to 7 torr contained in a 15 cc. cylinder were made. The three-body recombination coefficient k_1 with molecular nitrogen as the third body was found to be $(1.94 \pm 0.14) \times 10^{-32}$ cc.^{2} sec.$^{-1}$. The wall recombination probability γ of quartz ranged from 9×10^{-6} to 6×10^{-4}, decreasing with increasing oxygen impurity; γ ranged from 10^{-7} to 2.5×10^{-5} for teflon, increasing with increasing oxygen content. The sum of the two-body radiative recombination and two-body teflon-wall recombination was a significant part of the total atom recombination at lower pressures; the sum of the

coefficients was 2.5×10^{-16} cc. $sec.^{-1}$.

The electron paramagnetic resonance spectrometer was calibrated with molecular oxygen. The use of oxygen as a calibration standard was verified by comparison of its calibration constant with those of diphenylpicrylhydrazyl and Mn^{++} ions.

A specially constructed quartz cell externally silvered to form a resonant x-band cavity for a standard electron paramagnetic resonance spectrometer was used for the non-flowing gas experiments. This cavity was found to be especially sensitive for use in gaseous electron paramagnetic resonance spectrometry.

For intervals up to two seconds following atomic nitrogen formation, the data indicate a slower decrease of atom concentration than may be accounted for by known mechanisms of recombination. The possible existence of some atom-forming substance in the afterglow is discussed.

ATOMIC NITROGEN RECOMBINATION STUDIED BY ELECTRON PARAMAGNETIC RESONANCE

by

KENNETH MELVIN EVENSON

A THESIS

submitted to

OREGON STATE UNIVERSITY

in partial fulfillment of
the requirements for the
degree of

DOCTOR OF PHILOSOPHY

June 1964

APPROVED:

Redacted for Privacy

Associate Professor of Physics

In Charge of Major

Redacted for Privacy

Head of Department Physics

Redacted for Privacy

Dean of Graduate School

Date thesis is presented April 18, 1964

Typed by Muriel Davis

DEDICATION

To my wife, Vera, whose love and understanding are a constant source of inspiration.

To my parents for their continued love and guidance.

To my two children, Sally and Grant, who brightened every day since their arrivals.

ACKNOWLEDGMENTS

The author takes this opportunity to express his gratitude to the people who helped to bring this thesis to its completion. He thanks:

Dr. David S. Burch, the major professor, for the original idea of the experiment, for his guidance and assistance in bringing the experiment to its completion, and for his helpful suggestions in the preparation of the manuscript (i. e., for his many hours spent in reading sloppy copy),

Lee Shimmin, for his help and sense of humor in the laboratory,

and my wife, Vera, for her helpful suggestions in the preparation of this manuscript and for her many hours spent alone while the author was in the laboratory.

TABLE OF CONTENTS

LIST OF FIGURES

LIST OF TABLES

ATOMIC NITROGEN RECOMBINATION STUDIED BY ELECTRON PARAMAGNETIC RESONANCE

INTRODUCTION

The work to be presented in this report deals mainly with the use of electron paramagnetic resonance (hereafter abbreviated epr) as a tool to study the recombination of atomic nitrogen into its molecular form. The epr spectra of nitrogen and some other paramagnetic gases were also observed.

Atomic Nitrogen

Nitrogen is an element present in the earth's crust, in the proteins of all living matter, and in the atmosphere. Although nitrogen in all forms constitutes only a fraction of a percent of the total mass of the earth's crust, in its diatomic form it makes up an overwhelming 78% of the atmosphere at sea level.

Atomic nitrogen is a highly reactive gas which occurs naturally only in the upper atmosphere. There, two factors work together to maintain the atomic nitrogen concentration. The intensity of ultraviolet radiation from the sun is sufficiently high to effect appreciable dissociation of molecular nitrogen into atoms. Secondly, since the gases are rarefied, recombination is not frequent. At 100 kilometers, atomic nitrogen represents about 0.01% of the number density of

atomic and molecular particles as compared with 1% for atomic oxygen at the same altitude (36, p. 47). Although atomic nitrogen is not as concentrated in the upper atmosphere as atomic oxygen, it is present in sufficient quantities to play an important role there. In order to understand the upper atmosphere, it is important to have a knowledge of the rates of all chemical reactions which may occur there. One of the important reactions, the recombination of atomic nitrogen, is the chief subject of the work to be described herein.

Visual effects resulting from the recombination of atomic nitrogen were first observed by Lewis (32) in 1900; he observed a "chamois yellow fluorescence" in vacuum discharge tubes containing nearly pure nitrogen. Lewis noted that trace amounts of water or oxygen were necessary for this fluorescence which lasted for several seconds after the discharge was extinguished. Later, in the first quantitative work dealing with this afterglow, Lord Rayleigh (then R. J. Strutt) in 1911 named the energy carrier for the afterglow "active nitrogen" (45). The fluorescence is now called the Lewis-Rayleigh afterglow in honor of the first two people to do extensive work in the field.

The color of the afterglow arises chiefly from spectral bands originating from transitions between the different vibrational levels of the $^3\Pi$ and $^3\Sigma$ states shown in Figure 1. These spectral bands are called the first positive system of the molecular nitrogen

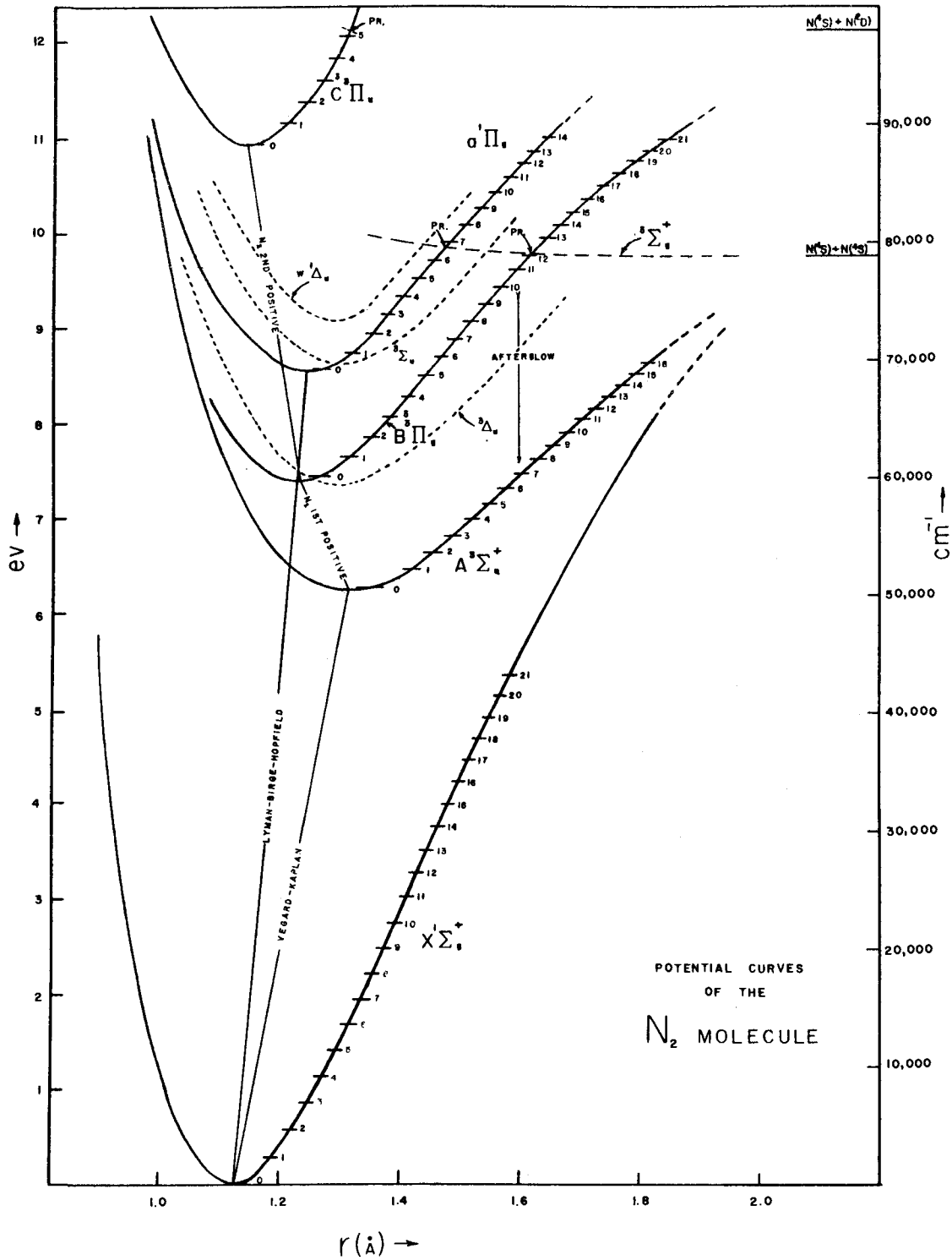

Figure 1. Potential Curves of the N_2 Molecule (31, p. 391)

spectrum.

Mitra has devoted an entire book to a theory of active nitrogen (37). Although Mitra's theory has now been abandoned (24, p. 121), a quotation from his book can best describe the general state of observations on active nitrogen (37, p. 3, 4):

> The chronicling of facts regarding active nitrogen which may be considered as established beyond doubt, is not always an easy task. Any one attempting to study the literature on the subject is not only struck by the large amount of experimental work done but, at the same time, is greatly confused by the divergent results and conflicting statements of the different authors and also, not infrequently, of the same author on different occasions.

Since the publication of Mitra's book, however, workers who have made the more quantitative measurements on the atomic nitrogen reactions are in better agreement. Only in the last fifteen years has it been firmly established that atomic nitrogen in its ground state $^4S_{3/2}$, which has the configuration $1s^2\ 2s^2\ 2p^3$, is the chief constituent of active nitrogen. Jennings and Linnet (24, p. 122) in their review article on atomic nitrogen stated further:

> The first positive evidence of the presence of ground-state atoms in the afterglow was obtained by examining the paramagnetic resonance spectrum of active nitrogen.

Once it was established that atomic nitrogen was the chief constituent of active nitrogen, a great deal of effort was made to elucidate its various chemical reactions including its own recombination. Three-body volume recombination is an important process by which

atomic nitrogen recombines at usual laboratory gas pressures, and it is in this process that the afterglow originates. The most widely accepted mechanism for this three-body recombination process (24, p. 124-129; 31, p. 388-404) is that in which two ground state (^4S) nitrogen atoms collide and form the weakly bound $^5\Sigma$ state shown in Figure 1. This excited molecule then loses sufficient energy in a collision with a third body to enter the 12th vibrational level of the $^3\Pi$ state by the process of inverse pre-dissociation (pre-association). This $^3\Pi$ state decays to the $^3\Sigma$ state with the emission of the characteristic nitrogen afterglow spectrum. The Vegard-Kaplan bands representing transitions from the $^3\Sigma$ state to the $^1\Sigma$ ground state are observed only in very pure nitrogen (24, p. 129).

The determination of the rate of recombination necessitates measurement of the absolute concentration of atomic nitrogen and the variation of this quantity with time; this measurement was effected in two different manners in the experiments to be described. 1) The atom concentration was measured in gas flowing in a cylindrical tube, the time being the spatial separation between the atom source and concentration-measuring regions divided by the flow velocity. 2) The atom concentration was continuously monitored in a chamber sealed off from the atom source; the time was determined directly from the recorder chart speed. In both cases the atom concentrations were measured by epr spectrometry.

There are several experimental approaches to the measurement of atomic nitrogen densities: mass spectrometry, Wrede gauge techniques, chemical titration, catalytic probe methods, and epr spectrometry. Berkowitz (8) used the mass spectrometer in his study of active nitrogen; however, he did not measure the recombination coefficient. Wentink, Sullivan, and Wray (50) were the first workers to determine a value for the recombination coefficient of atomic nitrogen. In 1958 they reported the use of a catalytic platinum wire resistance probe to measure the atomic nitrogen concentration. Since that time, four other groups of workers have published experimental values of the recombination coefficient, k_1. Three of these groups (15; 18; 35) used chemical titration with nitric oxide to determine the atomic nitrogen concentration. Very recently Marshall (33) used epr to measure the atomic nitrogen volume recombination coefficient.

Most atomic concentration measuring techniques depend upon the destruction of atoms, thus altering drastically the conditions normally occurring in the afterglow; this destruction gives rise to possible secondary effects which interfere with the measurement of k_1. Epr measurements, on the other hand, introduce only a slight perturbation of the electron spin states, and hence do not disturb the atoms to the extent that their concentration or recombination rates would be altered. In their determinations of atomic oxygen

recombinations, Krongelb and Strandberg (30, 1196-1210) were the first to use epr to measure gaseous reaction rates.

In any laboratory experiment recombination also occurs at the wall of the containing vessel. This fact necessitates the measurement of the wall recombination coefficient of the wall material. In the experiments to be described, wall recombination coefficients for quartz and teflon walls were obtained. Values of the wall recombination coefficient of atomic nitrogen on various wall materials have been reported by four groups (15; 18; 34; 52).

The measurement of the recombination coefficients is further complicated by gradients in the atomic nitrogen concentration brought about by a localized source of atoms and by recombination more rapid at the walls than in the volume. These gradients result in the diffusional flow of atoms which must be considered in a differential equation relating the decay of nitrogen to the diffusion coefficient, the volume recombination coefficient, and the wall recombination coefficient. Various simplifying assumptions are then made in solving this differential equation, which relates the measured experimental quantities to the recombination coefficients.

Electron Paramagnetic Resonance

Electron paramagnetic resonance is a phenomenon involving the absorption of electromagnetic energy of a particular frequency

by a paramagnetic substance placed in a magnetic field.

An atom or molecule of a paramagnetic material has a permanent magnetic moment due to the intrinsic magnetic moments of its electrons and nuclei and the orbital motion of its electrons. When a paramagnetic molecule is placed in a magnetic field, the perturbation of the interaction of its magnetic moment with the magnetic field results in a splitting of the unperturbed energy levels; the consequent splitting of the optical spectral lines is commonly known as the Zeeman effect of atomic spectroscopy. Transitions between these adjacent perturbed levels may be induced by an electromagnetic field whose photons have an energy equal to the difference in energy between the states. The resonant absorption of this electromagnetic energy is called electron paramagnetic resonance, electron spin resonance, or simply paramagnetic resonance when the difference in energy levels is due chiefly to the electrons' magnetic moments, and nuclear magnetic resonance when due to the nuclear magnetic moments.

The electron paramagnetic resonance condition is described by the basic equation: $h\nu = g\beta H_o$ where h is Planck's constant, ν is the frequency of the electromagnetic radiation illuminating a sample, g is the spectroscopic splitting factor (also called the Lande g factor), β is the Bohr magneton, and H_o is the polarizing magnetic field strength in which the sample is placed. Each

energy level of a substance has its own characteristic g value; however, magnetic perturbation does not necessarily result in a symmetric splitting of the energy levels as is described by the above simplified expression. Thus several closely spaced lines may result. Each of these lines may be further split into several components as a result of coupling between electrons and nuclei. To detect all the resonance lines corresponding to the different values of g and the components of these lines resulting from the magnetic perturbation and the nuclear splitting, the magnetic field H_o is varied and the frequency is held constant.

Any frequency may be used for spectral analysis. Resolution and sensitivity increase with increasing frequency, so the higher frequencies are usually chosen, commonly about 9,000 megacycles per second with a corresponding polarizing field of approximately 3,000 oersteds.

In 1926 quantum mechanical theory explained the anomalous Zeeman effect (17, p. 263-277). Since electron paramagnetic resonance is the phenomenon associated with the transitions between the Zeeman levels, the basic theory for the epr transitions was thus founded. However, electron paramagnetic resonance was not observed until 1945 by Zavoisky (54). The rapid development of the field since then has been considerably enhanced by the development during World War II of the high frequency radar and microwave

techniques.

Paramagnetic resonance in a gas was first observed in 1949 by Beringer and Castle (6) who studied the epr spectrum of molecular oxygen. Atomic nitrogen in its ground state (^4S) was first detected in 1954 by Heald and Beringer (16). Other paramagnetic gases which have been studied are NO_2, NO, O, H, OH, Cl, and F. A detailed theory of epr predicts the size of the resonance signal in terms of certain atomic and molecular constants and instrumental parameters (30; 47; 48). To determine these instrumental parameters most accurately, the use of a paramagnetic calibrating gas is desirable. The only paramagnetic calibrating gases stable at ordinary laboratory temperatures and pressures are nitrogen dioxide, nitric oxide, and molecular oxygen. For the present investigation, oxygen was chosen as the calibrating gas since the theory of the epr spectrum of the triatomic molecule of nitrogen dioxide has not been developed and the spectrum of nitric oxide occurs at a magnetic field that was unobtainable with the magnet available. The oxygen molecule has many spectral lines spread over a wide range of magnetic field strengths and the theory of the oxygen spectrum has been extensively formulated; therefore, it is an ideal calibrating substance for gaseous epr work.

THEORETICAL CONSIDERATIONS

The theoretical considerations pertinent to the experiments to be described in succeeding chapters include atom recombination theory and a discussion of flowing, recombining gases. In the discussion of atom recombination, various mechanisms by which atoms recombine are considered, the differential rate equations governing each type of recombination are illustrated, and theories of three-body rate coefficients are discussed. Next, solutions of the differential equations describing a flowing, recombining gas are considered.

Atom Recombination

Several possible mechanisms by which gases recombine are listed in Table 1 along with the differential rate equation for each mechanism. The first two of these mechanisms, three-body and radiative, represent the volume recombination processes which are of importance in the upper atmosphere. In mechanism I, two nitrogen atoms collide while in the vicinity of a third body. The presence of this third body allows simultaneous conservation of energy and momentum for any initial velocity of each of the three bodies, and every three-body collision can result in a recombination. However, in mechanism II, radiative recombination, only certain initial relative velocities allow for the conservation of both energy and momentum.

Table 1

Possible Mechanisms for Atomic Nitrogen Recombination

	Name	Mechanism	Equation	
I	Three-body	$N + N + M \rightarrow N_2$ (or N_2^*) $+ M$	$\frac{dn}{dt} = -k_1 n^2 [M]$	(2-1)
II	Radiative	$N + N \rightarrow N_2 + h\nu$	$\frac{dn}{dt} = -k_2 n^2$	(2-2)
III	Two-body wall	$N + N +$ wall $\rightarrow N_2 +$ wall	$(\frac{d\eta}{dt})_{wall} = -K_3 n^2_{wall}$	(2-3)
IV	Wall	N + N (adsorbed on wall) $\rightarrow N_2$	$(\frac{d\eta}{dt})_{wall} = -K_4 n_{wall}$	(2-4)
V	Complex	$N + N_2 \rightarrow N_3$, $N_3 + N \rightarrow 2N_2$, etc.	----	

In the above equations and in the remainder of the report, the following symbols are used:

n	the concentration of nitrogen atoms
$(\frac{d\eta}{dt})_{wall}$	the number of wall recombinations per unit time per unit area
$[M]$	the concentration of any other atomic or molecular specie
h	Planck's constant
ν	the frequency of radiation from an excited molecule
N_2^*	an excited nitrogen molecule

This restriction on the initial velocities makes process II less likely than I at common laboratory gas pressures, even though the number of two-body encounters greatly exceeds the number of three-body encounters. Radiative recombination may very well play an important role in atom recombination in the upper atmosphere where the gas densities are extremely low, thus making three-body encounters far less likely.

Mechanism III, two-body wall recombination, is similar to three-body recombination except that the wall assumes the role of the third body in the recombination process. Wall recombination (IV) may occur when an atom in the gas collides with an atom adsorbed on the wall. The rate of this reaction could therefore be written:

$$\left(\frac{d\eta}{dt}\right)_{wall} = -K_4^* n_w n_s , \qquad (2\text{-}5)$$

where K_4^* is a proportionality constant,

n_w is the atom gas concentration at the wall,

and n_s is the atom surface concentration on the wall.

However, the concentration of atoms adsorbed on the wall is independent of the gas concentration over a large range of gas densities; making $K_4^* n_s$ a constant, K_4.

There appears to be no definite experimental evidence for any complex recombination mechanism, such as V, at the present time,

although the possibility of reactions involving ions must be kept in mind.

The differential equations for the loss of atomic nitrogen by the various processes are listed in Table 1. In general, all the processes may be expected to participate, and the total rate of recombination depends upon all of the separate rates:

$$\left(\frac{dn}{dt}\right)_{volume} = -k_1 n^2 [M] - k_2 n^2 \qquad (2\text{-}6)$$

and

$$\left(\frac{d\eta}{dt}\right)_{wall} = (-K_3 n^2 - K_4 n)_{wall}. \qquad (2\text{-}7)$$

These differential equations express the rate of disappearance of atomic nitrogen at any point in the gas and are to be used as sink functions in the equation of continuity. The complete differential equation with added terms due to gradients in the atom density will be considered in the section on gas flow.

Current theories of the three-body recombination rate yield, at best, order of magnitude results for the rate constants. Three different methods of approach have been used to calculate three-body recombination coefficients. The earliest methods used a simple mechanistic view derived from the kinetic theory of gases (49, p. 245-250). Wigner's statistical theory (51) with recent modifications (5; 11; 28; 29) has been applied to atom recombinations other than nitrogen. A recent calculation of the atomic oxygen recombination coefficient has been made using a perturbed stationary state quantum

mechanical approximation (3). Neither the statistical nor the quantum mechanical approach has been used in the case of atomic nitrogen recombination because these calculations require a knowledge of all excited molecular states of nitrogen which are formed in the recombination process. Even when applied to other atomic species for which this knowledge is available, these methods have not yielded accurate values for k_1.

An approximate expression for the three-body recombination coefficient can be derived from the kinetic theory approach. In this theory the atoms and molecules are treated as hard spheres. The number of three-body collisions in which two nitrogen atoms are simultaneously in contact with any other gaseous atom or molecule is infinitesimally small, far too small to account for the observed three-body recombination rates, and so it is further assumed that a recombination takes place whenever a third body and two atoms are separated by less than some critical reaction distance of the range of the van der Waal force (approximately 1 1/2 atom diameters). The values of k_1 resulting from this approximate calculation are of the order of 10^{-32} cc.^{2} sec.$^{-1}$.

The recombination coefficient k_1 is occasionally defined in an alternative way, different from Equation (2-1) by a factor of two:

$$\frac{dn}{dt} = -2k_1' [M] n^2 ; \qquad (2\text{-}8)$$

therefore,

$$2k_1' = k_1 . \qquad (2\text{-}9)$$

Thus, care must be exercised in comparing values of the recombination coefficient from different sources.

Gas Flow Theory

In this section a relationship between the atom concentration of a recombining gas flowing in a cylindrical tube and the various parameters of the flow system will be derived.

To describe completely the flow of fluids, taking into account viscosity, compressibility, the effect of body forces, pressure changes, heat flow, diffusion, and recombination, three equations are required: the Navier-Stokes equation which expresses the conservation of momentum, the equation of thermal energy which expresses the conservation of energy; and the equation of continuity which expresses the conservation of matter. A simultaneous exact solution of all three equations is impossible without several simplifying assumptions, the first of which is that the flowing gas is at a constant temperature. Therefore, the equation of heat flow may be discarded. The Navier-Stokes equation may also be discarded if it is further assumed that the gas is non-viscous and imcompressible.

The equation of continuity which describes the rate of concentration change of the nitrogen atoms at each point in the volume of

the gas is:

$$\frac{\partial n}{\partial t} = -\nabla \cdot (\vec{\Gamma}) + \phi \qquad (2\text{-}10)$$

where $\vec{\Gamma}$ is the flux density, $\Gamma = n\vec{v} - D\nabla\vec{n}$,

n is the concentration of atomic nitrogen,

$\vec{v}$ is the flow velocity,

D is the diffusion coefficient,

and ϕ is the volume rate of formation of atomic nitrogen.

In the steady state $\frac{\partial n}{\partial t} = 0$, and the substitution of this and $\vec{\Gamma}$ into the equation of continuity yields;

$$\nabla \cdot \vec{\Gamma} = \vec{v} \cdot \nabla n + n\nabla \cdot \vec{v} - D\nabla^2 n = \phi = -(k_1[M] + k_2)n^2$$

with the boundary condition that the radial current to the wall shall equal the number of wall recombinations per unit time. The atom velocity $\vec{v}$ is equal to the gas velocity $\vec{v}_{gas}$ for which

$$\nabla \cdot \vec{\Gamma}_{gas} = \vec{v} \cdot \nabla n_{gas} + n_{gas} \nabla \cdot \vec{v} - D\nabla^2 n = 0,$$

and, assuming incompressibility so that $\nabla n = 0$ and $\nabla^2 n = 0$; therefore, $\nabla \cdot \vec{v} = 0$. Additional assumptions which result in what will be called uniform flow are that the radial diffusion is sufficiently rapid to result in a radially uniform concentration of atoms in the flow tube, so that $\vec{v} \cdot \nabla n = v \frac{dn}{dz}$, and that the diffusional velocity in the z direction is negligible compared with the flow velocity, so that $D\nabla^2 n = 0$. Thus n is a function of z only, $n \cong n(z)$, and the resulting differential equation for this uniform flow is:

$$v \frac{dn}{dz} = -(k_1[M] + k_2 + k_3)n^2 - k_4 n \qquad (2\text{-}11)$$

where the number of wall recombinations per second,

$$(\frac{d\mathcal{N}}{dt})(\text{area}) = (-K_3 n^2 - K_4 n)(2\pi r_o \delta z)$$

has been replaced by an equivalent number of volume recombinations per second,

$$(\frac{dn}{dt})(\text{volume}) = (-k_3 n^2 - k_4 n)(\pi r_o^2 \delta z).$$

For a cylindrical tube, equating these recombination rates yields:

$$k_3 = K_3 \frac{2}{r_o} \quad \text{and} \quad k_4 = K_4 \frac{2}{r_o} .$$

The coefficient k_4 may be expressed in terms of the wall recombination probability γ, which is defined as the ratio of the number of wall recombinations per second per unit area to the total number of wall collisions per second per unit area. The rate of atom collisions per unit wall area predicted by the kinetic theory of gases is $(\frac{1}{4} n \bar{c})$ where $\bar{c}$ is the average thermal velocity of the atoms; therefore, the rate of recombination per unit wall area is $\gamma(\frac{1}{4})n\bar{c}$. Since for any short sections of the flow tube with wall area $2\pi r_o \delta z$ and volume $\pi r_o^2 \delta z$ the number of wall recombinations equals the number of equivalent volume recombinations, then

$$\gamma \frac{1}{4} n\bar{c}\, 2\pi r_o \delta z = k_4 n \pi r_o^2 \delta z, \qquad (2\text{-}11A)$$

and solving for k_4,

$$k_4 = \frac{\gamma \bar{c}}{2r_o} \quad . \tag{2-12}$$

Equation (2-11) can be integrated, yielding:

$$\frac{n(n_o + \frac{k_4}{k_1[M] + k_2 + k_3})}{n_o(n + \frac{k_4}{k_1[M] + k_2 + k_3})} = e^{-k_4 \frac{z}{\bar{v}}} \tag{2-13}$$

Special cases of interest are

$$k_4 = 0 \qquad : \quad \frac{1}{n} = \frac{1}{n_o} + (k_1[M] + k_2 + k_3)\frac{z}{\bar{v}} \tag{2-14}$$

and

$$k_1, k_2, k_3 = 0 : \quad n = n_o e^{-k_4 \frac{z}{\bar{v}}} \quad . \tag{2-15}$$

At large atom concentrations, the $(k_1[M] + k_2 + k_3)n^2$ term in Equation (2-11) will govern the recombination, while at low concentrations the $k_4 n$ term will dominate; therefore, the atom concentration may be expected to decay as in Equation (2-14) for large values of n, and as in Equation (2-15) for small values of n.

In determining values of k_1, it will be assumed that a linear plot of $\frac{1}{n}$ versus $\frac{z}{\bar{v}}$ (or time, t) is an indication of negligible wall recombination; thus, the slope of this curve is $k_1[M] + k_2 + k_3$. The errors resulting from this assumption will now be discussed. Equation (2-13) containing both three-body and wall recombination terms may be expanded using the approximation:

$$e^{k_4 t} = 1 + k_4 t + \frac{(k_4 t)^2}{2} \qquad (2\text{-}16)$$

The result is:

$$\frac{1}{n} = \frac{1}{n_o} + \left\{ (k_1[M] + k_2 + k_3) + \frac{k_4}{n_o} \right\} (t) \left(1 + \frac{k_4 t}{2} \right) \qquad (2\text{-}17)$$

The non-linearity of a plot of $\frac{1}{n}$ versus $t (t = \frac{z}{v})$ is given by the $\frac{k_4 t}{2}$ term in the above expression. From observations of trial plots of the above equation, it was determined that if $\frac{k_4 t}{2}$ was greater than 0.03 then the curve beyond this time, defined as t_c, would be clearly non-linear and would not be used in the determination of k_1. Thus t_c is the time after which plots of $\frac{1}{n}$ versus t appear non-linear. The maximum errors which result from calculating $(k_1[M] + k_2 + k_3)$ from the apparently linear slopes of plots of $\frac{1}{n}$ versus t may be calculated from Equation (2-17). If we let n_c be the value of n at t_c and substitute $\frac{k_4 t_c}{2} = 0.03$, then the value of $(k_1[M] + k_2 + k_3)$ determined by the end points ($n = n_o$ at $t = 0$ and $n = n_c$ at $t = t_c$) of the graph is

$$k_1[M] + k_2 + k_3 = \frac{1}{n_o t_c} \left(\left[\frac{n_o}{n_c} - 1 \right] - 0.06 \right) \left(\frac{1}{1.03} \right).$$

The inaccuracies due to the presence of k_4 result in the -0.06 term and the 1.03 factor. The maximum percent error ϵ due to these effects is thus approximately

$$\epsilon = \left(\frac{0.06}{\frac{n_o}{n_c} - 1} + 0.03 \right) 100.$$

Thus the larger the value of $\frac{n_o}{n}$ for which the slopes appear linear, the greater will be the accuracy in the value of k_1. Some typical values of ϵ for different $\frac{n_o}{n_c}$ are:

$$\text{if } \frac{n_o}{n_c} = 1.5, \text{ then } \epsilon = 15\%;$$

$$\text{if } \frac{n_o}{n_c} = 2, \text{ then } \epsilon = 11\%;$$

$$\text{if } \frac{n_o}{n_c} = 3, \text{ then } \epsilon = 6\%;$$

and

$$\text{if } \frac{n_o}{n_c} = 8, \text{ then } \epsilon = 4\%.$$

As a further justification for the use of these uniform flow equations, we can compare their predictions with the theory of Krongelb and Strandberg (30,p.1205) who made several numerical solutions of the differential equations describing the flow of recombining atoms in a cylindrical tube, without the assumption of a radially uniform atom concentration. Their solutions were made with the assumptions that the fluid is incompressible, that the effect of body forces is negligible, and that the flow is laminar. The solution of the simplified Navier-Stokes equation results in an equation for the so-called Poiseuille flow. Poiseuille flow results in a parabolic velocity profile (25, p. 215):

$$v = v_o \left(1 - \frac{r^2}{r_o^2}\right) \qquad (2\text{-}18)$$

where v is the flow velocity in the tube,

v_o is the flow velocity at the center of the tube,

r is the distance from the center of the tube,

and r_o is the radius of the tube.

Krongelb and Strandberg then substituted this equation for the velocity into the equation of continuity and obtained numerical solutions. Their solutions for two specific cases both with no wall recombination, one with no radial diffusion and one with a fairly large radial diffusion, are shown respectively in curves "a" and "b" of Figure 2. The solution of our uniform flow equation in the absence of wall recombination is plotted in curve "c". The agreement between these three curves is excellent; curves "b" and "c" are colinear and the slope of "a" is identical to that of "b" and "c" for values of $\frac{n_o}{n}$ larger than two. The compatibility of these three curves is added justification for the validity of the uniform flow equation in the case where wall recombination is negligible.

A criterion to determine when uniform flow is a valid approximation in case wall recombination is not negligible will be assumed to be the following: the mean time for diffusion of atoms across the radius of the tube must be less than the time constant for wall recombination. The time constant for wall recombination is the reciprocal of k_4, while the time for diffusion may be taken as the radius of the tube, r_o, divided by the velocity of diffusion v_D. Since

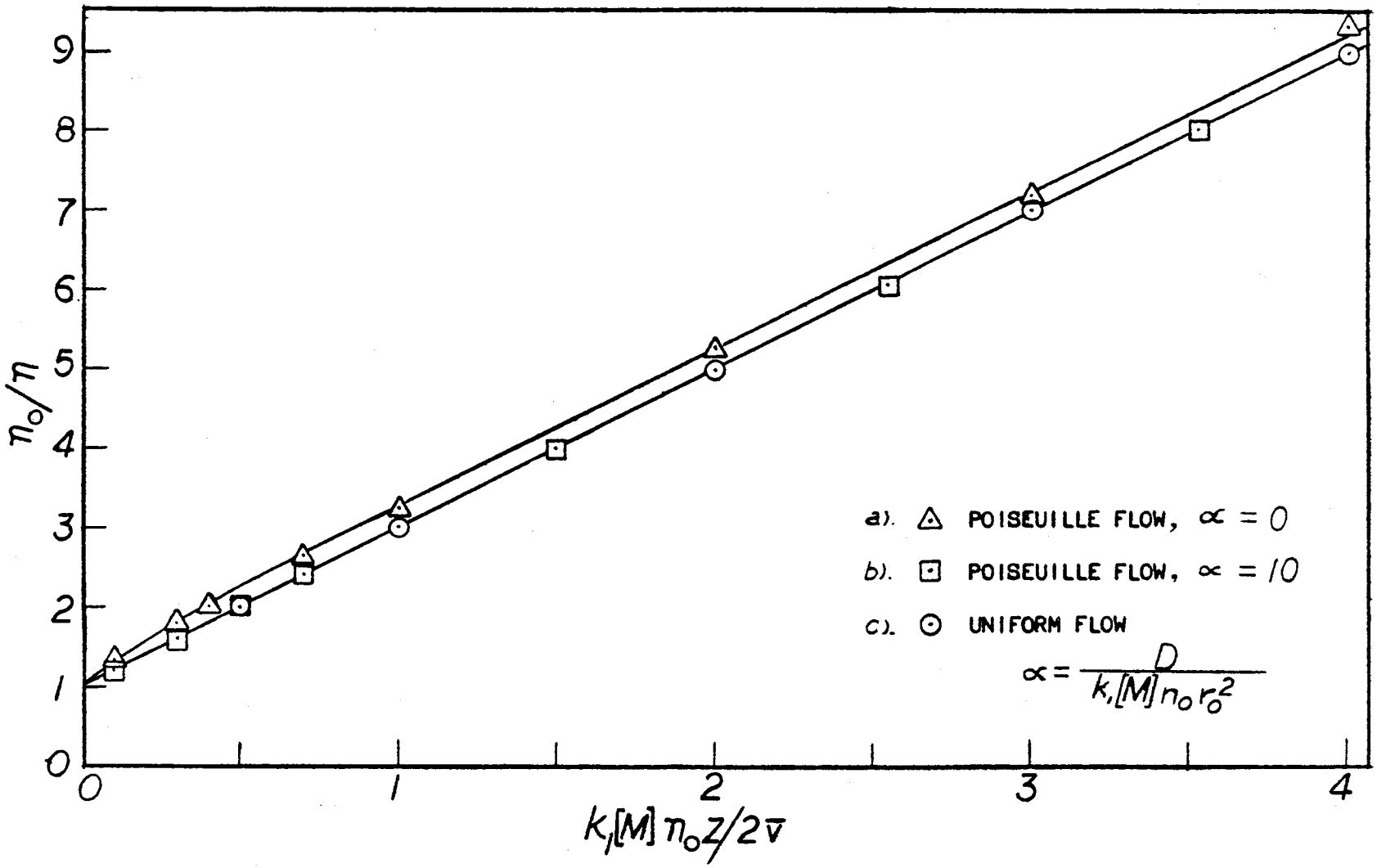

Figure 2. Three-Body Recombination Curves for Poiseuille Flow and Uniform Flow

$v_D = D \frac{\nabla n}{n}$, and if we make the gross approximation that

$$\frac{\nabla n}{n} = \frac{\Delta n}{n_m r_o} , \quad n_m \text{ is } n_{\text{maximum}} ,$$

and we want a radial variation of concentration of no more than 5%,

$$\Delta n = 0.05 n_m ,$$

then the criterion becomes

$$\frac{r_o^2}{(0.05)(D)} < \frac{1}{k_4} . \qquad (2\text{-}19)$$

ELECTRON PARAMAGNETIC RESONANCE

Only those aspects of the electron paramagnetic resonance phenomenon which contribute to an understanding of the spectrum of atomic nitrogen and to the measurement of absolute concentrations of atom densities will be discussed in this chapter.

Theory

In a discussion of the epr spectrum of atomic nitrogen, an energy level diagram is useful in predicting the location of the epr spectral lines. An energy level diagram for the isotope N^{14} (which has a nuclear spin $I = 1$) in a magnetic field is shown in Figure 3. The ground state of atomic nitrogen is a $^4S_{3/2}$ state; i. e., $L = 0$, $J = S = 3/2$. The next four higher excited states $^2D_{5/2}$, $^2D_{3/2}$, $^2P_{3/2}$, and $^2P_{1/2}$ are also shown. In considering transitions between the four upper levels and the ground state, one applies the selection rules for electric dipole transitions which are:

$$\Delta L = 0, \pm 1$$

$$\Delta S = 0$$

$$\Delta J = 0, \pm 1 \quad \text{but } J = 0 \not\rightarrow J = 0$$

$$\Delta M_J = 0, \pm 1 \quad \text{but } M_J = 0 \not\rightarrow M_J = 0 \text{ if } \Delta J = 0.$$

The change in S is not equal to 0 for transitions between the ground state and the other four states shown; these transitions are

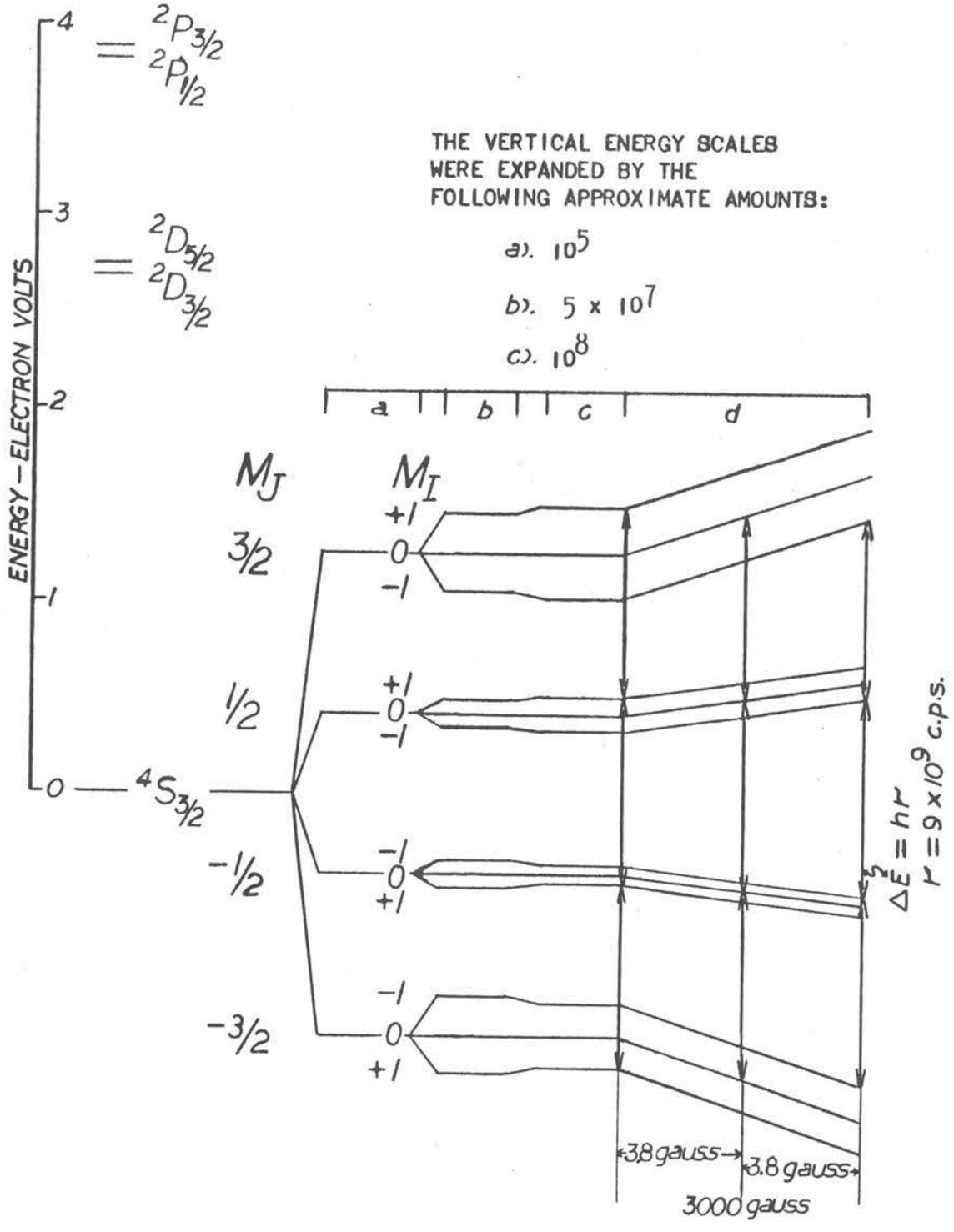

Figure 3. Energy Level Diagram of the Nitrogen Atom

therefore forbidden and the upper states are then metastable states of atomic nitrogen.

In describing the splitting of the ground state energy levels due to the interaction of the nuclear magnetic moment, the spin and orbital magnetic moment of the electrons, and the external magnetic field H_o in the z direction, the hamiltonian including the interaction may be written:

$$\mathbf{H} = \mathbf{H}_o + g\beta H_o J_z - g_n\beta_n H_o I_z + A\vec{I}\cdot\vec{J} \qquad (3\text{-}1)$$

where $\mathbf{H}_o$ is the unperturbed hamiltonian,

g_n is the nuclear g factor,

β_n is the nuclear magneton,

A represents the constant for the coupling of the nuclear magnetic moment to the electronic magnetic moment.

The energy levels are obtained by diagonalizing this hamiltonian. In a magnetic field where I is decoupled from J, as it is in the case of the nitrogen atom in a field of 3,000 gauss, a first order perturbation calculation instead of the diagonalization yields the following approximate energy levels (38, p. 75):

$$E(M_I, M_J) = E_o + g\beta H_o M_J - g_n\beta_n H_o M_J + AM_I M_J. \qquad (3\text{-}2)$$

In the energy level diagram, Figure 3, the levels due to the addition of $g\beta H_o M_J$ to the ground state are shown on a greatly expanded vertical scale in column a); in column b) the effect of including the

AM_IM_J term, and in column c) the effect of adding the $g_n\beta_n H_o M_I$ term to the levels shown in column b) are represented on still further expanded scales. In column d) the result of increasing the magnetic field by 7.6 gauss is shown.

For magnetic dipole induced transitions the selection rules are:

$$\text{either } \Delta M_J = \pm 1 \text{ and } \Delta M_I = 0$$

$$\text{or } \Delta M_J = 0 \text{ and } \Delta M_I = \pm 1.$$

Electron paramagnetic resonance is the phenomenon associated with the absorption of energy for the $\Delta M_J = \pm 1$ transition; $\Delta M_J = \pm 1$ transitions for a constant ΔE are represented by vertical lines in column d in the energy level diagram. The energy of this transition is

$$\Delta E_{(\Delta M_J = \pm 1)} = \pm (g\beta H_o + AM_I) \qquad (3\text{-}3)$$

and is seen to be independent of the $g_n\beta_n H_o M_I$ term added in column b) of Figure 3.

In the case of N^{14} the $g\beta H_o$ term is nearly 1000 times larger than the AM_1 term and the three values of $M_I(+1, 0, -1)$ produce the three closely spaced epr lines of atomic nitrogen. The absorption is called a resonance phenomenon because it is strongly dependent upon the magnetic field. The value of A for N^{14} was first measured using epr by Beringer and Heald (7) who obtained a value of 10.45 ± 0.02 megacycles per second for $\frac{A}{h}$ where h is Planck's constant. More recently a group of workers (20) obtained 10,450,925 ± 20 cycles per second for the value of $\frac{A_{N^{14}}}{h}$ and

16,645,441 ± 20 cycles per second for $\frac{A_N{}^{15}}{h}$ by a technique using optical pumping and spin exchange.

For the $\Delta M_J = 0$ and $\Delta M_I = \pm 1$ transitions

$$\Delta E = \pm(-g_n \beta_n H_o + A M_J) \qquad (3\text{-}4)$$

and for N^{14} the AM_J term has values about 10 times larger than $g_n \beta_n H_o$ in a field of 3,000 gauss. These transitions, which would then be observable in the absence of a magnetic field, would be only slightly dependent upon the magnetic field. The expression, magnetic resonance, however, is generally reserved for situations where the $g_n \beta_n H_o$ term dominates the energy absorption expression, and the energy of absorption is hence highly dependent upon the magnetic field.

The other stable isotope of nitrogen, N^{15}, has a nuclear spin of 1/2 and therefore an epr spectrum consisting of just two lines.

An expanded scale for the M_J and M_I levels of the ^2P and ^2D states is not illustrated in the energy level diagram in Figure 3. Although the vacuum ultraviolet absorption spectra of the ^2P and ^2D states have demonstrated the presence of ^2P and ^2D states in small amounts in the nitrogen afterglow (46), the epr spectra of these two states have never been observed, presumably because their concentrations are too small.

In dealing with the more quantitative effects of epr, the magnetic state of a substance can be described in terms of its magnetic

moment per unit volume, or magnetization vector. In an isotropic medium the magnetization M is proportional to the external field, H, which produces it:

$$\vec{M} = \chi \vec{H}$$

The proportionality constant, χ is called the magnetic susceptibility.

Consider the situation in which there is applied to a sample a steady magnetic field H_o in, say, the z direction, and an oscillating magnetic field H_x in the x direction. The action of both H_o and H_x gives rise to changing components of the magnetization in the x and y directions. Then M_x has some definite phase relationship with respect to H_x. Mathematically, these components of the magnetization are most easily dealt with by assigning real and imaginary parts to χ :

$$\chi = \chi' - i\chi''$$

The field H_x can then be taken as the real part of $2H_1 e^{i\omega t}$

then

$$M_x = \text{Real Part of } \chi H \tag{3-5}$$

and

$$M_x = \chi'(2H_1 \cos \omega t) + \chi''(2H_1 \sin \omega t).$$

$2H_1$ is conventionally used as the magnitude of the oscillating field H_x because of a convenience in the solution of the Bloch equations describing the phenomenological character of magnetic resonance.

The power per unit volume expended in changing the magnetic flux is (39, p. 153):

$$P = \mu_o \vec{H} \cdot \frac{\partial \vec{B}}{\partial t} . \qquad (3\text{-}6)$$

But $\vec{B} = \mu_o (\vec{H} + \vec{M})$,

so that $\frac{\partial \vec{B}}{\partial t} = \mu_o \left(\frac{\partial \vec{H}}{\partial t} + \frac{\partial \vec{M}}{\partial t} \right)$;

therefore, $P = \mu_o \vec{H} \cdot \left(\frac{\partial \vec{H}}{\partial t} + \frac{\partial \vec{M}}{\partial t} \right)$.

Now $\vec{H} \cdot \frac{\partial \vec{H}}{\partial t}$ is the power associated with the magnetic field in free space; therefore, the power absorbed by the sample per unit volume is

$$P = \mu_o \vec{H} \cdot \frac{\partial \vec{M}}{\partial t} , \qquad (3\text{-}7)$$

then $$P = \chi'(4H_1^2)\omega \sin \omega t \cos \omega t + \chi''(4H_1^2)\omega \cos^2 \omega t . \qquad (3\text{-}8)$$

By integrating the above expression over one cycle of H_x, the average power absorbed per unit volume per cycle becomes

$$P = 2H_1^2 \omega \chi''. \qquad (3\text{-}9)$$

The absorbed power P is the quantity which is eventually measured by the epr spectrometer and is thus proportional to χ''.

Krongelb and Strandberg (30, p. 1199) have carried out the calculations relating the number density of molecular oxygen and atomic gases to $\int_{-\infty}^{+\infty} \chi'' \, dH$. By using molecular oxygen as a calibration standard, these workers eliminated unknown instrumental parameters. Their result for atoms, after we corrected for a numerical error of 1/2 because the integral of the line shape factor is π and not $\frac{\pi}{2}$, is (30, p. 1199):

$$\int \chi'' \, dH = n(\pi) \left(\frac{\hbar \omega_o}{g \beta k T} \right) \frac{1}{Z} \sum_{JM} \left\{ e^{-\frac{E_{JM}}{kT}} \left| (\mu_r)_{JM, J'M'} \right|^2 \right\} \qquad (3\text{-}10)$$

where ω_o = angular frequency of H_x,

g = spectroscopic splitting factor (Lande g factor) which is $\left[1 + \frac{J(J+1) + S(S+1) - L(L+1)}{2J(J+1)} \right]$,

J = total angular momentum quantum number,

L = orbital angular momentum quantum number,

S = spin angular momentum quantum number,

β = Bohr magneton

Z = partition sum $= \sum_{JM} e^{-\frac{E_{JM}}{kT}}$,

$\left| (\mu_r)_{JM, J'M'} \right|^2$ = absolute square of the transition matrix element in the direction of the RF field,

$\left| (\mu_r)_{JM, J'M'} \right|^2 = g^2 \beta^2 \frac{f^+}{2} (J - M)(J + M + 1)$,

f^+ is basically a geometrical factor which is identical for all samples having the same geometry,

M = magnetic quantum number.

The primed and unprimed symbols represent the final and initial states, respectively.

For atomic nitrogen in the $^4S_{3/2}$ ground states, $L = 0$, $S = 3/2$, and $J = 3/2$; therefore,

$$g = 2,$$

$$e^{\frac{-E_{JM}}{kT}} = e^{0} = 1,$$

$$Z = 2J + 1,$$

$$\sum_{JM} = (J + M)(J + M + 1) = \frac{2}{3} J(J + 1)(2J + 1) = 2.25,$$

and $$\int \chi''_N dH = n_N \left(\pi \frac{\hbar\omega}{\beta kT}\right) \frac{f^+}{2} \beta^2 (2)(2.25). \qquad (3\text{-}11)$$

For molecular oxygen, Krongelb and Strandberg (30, p. 1199) obtained, again after inserting the correction factor of two,

$$\int \chi''_{O_2} dH = n_{O_2} \left(\frac{\pi \hbar \omega_o}{\beta kT}\right)^2 \frac{e^{-\left(\frac{E_{JM}}{kT}\right)}}{Z} \frac{|(\mu_r)_{JM, J'M'}|^2}{g_{eff.}} \qquad (3\text{-}12)$$

where

$$|(\mu_r)_{JM, J'M'}|^2 = g^2 \beta^2 \left(\frac{f^+}{2}\right) \{4|(JM|S_x|J'M')|\}^2,$$

$$g_{eff.} = \frac{\hbar}{\beta} \frac{d\omega_o}{dH},$$

$$g = 2$$

$$Z \approx \frac{3kT}{2B}$$

$$B = 43,100 \text{ Mc./sec.} = \text{the rotational temperature}$$

$$(43,100 \text{ Mc.} \rightarrow 2.1 \ ^{o}K).$$

The $K = 5$, $J = 4 \rightarrow 6$, and $M = 1 \rightarrow 2$ transition which Krongelb and Strandberg used was also employed in the present experiments because this transition produced a line which was one of the most

prominent lines and was isolated from nearby interfering lines in the low magnetic field region. The theory of the Zeeman effect for molecular oxygen is worked out by Tinkham and Strandberg (48, p. 963) who obtained a value of 0.37 for $[4|(JM|S_x|J'M')|^2 e^{\frac{-E_{JM}}{kt}}]$ for the $K = 5$, $J = 4 \rightarrow 6$, and $M = 1 \rightarrow 2$ transition and a value of 1.313 for $g_{eff.}$. Substitution of these values and the above values for Z, B, and g into Equation (3-12), and division by the corresponding expression for nitrogen yields the following expression:

$$n_N = n_{O_2} (1.033 \times 10^{-3}) \frac{\int \chi''_N \, dH}{\int \chi''_{O_2} \, dH} \qquad (3\text{-}13)$$

The two corrections which were made in the expressions for both nitrogen and oxygen cancelled out, and the resulting expression is of the same form as that of Krongelb and Strandberg (30, p. 1199) except, of course, that their expression described the determination of atomic oxygen concentrations and not those of nitrogen.

To achieve the maximum sensitivity, an ac detection scheme was employed in the epr spectrometer and χ'' was not measured directly. In this scheme, the magnetic field was modulated at a frequency ω_m and amplitude H_m, and a narrow band receiver detected the ac signal at frequency ω_m resulting from this modulation. Halbach (14) has derived the following expression relating this measured ac signal to $\int \chi'' \, dH$:

$$\int \chi'' \, dH = C \frac{1}{H_m H_1 (S_L)} \int \Delta H \, Y dH \qquad (3\text{-}14)$$

where $\int \Delta H \, Y dH$ is called the first moment of the signal,

C is a proportionality constant,

H_m is the magnitude of the magnetic modulation field,

H_1 is the magnitude of the 9 gigacycles per second magnetic field,

S_L is the signal level of the amplifier (gain),

H is the polarizing magnetic field strength,

$\Delta H = H - Hc$,

$Hc = H$ at center of line,

and Y is the recorder output of the epr spectrometer.

A somewhat more generalized derivation of the above expression following the methods of Primas (40) yields the same expression. The expression is valid for all modulation frequencies and amplitudes (even those frequencies greater than the reciprocal of the relaxation times and amplitudes in excess of the line width).

The independency of the expression with respect to ω_m and the linearity of its first moment with H_m were verified for 100 kilo - cycles per second modulation and 400 cycles per second modulation in the case of nitrogen in two ways. First, the ratio of the moments of nitrogen taken at both 100 kilocycles per second and 400 cycles per second modulation to that of a standard DPPH (diphenylpicrylhydrazyl)

were the same. The DPPH has a line width which is sufficiently large so that its shape is undistorted by the effects of the higher modulation frequency. A modulation amplitude about one-tenth of its line width was used in measuring the DPPH moment. Secondly, the nitrogen moments at both 100 kilocycles per second and 400 cycles per second taken at a constant nitrogen concentration and varying modulation amplitude were proportional to the modulation amplitude even though it was increased to several times the minimum observed line width.

If we take the ratio of two integrated susceptibilities in Equation (3-14):

$$\frac{\left(\int \chi'' \, dH\right)_N}{\left(\int \chi'' \, dH\right)_{O_2}} = \frac{(H_m)(H_1)(S_L)_{O_2} \left(\int \Delta H \, Y \, dH\right)_N}{(H_m)(H_1)(S_L)_N \left(\int \Delta H \, Y \, dH\right)_{O_2}} \qquad (3\text{-}15)$$

C cancels out, and we can substitute the resulting expression into Equation (3-13), yielding the equation used in measuring the nitrogen atom concentration:

$$n_N = (1.033 \times 10^{-3})(n_{O_2}) \frac{\left\{H_m H_1 (S_L)\right\}_{O_2} \left\{\int \Delta H \, Y \, dH\right\}_N}{\left\{H_m H_1 (S_L)\right\}_N \left\{\int \Delta H \, Y \, dH\right\}_{O_2}} \qquad (3\text{-}16)$$

Because the spectrum of atomic nitrogen consists of three lines due to the splitting caused by the N^{14} nucleus, the value of $\int \Delta H \, Y \, dH$ to be used in Equation (3-16) was obtained by finding the value of $\int \Delta H \, Y \, dH$ for one of the three lines and multiplying by three.

The Epr Spectrometer

A standard Varian epr spectrometer with a V-4500 epr console, a V-4560 100 kilocycles per second field modulation unit, a V-4500-41A low-high power microwave bridge, a V-4531 resonant cavity, a V-4007 six inch magnet with 2-3/4 inch gap and Rose shimmed pole faces, and a V-2200-A magnet power supply was employed. This epr spectrometer was used as shown in Figure 4 in all experiments except two, for which minor modifications were made. A low frequency modulation unit was substituted for the 100 kilocycles per second modulation unit to measure the epr line shape of atomic nitrogen, and a specially constructed quartz cavity was substituted for the Varian cavity when required. The individual components of the epr spectrometer will not be discussed separately since the instrument is a standard unit and is described adequately by the Varian instruction manuals.

The microwave bridge is represented in Figure 4 by the group of blocks connected by double lines which represent waveguides. The cryostat isolator attenuated the microwave power traveling to the resonant epr cavity, but did not attenuate the epr signal returning from the cavity. Adjustment over a range of about 70 decibels of microwave power in the resonant cavity was possible with the use of both the cryostat isolator and the variable attenuator. For

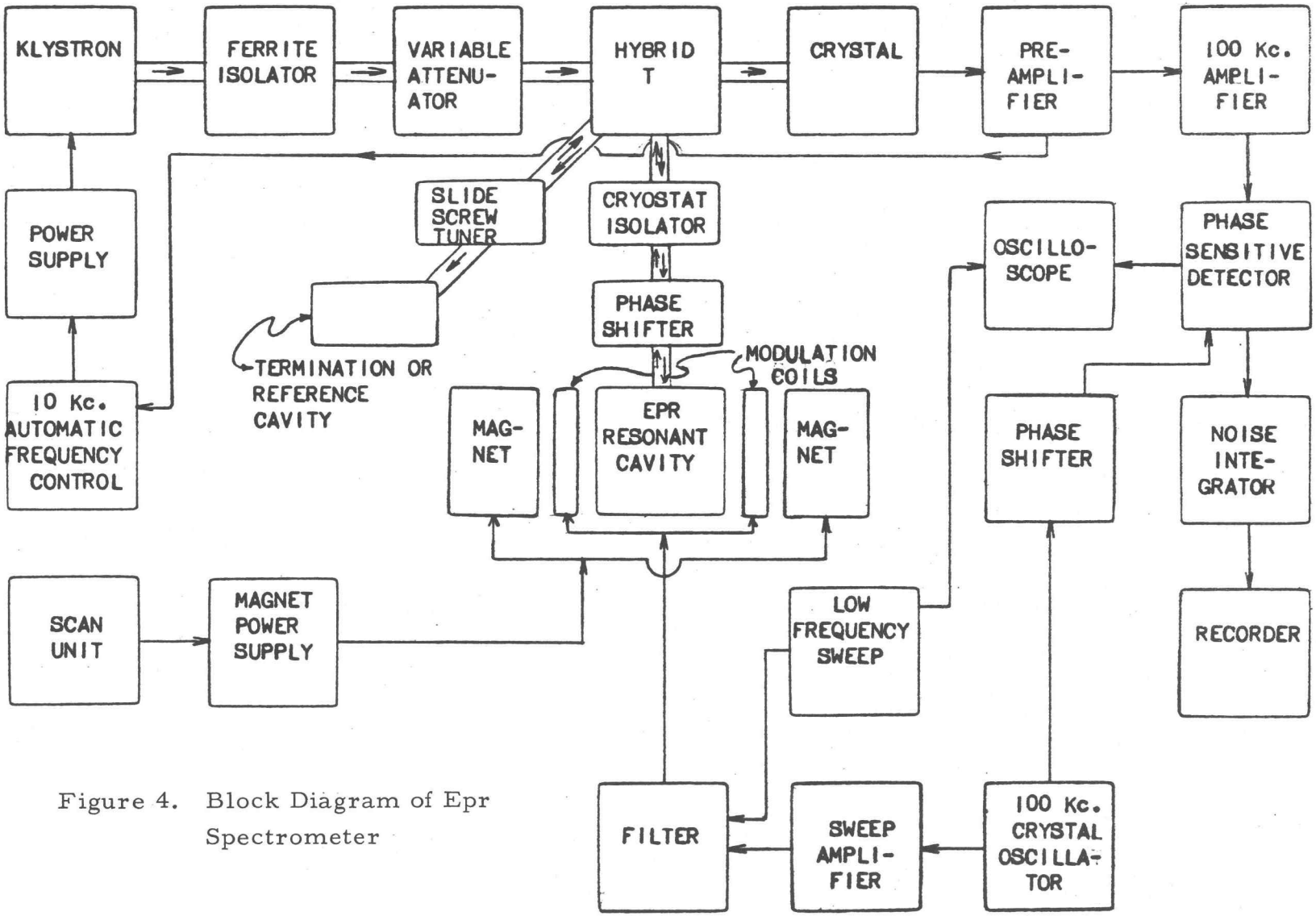

Figure 4. Block Diagram of Epr Spectrometer

extremely low power measurements, in the vicinity of 60 decibels of attenuation of the 100 milliwatt maximum power at the sample, the frequency of the klystron was locked to a reference cavity by the automatic frequency control rather than to the main epr cavity because the automatic frequency control signal reflected from the main epr cavity was too weak to provide stability at this attenuation. With this reference cavity arrangement, a microwave phase shifter in the waveguide leading to the main epr cavity could be adjusted to allow the observation of the χ' component, χ'' component, or some mixture of these components of the signal.

When the epr spectrometer was operated in high power (i.e., the klystron was locked to the resonant epr cavity), only the χ'' component was observed. To insure that only the χ'' component was being observed when the klystron was locked to the reference cavity, the signal from a reference sample of DPPH placed permanently in the epr cavity external to the flow tube was monitored periodically throughout the various experiments, permitting compensation for any drift in the settings of the instrument. The shapes of the DPPH signal at high and low power were compared to determine the proper setting of the phase shifter for detection of the pure χ'' component.

The experimental measurement of all factors appearing in the atom density equation (3-16):

$$n_N = (1.033 \times 10^{-3})(n_{O_2}) \frac{\left\{H_m H_1 (S_L)\right\}_{O_2}}{\left\{H_m H_1 (S_L)\right\}_N} \frac{\left\{\int \Delta H\, Y\, dH\right\}_N}{\left\{\int \Delta H\, Y\, dH\right\}_{O_2}}$$

will now be described. All of the factors before the integral sign in the preceding equation appear as ratios so that the absolute values of these factors need not be known. The 100 kilocycles per second amplifier had S_L numbers posted on the S_L dial; however, the numbers were found to be insufficiently accurate. The S_L numbers were therefore redetermined to an accuracy of better than 1% by measuring the signal height from a reference sample of solid DPPH at different S_L settings.

The modulation dial setting, H_m, was checked in a similar manner using a solid sample of DPPH and a 0.001 molar aqueous solution of $MnSO_4$ contained in a small capillary extending through the epr cavity. The $MnSO_4$ solution exhibited a resonance signal containing six lines each 25 gauss wide while the signal from DPPH was only about two gauss wide. The signal height of the epr signal is proportional to H_m only for the values of H_m small compared with the natural line width, so the broader signal from $MnSO_4$ was useful in measuring H_m for the larger values of H_m.

The oscillating field strength H_1 had to be set at low values $(H_1)_N$ to prevent saturation of the atomic nitrogen signal and at high values $(H_1)_{O_2}$ for the oxygen signal to achieve a satisfactory

signal-to-noise ratio. From Equation (3-14) one finds for a line of constant width that the signal height $Y_{max.}$ divided by the gain S_L is proportional to H_1, then

$$\frac{(H_1)_{O_2}}{(H_1)_N} = \frac{\frac{Y_{1,max.}}{(S_L)_1}}{\frac{Y_{2,max.}}{(S_L)_2}} \tag{3-18}$$

where Y_1 and Y_2 are the signal heights obtained from the same reference sample at the respective attenuator settings used for the molecular oxygen and atomic nitrogen calibration. S_{L1} and S_{L2} were the respective gain settings ; the modulation H_m was unchanged. A DPPH sample permanently located in the cavity external to the flow tube was used as a secondary reference sample with the Varian cavity and, since the quartz cavity experiments were performed in a much shorter time than the flow experiments, only molecular oxygen was used as the reference sample in the quartz resonant cavity.

The factor Y under the integral in Equation (3-16) is simply the height of the recorded signal at H. The magnetic field is varied at some specific rate r with respect to time ($\frac{dH}{dt} = r$), and the chart of the recorder moves at some speed s ($s = \frac{dx}{dt}$). Then

$$dH = \frac{r}{s}\, dx. \tag{3-19}$$

If r and s are constant,

$$\Delta H = \frac{r}{s}\Delta x. \qquad (3\text{-}20)$$

The speed x of the recorder is printed on the recorder; the determination of r, which is somewhat more difficult, will now be described.

The magnetic field H as a function of the magnet current I was measured with the use of a nuclear magnetic resonance proton probe; the current I was read on the magnet power supply ammeter. The magnetic field H was an approximately linear function of I, and $\frac{dH}{dI}$ could be considered constant over the width of each line observed. The current from the magnet power supply was a linear function of the scan voltage V into the magnet power supply: $\frac{dI}{dV} = C_m$. However, C_m was a function of both the "sweep rate" setting on the magnet and the value I_o of the magnetic current when V = 0. I_o was changed by varying the "coarse current" and "fine current" settings of the magnet power supply. The values of C_m were measured to 1% accuracy for the two settings of the sweep rate and the different values of I_o used in recording signals from atomic nitrogen and molecular oxygen.

The voltage driving the magnet power supply sweep originated in the scan unit in which a choice of 12 maximum output voltages, V_m was possible; each of these voltages was varied by a 15-turn potentiometer driven by a synchronous motor. Two different motors

with speeds S, each with three different gears with relative speeds n_1, n_2, and n_3 could be used to drive the potentiometer. Relative values of the 12 output voltages V_m were measured at a fixed setting on the 15-turn potentiometer to 0.5% accuracy with a Leeds-Northrup K-2 potentiometer while the scan unit was connected to the magnet power supply. The rate of change $\frac{dV}{dt}$ of the scan voltage was therefore proportional to $(V_m)(S)(n)$.

The rate r is given by

$$r = \frac{dH}{dt} = \left(\frac{dH}{dI}\right)\left(\frac{dI}{dV}\right)\left(\frac{dV}{dt}\right), \tag{3-21}$$

and substituting for $\frac{dV}{dt}$ and $dt = \frac{dx}{s}$, then

$$dH \propto \left(\frac{dH}{dI}\right)\left(\frac{dI}{dV}\right)(V_m)(S)(n)\left(\frac{dx}{s}\right). \tag{3-22}$$

Since $\frac{dH}{dI}$, $\frac{dI}{dV}$, V_m, S, n, and s are approximately constant over a line width, the above equation can be integrated, yielding

$$\Delta H \propto \left(\frac{dH}{dI}\right)\left(\frac{dI}{dV}\right)\frac{(V_m)(S)(n)}{(s)}\Delta x. \tag{3-23}$$

The above two expressions may be substituted into Equation (3-16) giving:

$$n_N = (1.033\times10^{-3})(n_{O_2})\frac{\left[\left\{\left(\frac{dH}{dI}\right)\left(\frac{dI}{dV}\right)\frac{(V)(S)(n)}{(s)}\right\}^2\right]_N\left[\int \Delta x\, Y\, dx\right]_N}{\left[\left\{\left(\frac{dH}{dI}\right)\left(\frac{dI}{dV}\right)\frac{(V)(S)(n)}{(s)}\right\}^2\right]_{O_2}\left[\int \Delta x\, Y\, dx\right]_{O_2}} \tag{3-24}$$

In any one experimental calibration, S, n, and s were the same for

both oxygen and nitrogen, so these factors cancelled out.

To compute $\int \Delta x\ Y\ dx$, $\Delta x Y$ was plotted versus x and the area under the resulting curve was measured with a Keuffel-Esser planimeter accurate to about 0.5%. The natural shapes of χ'' are Lorenzian (38, p. 30-34); a calculation of the contribution of the tail portions of a Lorenzian curve shows that 5% of $\int \Delta x\ Y\ dx$ is located beyond the point where $Y = \frac{Y_{max.}}{600}$. This means that great care must be taken in obtaining the value of $\int \Delta x\ Y\ dx$. At best, 5% is the accuracy obtainable in this computation.

Epr Calibration Check

To ascertain the validity of using oxygen as a calibration standard, the epr moments of two other commonly used calibration standards, solid DPPH and $MnSO_4$ in water, were compared with the moment of molecular oxygen. The general relationship between the number densities of those atomic species with angular moments J, and Lande g factors g may be obtained from Equations (3-10) (3-11) and (3-14):

$$R = \left[\frac{n_{atom}(J)(J+1)g}{\left\{\left(\frac{dH}{dI}\right)\left(\frac{dI}{dV}\right)V\right\}^2 \int \Delta x\ Y\ dx}{H_m H_1 (S \cdot L)}\right]_{atom} = \left[\frac{7.753 \times 10^{-3} n_{O_2}}{\left\{\left(\frac{dH}{dI}\right)\left(\frac{dI}{dV}\right)V\right\}^2 \int \Delta x\ Y\ dx}{H_m H_1 (S \cdot L)}\right]_{O_2} \qquad (3\text{-}25)$$

where R should be a constant for any particular epr spectrometer.

One of the difficulties in attempting to verify the above equation is that the sensitivity of the epr spectrometer is a function of sample position in the resonant cavity and the above expression is valid only for samples of identical geometry. The three samples tested differed markedly in this respect: DPPH was a solid sample which occupied a negligible volume at the cavity center (position 1), the $MnSO_4$ solution was contained in a one mm. I. D. quartz capillary tube extending through the center of the cavity (position 2), and molecular oxygen filled a nine mm. I. D. quartz flow tube also extending through the cavity (position 3). To account for changes in sensitivity at these three different sample positions, the ratio of the average sensitivity within position 3 to that at position 1, and the ratio of this same average sensitivity at position 2 were measured using two different probing samples, a point sample of DPPH and an approximately uniform linear sample of DPPH. The results of these comparisons were:

$$\frac{\text{average sensitivity at position 2}}{\text{average sensitivity at position 1}} = 0.40 \pm 6\%,$$

$$\frac{\text{average sensitivity at position 3}}{\text{average sensitivity at position 2}} = 1.1 \pm 12\%,$$

so that

$$\frac{\text{average sensitivity at position 3}}{\text{average sensitivity at position 1}} = 0.44 \pm 14\%.$$

The presence of water lowers the Q of the cavity and hence

the overall sensitivity of the spectrometer. To measure this change in Q, the epr signal height from a small sample of DPPH encapsulated in quartz and placed in the cavity external to the quartz flow tube was monitored. A length of quartz tubing inserted in place of the quartz flow tube was used to keep the amount of quartz in the cavity approximately the same for all measurements taken. The ratio of the relative sensitivities with and without the aqueous solution of $MnSO_4$ in the quartz capillary in place was:

$$\frac{Y_{max,\ DPPH\ \text{with}\ MnSO_4}}{Y_{max,\ DPPH\ \text{without}\ MnSO_4}} = \frac{6.4}{9.3} = 0.69$$

The signal observed with the $MnSO_4$ solution in place is due to the Mn^{++} ion which is in the $^6S_{5/2}$ state with $J = S = 5/2$ and $g = 2$. DPPH has a loosely-bound electron so that $J = S = 1/2$ and $g = 2$.

The experimental measurement of the relative values of R after making the corrections for geometry and sensitivity were:

$$R_{DPPH} = 3.30 \times 10^{16} \pm 13\%$$

$$R_{O_2} = 3.13 \times 10^{16} \pm 11\%$$

$$R_{MnSO_4} = 2.52 \times 10^{16} \pm 16\%.$$

The high value of R in the case of DPPH is to be expected since it is dubious if very pure samples of DPPH can be obtained; DPPH also disintegrates a few percent per year. Its R value is, however, still within the experimental accuracy. The R values for $MnSO_4$

and O_2 differed by 19% which is within the experimental accuracy. Therefore, it is concluded from this calibration check that molecular oxygen is an excellent calibrating standard for the epr measurement of gas concentrations.

EXPERIMENTAL APPARATUS

The description of the experimental apparatus will be divided into three parts: the gas handling system, the quartz resonant cavity, and the atomic nitrogen source.

Gas Handling System

A diagram of the gas handling system is shown in Figure 5. The apparatus consists of two parts: the main nitrogen flow unit and the foreign gas adding unit. The discharge unit, which dissociates the nitrogen, and the epr unit are also shown in the diagram but they will be described in another section. Each component of the gas handling system will be discussed starting with the supply tank and proceeding in the direction of gas flow.

Gas tanks of either Airco water-pumped nitrogen or Matheson prepurified nitrogen were equipped with pressure regulators to maintain atmospheric pressure in that part of the system up to the needle valve.

The entire flow system was constructed of pyrex from the helium-tested bellows valve at the pressure regulator to the inlet of the smoothing tank except at the following places: brass connectors with neoprene 0 rings were silver-soldered to kovar-to-glass seals at the input of the flowmeter and on the low pressure side of

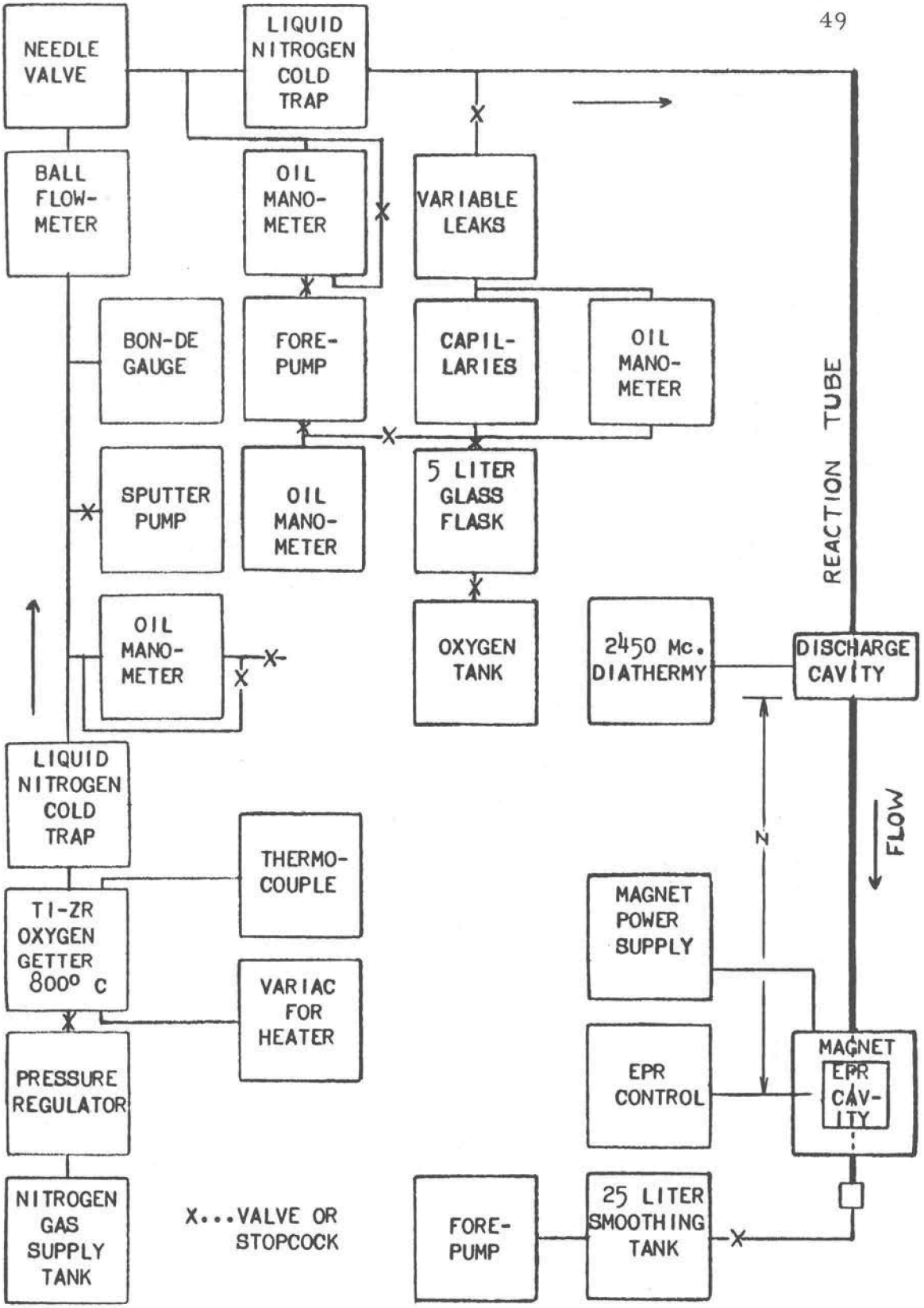

Figure 5. Gas Handling System for Flow Tube

the needle valve; a brass tube with 0 ring seals on each end connected the flowmeter and the needle valve; a brass tube with 0 ring seals on each end connected the bottom of the quartz flow tube to the pyrex tube which led to the stopcock at the stainless steel smoothing tank.

The titanium-zirconium (50-50 alloy) oxygen getter was constructed of 1.8 cm. diameter vycor tubing 18 cm. long and was filled with thin chips of the alloy. To remove oxygen in the gas flowing through the getter, the unit was heated to 800°C by a nichrome wire spiraled around the outside of the vycor tube. The entire unit was insulated by a 3/8 inch layer of micro-quartz, then was surrounded with asbestos tape, and finally was wrapped with an outer layer of aluminum foil. An iron-constantan thermocouple in contact with the vycor tube was used to measure the temperature of the getter.

A standard coaxial pyrex cold trap surrounded by liquid nitrogen was utilized to trap condensable vapors from the flowing gas.

A U-tube manometer filled with Octoil S oil and having one side open to the atmosphere was employed to measure the nearly atmospheric pressure in this part of the system. All manometers used were filled with Octoil S oil which was very effectively outgassed when the system was under vacuum by heating the manometers to about 80°C with a heat gun, and by then stirring the oil with a steel

ball bearing agitated by hand-held magnets.

The entire system from the pressure regulator to the smoothing tank was cleaned by evacuation to about 10^{-6} torr with a sputter pump. The pyrex-enclosed sputter pump was modeled after the one liter per second Varian "Vac-Ion" pump. A "Bon-De" ion gauge was used to calibrate the ion current of the sputter pump in terms of pressure.

The volume flow rate of gas, from 0.1 to 12 cc.$_{STP}$/ second, was determined by a 1/8 inch Matheson sapphire-ball flowmeter which was calibrated by measuring the rate of pressure change with time as nitrogen flowed into a known volume. The calibration was checked by measuring the time of flight of a pulse of the nitrogen afterglow while it flowed a definite distance down the reaction tube. The afterglow pulse was timed either visually or by the use of photomultipliers.

The flow velocity and pressure in the reaction tube were adjusted with an Edward's needle valve and with the stopcocks greased with outgassed Apiezon-N grease. The maximum flow velocity was 1000 cm./second; the pressure was measurable from 0.1 to 40 torr.

A second U-tube oil manometer used to measure the pressure in the part of the flow system from the needle valve to the stopcock at the smoothing tank was followed by another liquid nitrogen cold

trap to remove any condensable vapors originating in the oil manometer or the 0 ring fittings.

The reaction tube illustrated in the diagram in Figure 5 was the vessel in which the gas molecules were dissociated, in which the atoms then recombined, and in which the atom density was measured. Possible materials for this reaction tube must be heat resistant, vacuum tight, have a low wall recombination and a low vapor pressure, and exhibit low dielectric loss at 9 gigacycles per second. Four different types of reaction tubes were tested in an effort to satisfy these criteria. The reaction tubes were: a fused quartz tube, a teflon tube, a quartz tube lined with a thin layer of teflon finish, and a teflon tube inside a fused quartz tube. Initially a standard General Electric fused quartz tube which measured 1.2 meters in length and had an inside diameter of 9 mm. and an outside diameter of 11 mm. was selected. The tube was scrubbed with "Haemo-Sol" laboratory detergent and hot distilled water; then it was etched for 10 minutes in concentrated hydrofluoric acid diluted three to one with distilled water and finally thoroughly rinsed in twice distilled water. Measurements of the wall and volume recombination coefficients were made using this tube; however, it was found to exhibit variable wall recombination. Then a 11.5 mm. O.D. teflon tube with 0.8 mm. walls and a length of 1.2 meters was substituted for the fused quartz tube; however, the teflon tube was immediately

abandoned because it was so porous that large amounts of air diffused through the walls. Visual observations of the afterglow in this teflon tube, however, seemed to indicate a desirably low wall recombination. Efforts were then made to line a quartz tube with Dupont 852-201 clear teflon finish. However, a uniform wall could not be achieved with this lining technique because of the difficulties encountered in applying the teflon uniformly to the inside of a small diameter tube of such length.

Finally a satisfactory combination of the quartz and teflon tubes was achieved by stretching lengthwise and squeezing diametrically the original 11.5 mm. O.D. teflon tube to a proper diameter to allow its insertion inside the original quartz flow tube. Additional data were finally taken using this arrangement.

The presence of a large smoothing tank shown in Figure 5 was found to be necessary to prevent velocity fluctuations in the reaction tube caused by the action of the "Hyvac-7" forepump.

The gas adding unit was attached to the main flow unit so that measurable amounts of foreign gases could be added to the flowing nitrogen. A five liter glass flask, used to store mixtures of nitrogen and oxygen, was followed by a U-tube oil manometer employed to measure the pressure in the flask. The gas flow was determined by measuring the pressure drop across any one of three different sized glass capillaries with a U-tube oil manometer connected

across the capillary system. The capillary system was calibrated by measuring the rate of change of pressure with time as gas flowed into a known volume; the flow rate was measurable from 0.0001 to 0.25 cc.$_{STP}$/second.

The gas flow was varied by changing the gas pressure in the 5 liter flask and by adjusting a system of four all-glass leaks (21).

Quartz Resonant Cavity

In an attempt to measure the volume recombination coefficient of atomic nitrogen in a non-flowing gas, measurements of the atom density were made in a fused quartz chamber which could be sealed off from the atomic nitrogen source. This chamber, coated externally with silver, and lined internally with teflon, formed the resonant cavity of the epr spectrometer, permitting measurement of the nitrogen atom density in the same region in which the atoms were recombining.

A cylindrical quartz chamber was chosen because this shape was the simplest to construct; also the cylindrical geometry exhibits high Q values, significant because the sensitivity of the spectrometer is directly proportional to the Q of the cavity. The TM_{010} mode was chosen for three reasons: 1) Since in the TM_{010} mode the frequency is not a function of the length of the cavity, any length could be used; the length of the cavity was chosen so that it would

nearly fill the epr magnet gap of 2-3/4 inches. 2) In this TM_{010} mode the oscillating magnetic field is azimuthal and hence, at right angles to the axis of the cylinder at all points. Therefore when the axis is lined up with the polarizing magnetic field the oscillating magnetic field is in the proper direction to effect epr transitions at all points. 3) The nine gigacycle magnetic field has constant magnitude over most of the cavity, making saturation less likely.

A silver coating on the chamber was used because of the high electrical conductivity of this metal. The layer of silver had to be thin enough so that the 100 kilocycles per second modulation field would penetrate but thick enough so that the cavity would still have a high Q at nine gigacycles per second. The required thickness of the silver layer was calculated in terms of "skin depth" which is defined as the depth in a conductor at which incident electromagnetic energy is reduced by a factor of $\frac{1}{e}$. A layer of silver 12 skin depths thick at nine gigacycles per second is sufficiently thick to allow only $(\frac{1}{e})^{12}$ or $\frac{1}{160,000}$ of the incident electromagnetic radiation to escape, but this thickness is still only $\frac{1}{30}$ of the skin depth at 100 kilocycles per second. A layer 12 skin depths or 8×10^{-4} cm. was applied to the chamber in about 11 applications by the Brashear chemical process (44, p. 152-157). The amount of silver deposited in each layer was monitored by weighing a reference pyrex sample silvered along with the quartz cavity.

The physical details of the quartz resonant cavity are shown in Figure 6. The cavity was coupled to a waveguide, which connected to the epr spectrometer through a 1/4 inch diameter area on the side of the cylindrical cavity from which the silver was removed. A brass connector with a 1/4 inch diameter hole lined up with the silver-free area on the cylinder, and fit closely around 1/3 of the circumference of the cavity (see Figure 6). An adjustable microwave coupling pin was located on a radius of this hole. The entire brass connector was soldered to the end of a waveguide coming from the epr spectrometer.

The 100 kilocycles per second modulation coils each consisted of 250 turns of #40 single enameled wire wound on composition forms slipped over each end of the cylindrical cavity as shown in Figure 6. The coils were connected in series and were coupled directly to the epr modulation output.

To minimize wall recombination, it was decided to use teflon walls inside the externally silvered chamber. External silvering rather than internal silvering was used because metals have wall recombination coefficients nearly a million times greater than teflon; therefore, even though the silver were nearly completely covered with teflon, a tiny hole in the teflon which exposed a metal surface would result in a large wall recombination. The wall recombination coefficient of quartz is from 10 to 100 times greater than that of teflon; therefore, a small hole which exposed the quartz would not be

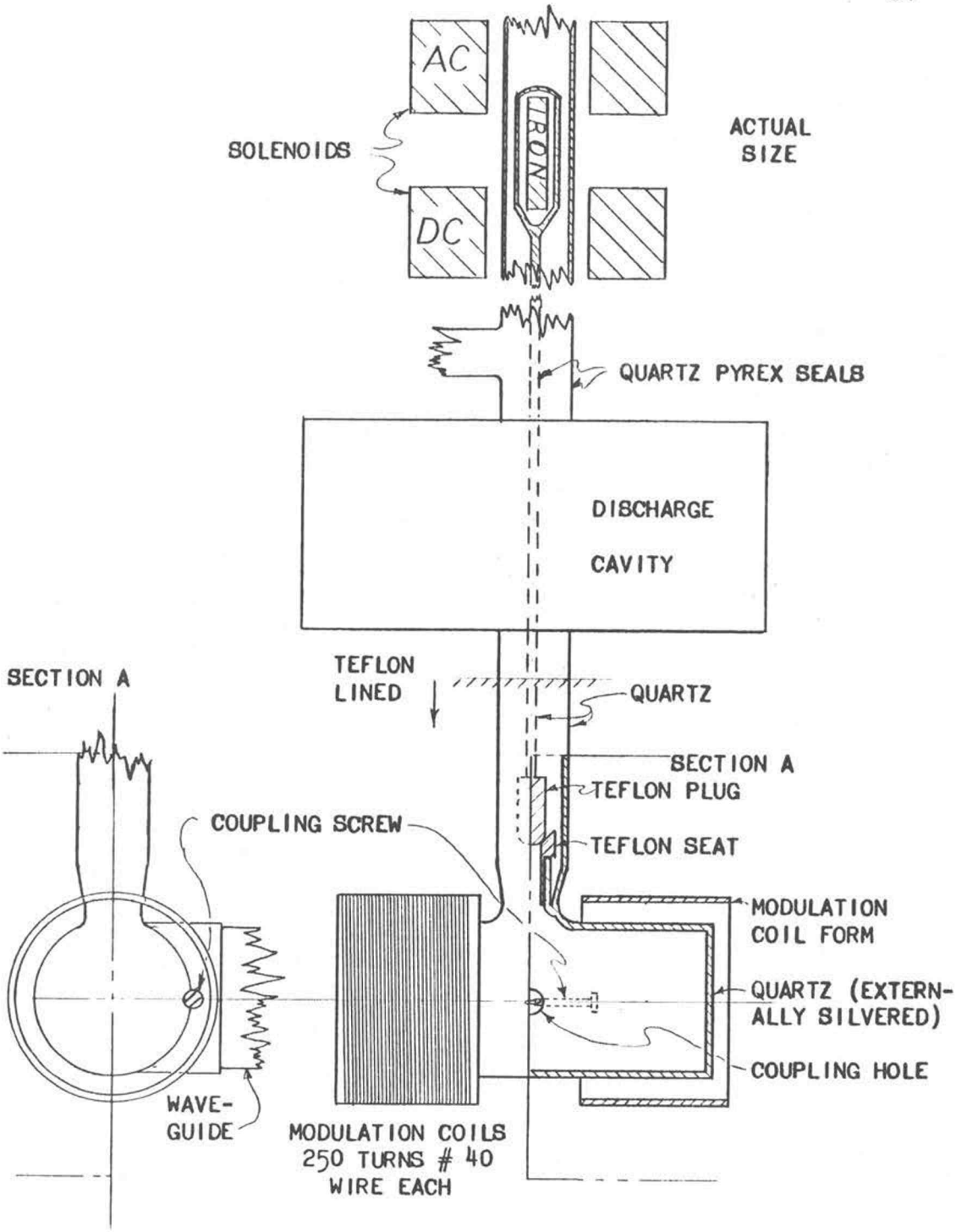

Figure 6. Quartz Cavity

so deleterious.

The cavity was constructed of a fused quartz cylinder with walls approximately one mm. thick, an inside diameter of 22 mm., and an inside length of 55 mm. The ends of the cavity were initially 1.6 mm. thick quartz discs which were fused to the ends of the cylindrical tube and then ground down to one mm. thickness in order to minimize dielectric losses due to the quartz. An eight mm. O.D. quartz tube 12 mm. long was then fused at right angles to the middle of this main cylinder, forming a short side arm. A second quartz tube 11 mm. in outside diameter, fused concentrically outside this arm is shown in Figure 6, and was attached to the gas system above the discharge cavity.

A valve to seal off the cavity from the nitrogen source was located at the end of the small inside arm. This valve consisted of a teflon plug, spherically shaped at its end, which could be raised or lowered into a cone-shaped teflon seat which had been forced into the inner arm extending from the top of the cavity. To assure a tight fit, the plug and seat were lapped together with #1500 aluminum oxide grinding compound. The plug could be raised by activating an ac solenoid whose magnetic field reacted with a pyrex encapsulated iron slug fastened to the teflon plug by a quartz rod. The solenoid was located 60 cm. above the cavity to prevent the interaction of the magnetic field of the solenoid with that of the epr

magnet. To close the valve, the ac solenoid was deactivated and to achieve a tight seal, a dc solenoid was used to create a downward force on the valve.

Starting at 6 cm. above the quartz chamber, the entire resonant cavity system was lined with two thin coats of Dupont 852-201 clear teflon finish.

The resonant frequency of 9,062 megacycles per second and the Q of 6,300 of the quartz resonant cavity were measured with the aid of a Hewlet Packard cavity wavemeter. The Q of the Varian V-4531 rectangular TM_{012} resonant cavity, which is standard equipment with the Varian epr spectrometer used, was 3,900 with the quartz flow tube in place. Therefore the specially constructed quartz cavity afforded a considerable gain in sensitivity. An additional increase in sensitivity was achieved with the quartz cavity because the gas sample filled its entire volume while at best only 1/3 of the volume of the Varian cavity could be filled.

The quartz cavity was positioned in the center of the polarizing magnet with its axis parallel to the polarizing magnetic field. The changes made in the gas handling system by attaching the quartz cavity are shown in Figure 7. An additional titanium-zirconium oxygen getter was added to prevent the back diffusion of oxygen from the forepump. An aluminum oxide trap kept the forepump vapors from back diffusing into the cavity system.

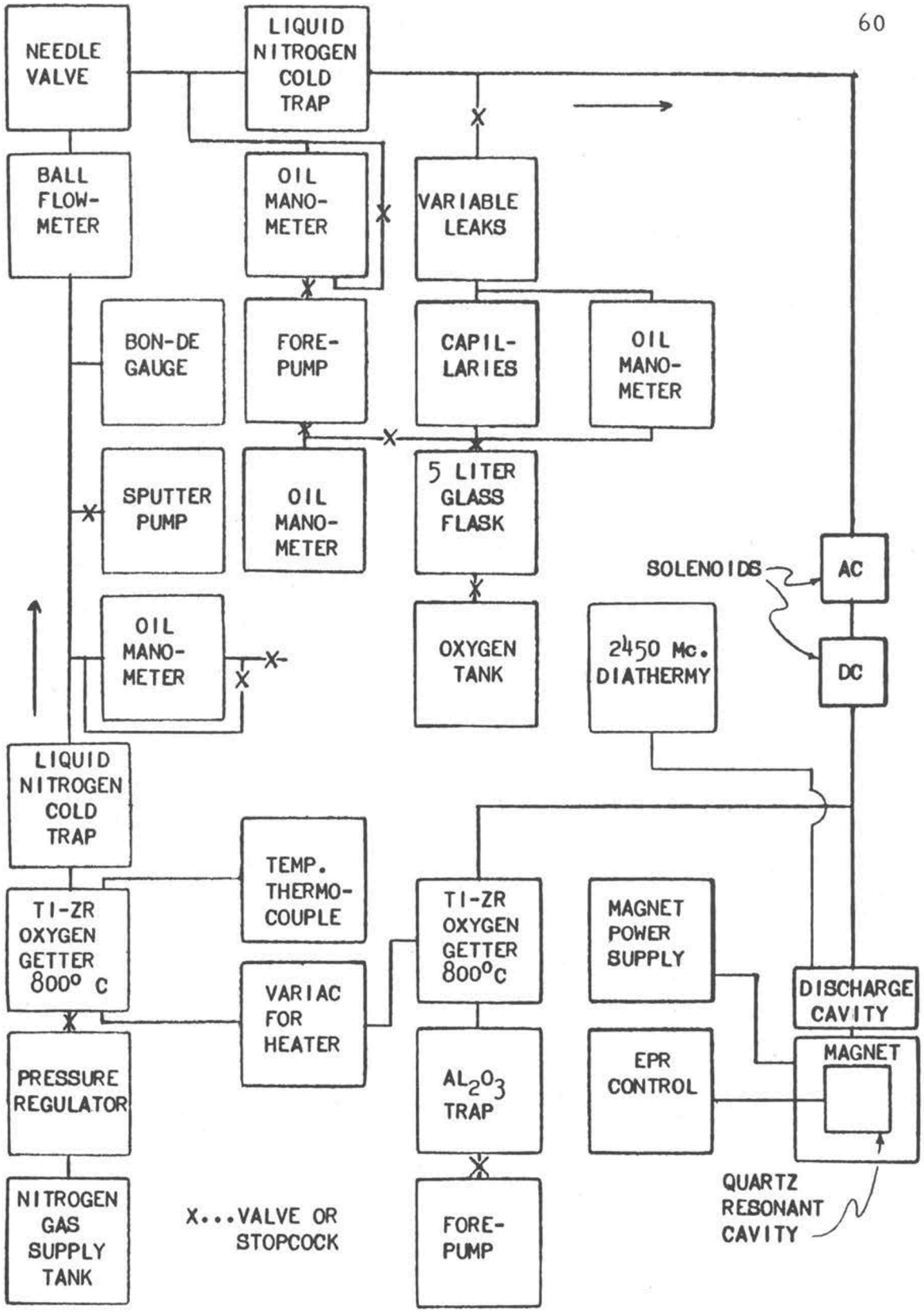

Figure 7. Gas Handling System for Quartz Cavity

Atomic nitrogen, formed within the 11 mm. quartz arm of the cavity by a 2,450 megacycles per second electrical discharge situated 7.5 cm. above the quartz chamber, traveled to the quartz chamber by diffusion. When a constant concentration of atomic nitrogen atoms was reached in the cavity, the valve was closed, and the decay of the atomic nitrogen signal was continuously monitored by the epr spectrometer.

Atomic Nitrogen Source

A high frequency 2,450 megacycles per second discharge was employed to dissociate the molecular nitrogen in all experiments. A Burdick medical diathermy unit with an output adjustable from 0 to 100 watts was the source of the high frequency energy. A specially constructed, quarter-wavelength, cylindrical, coaxial cavity connected to the diathermy was used to maintain the discharge in the flow tube located coaxially in the center of this discharge cavity. The discharge cavity was constructed of brass and measured three inches in diameter and one inch in length. Its tunable, hollow, center electrode was 3/4 inch long with a 3/4 inch O.D. and a 1/2 inch I.D.

The discharge cavity could be slid along the reaction tube to vary the distance, z, between the discharge and the epr cavity where the atomic nitrogen density was measured (see Figure 5).

The electric fields in the discharge cavity were sufficiently high to initiate the discharge from about 0.1 torr to 15 torr and to maintain the discharge from below 0.1 torr to above 80 torr.

RESULTS AND DISCUSSION

Using the apparatus and procedures described in the previous chapters, the following experiments were performed: epr spectra and line widths and shapes for atomic hydrogen, atomic nitrogen, atomic oxygen, molecular oxygen, and nitrogen dioxide were observed; the wall and volume recombination coefficients of atomic nitrogen were measured as a function of oxygen added to molecular nitrogen flowing in a quartz tube; and the wall and volume recombination coefficients of atomic nitrogen were measured in a quartz flow tube plus teflon liner and in a sealed quartz cavity.

Epr Spectra of Gases

The epr spectra of atomic hydrogen, atomic nitrogen, atomic oxygen, molecular oxygen, and nitrogen dioxide were observed primarily to become familiar with the operation of the epr spectrometer and to investigate its use as an atom concentration measuring tool. All of the spectra were taken with the use of the Varian epr spectrometer equipped with the Varian resonance cavity, with the exception of the molecular oxygen spectrum and one atomic nitrogen line which were taken using the Varian epr spectrometer with the quartz cavity. The Varian cavity with the 11mm. quartz tube inserted resonates at 9,160 megacycles per second, and the quartz cavity at 9,060 megacycles

per second. The 100 kilocycles per second modulation unit was employed for all experiments unless otherwise mentioned. The epr spectrum of each of the gases will be illustrated along with the shapes and widths of some of the epr spectral lines. The three atomic gases, atomic hydrogen, atomic nitrogen, and atomic oxygen, are unstable and were produced by an electrical discharge.

Atomic hydrogen. The observed atomic hydrogen epr spectrum was found to be identical with that observed by Beringer and Castle (6) who first described it in 1954. The spectrum of atomic hydrogen in its ground state, $^2S_{1/2}$, is shown in Figure 8 and consists of two identical lines resulting from the coupling between the nuclear magnetic moment and the electronic magnetic moment. The line at 3,000 gauss is due to the $M_J = \frac{1}{2} \rightarrow -\frac{1}{2}$, $M_I = +\frac{1}{2}$ transition, while at 3,500 gauss the line is due to the $M_J = \frac{1}{2} \rightarrow -\frac{1}{2}$, $M_I = -\frac{1}{2}$ transition. The widths of the lines, which were found to vary linearly with atomic hydrogen concentration, were approximately independent of molecular hydrogen concentration. These observations were in agreement with those of Hildebrandt, Booth, and Barth (19). The shape of each line was Lorenzian as predicted for collision-broadened lines (22, p. 72-73).

Atomic nitrogen. In the case of atomic nitrogen the coupling between the electronic magnetic moment and the nuclear magnetic moment is much smaller than in the case of hydrogen, producing

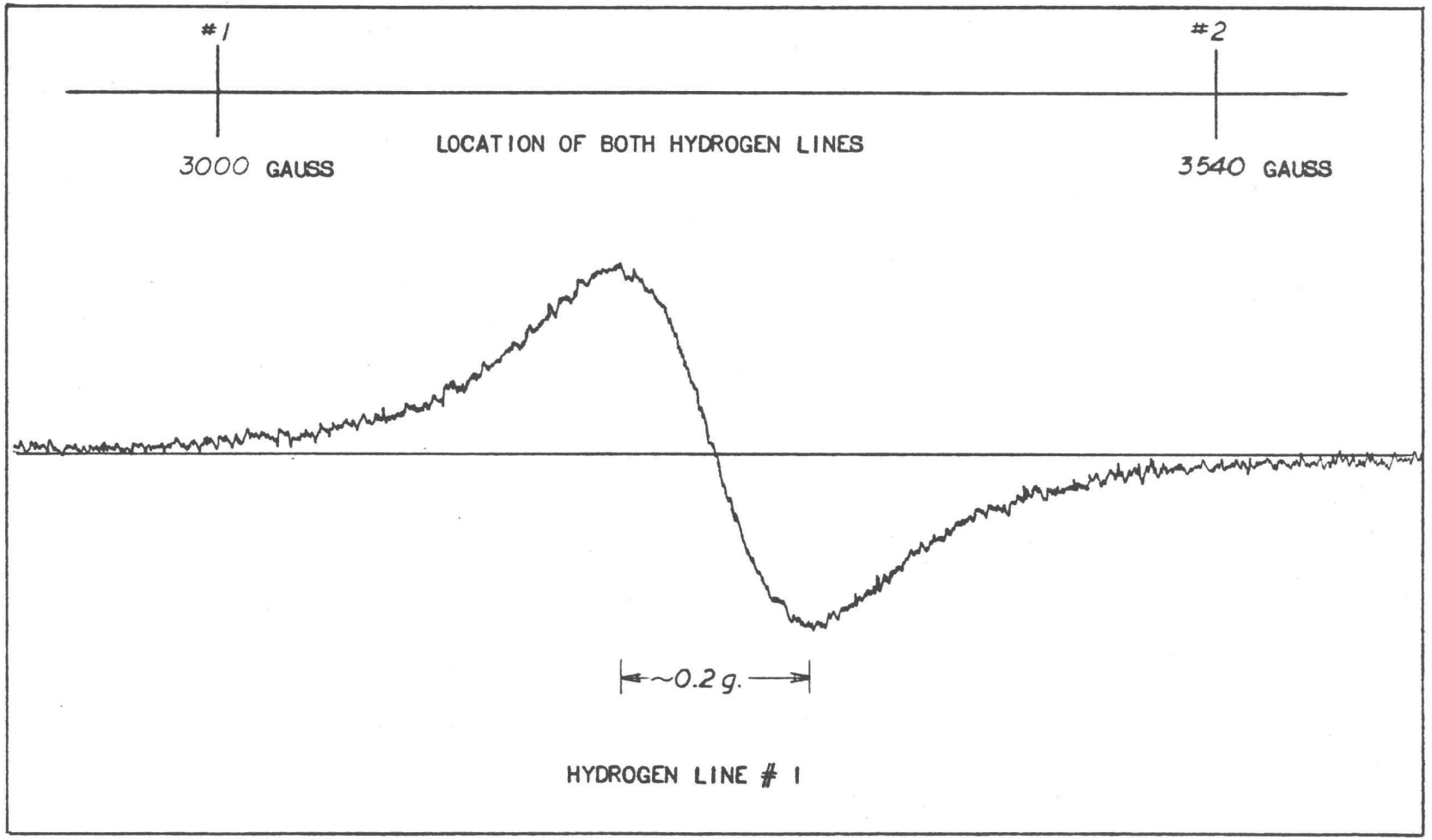

Figure 8. Epr Spectrum and Line Shape of Atomic Hydrogen

three closely-spaced hyperfine lines of equal intensity as shown in Figure 9. The energy level diagram describing this transition was shown in Figure 3. The double-lined spectrum of N^{15} was also observed, however this spectrum is not reproduced here. In the present experiments when the atomic nitrogen spectrum was first observed, the signals were found to increase with a decrease in microwave power, indicating a high degree of saturation at this initial power level of about 10 milliwatts in the sample cavity. The derivation of the calibration equation (3- 16) is valid only if saturation of the sample is not occurring. Saturation occurs when the electromagnetic radiation is inducing transitions between states at such a high rate that the population density of atoms in these states is sufficiently altered so that the difference in population between these states is no longer given by the usual Boltzmann factor $e^{-\Delta E/kT}$. When saturation occurs, the power absorbed will no longer be proportional to H_1; therefore, to check on the saturation of a sample one need only plot the signal height of the substance versus relative values of H_1. The signal height of a substance such as DPPH, which does not saturate at the values of H_1 used in all experiments reported here, is proportional to H_1. Therefore the signal height from the possibly saturated sample was plotted versus the signal height for DPPH. The values of H_1 for which the sample was undergoing negligible saturation were those at which the signal height

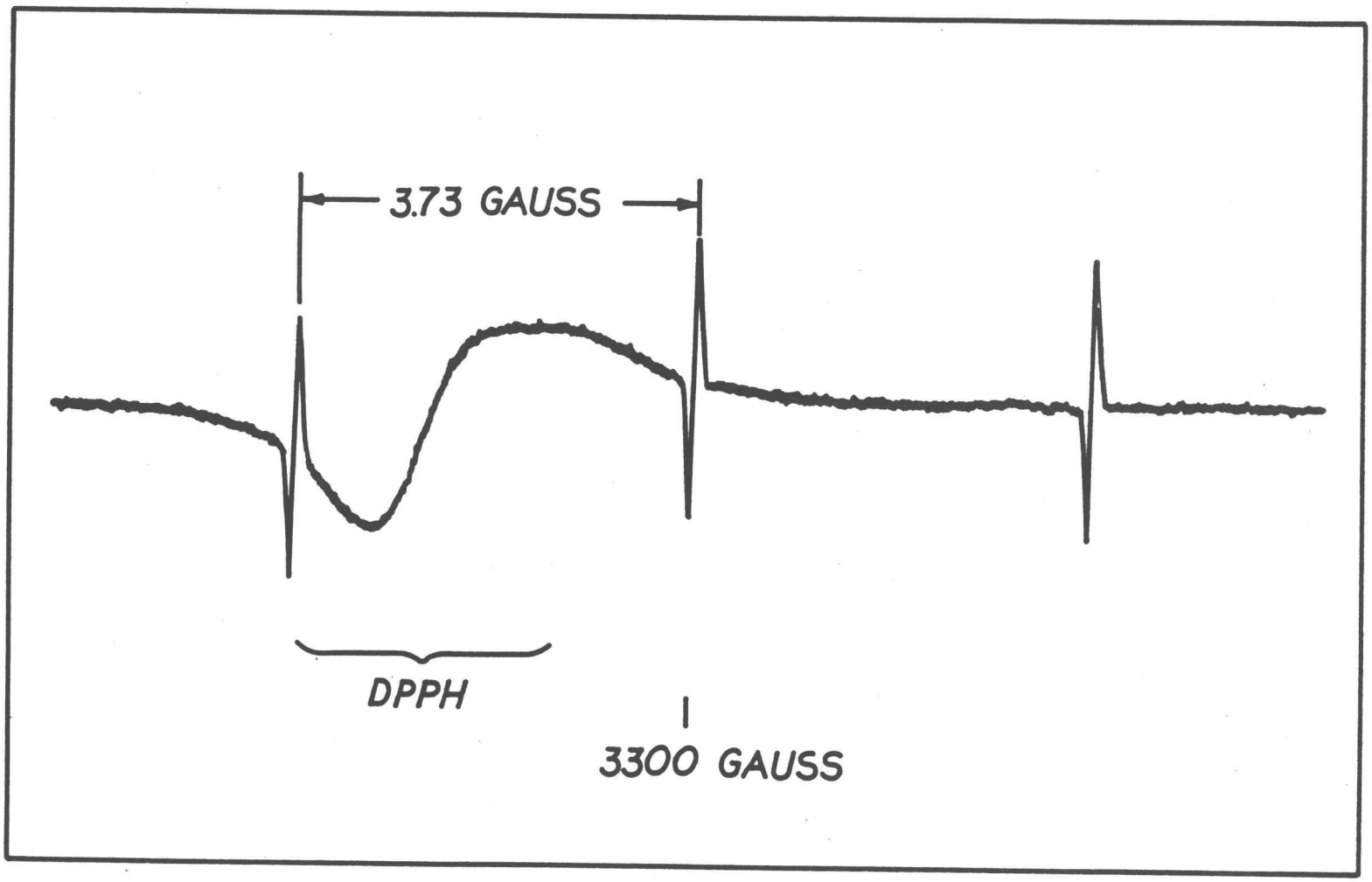

Figure 9. Epr Spectrum of Atomic Nitrogen

from the sample was directly proportional to the DPPH signal height as is shown in Figure 10. The atomic nitrogen spectrum was thereafter always taken in the non-saturated condition.

Two traces of an individual nitrogen line are presented in Figure 11; the top trace represents an atomic nitrogen line observed by the use of modulation at 400 cycles per second while the lower trace exhibits the result for 100 kilocycles per second modulation. The modulation amplitudes were in the range from about one-fourth to one-tenth of the line width for each case. A comparison of the shape of either of these atomic nitrogen lines with the nearly Lorenzian shape of the atomic hydrogen line shown in Figure 8 reveals little similarity.

The widths of the two atomic nitrogen traces were 80 milligauss for 100 kilocycles per second modulation and 49 milligauss for 400 cycles per second modulation. A study of the details of the shape obtained utilizing 100 kilocycles per second modulation led to the conclusion that the line was distorted due to effects connected with the comparable magnitudes of modulation period and spin relaxation time. The width and shape of the line taken at 400 cycles per second modulation were found to be almost unchanged by any of the following factors which are known to affect line widths and shapes (22, p. 71): increase of the overall pressure, increase in the concentration of atomic nitrogen, reduction in the microwave power, and

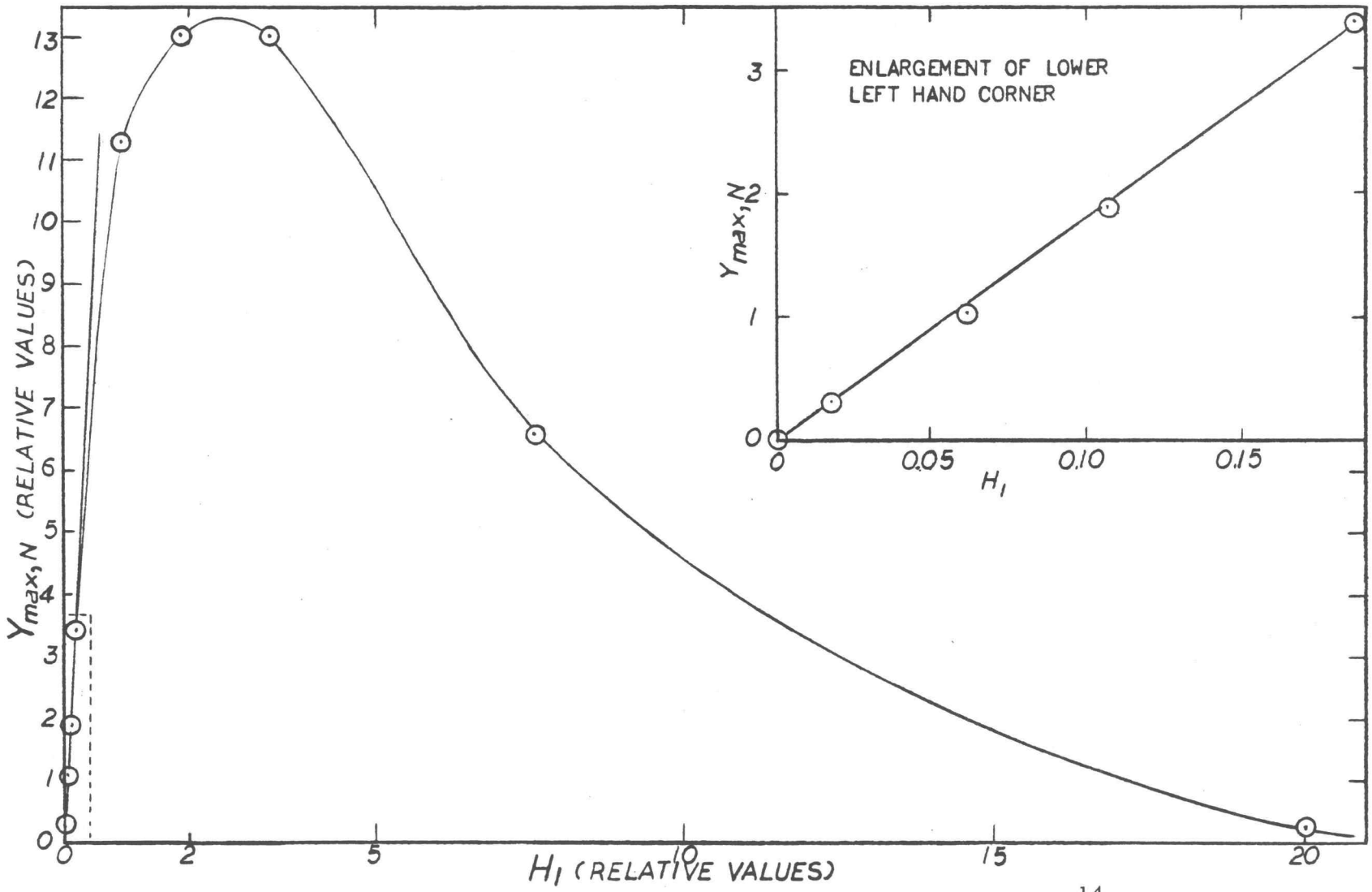

Figure 10. Saturation Curve for a Nitrogen Concentration of 5×10^{14} atoms/cc.

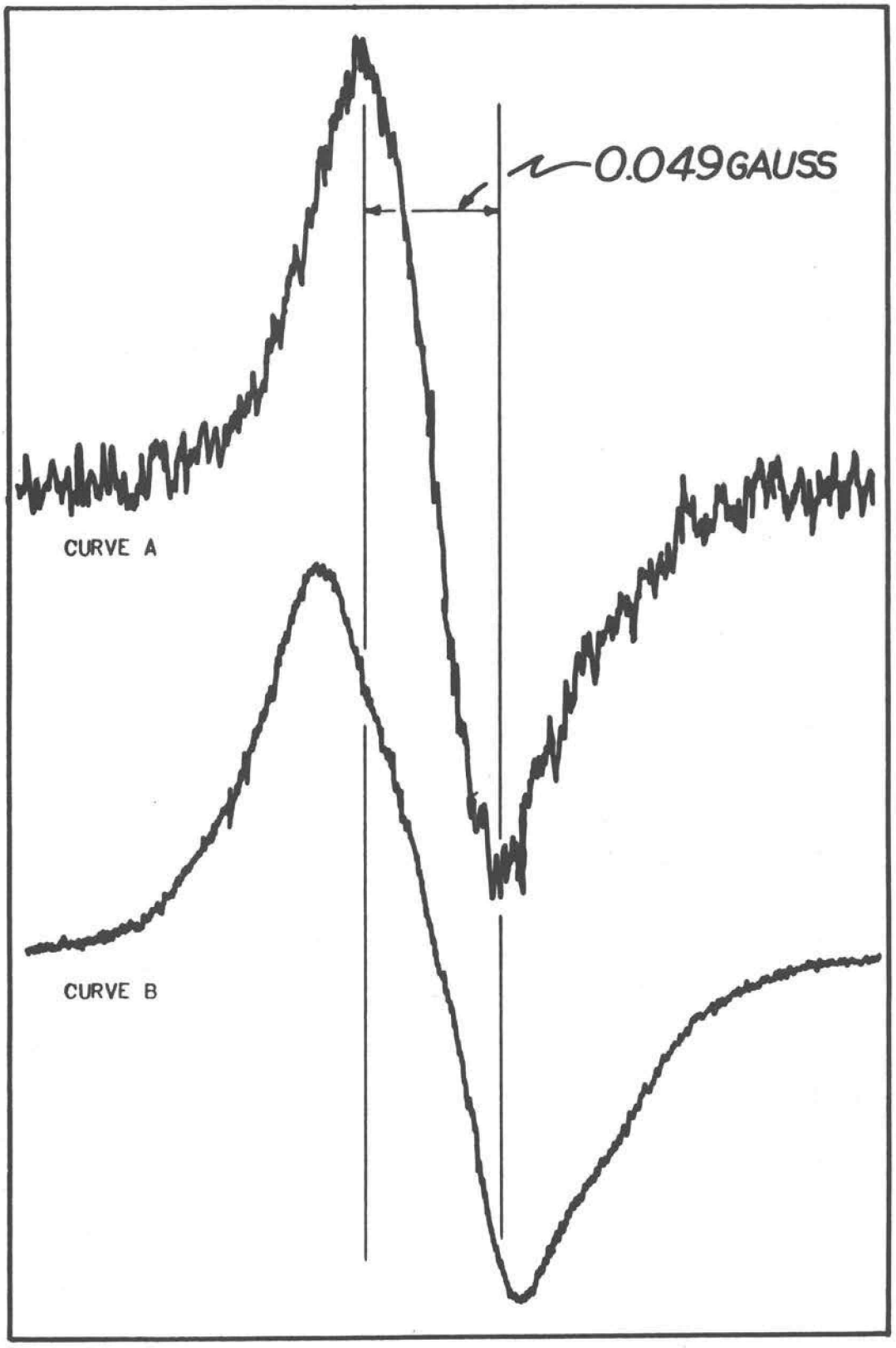

Figure 11. Atomic Nitrogen Epr Line Shape: Curve A, 400 cps. Modulation, Curve B, 100 kc. Modulation

decrease of the modulation amplitude. The width and shape of the epr line were found, however, to vary greatly with the positioning of the sample in the magnetic field; the observed shape of this line was therefore assumed to be due to the inhomogeneity of the magnetic field. A very careful measurement of the width of the atomic nitrogen line, taken at 100 kilocycles per second modulation in the Varian cavity, as the nitrogen atom concentration was increased by a factor of 25 (covering the entire range of concentrations observed in the experiments), revealed a change in width of less than 6%. In measuring concentrations of atomic nitrogen this constancy of the shape of the epr line is very useful, as can be noted from the following considerations:

$$\begin{array}{ll} \text{since (as shown by Equation (3-24))} & n \propto \int Y(\Delta x)\, dx, \\ \text{then, if the shape is constant so that} & \\ \quad Y = (Y_{max})(\text{f of } \Delta x), & n \propto Y_{max.}; \end{array} \qquad (4\text{-}1)$$

therefore, it was necessary to perform the time consuming evaluation of $\int Y(\Delta x)\, dx$ only once to obtain the proportionality factor between the atom density and the signal height.

Since the gas sample in the quartz resonant cavity occupied a much larger volume than the space occupied by the gas sample in the Varian cavity, one would expect a much greater inhomogeneity in the magnetic field with the use of this cavity. The atomic nitrogen signal obtained from the use of the quartz cavity is shown in Figure 12; the effect of the increased inhomogeneities has, indeed,

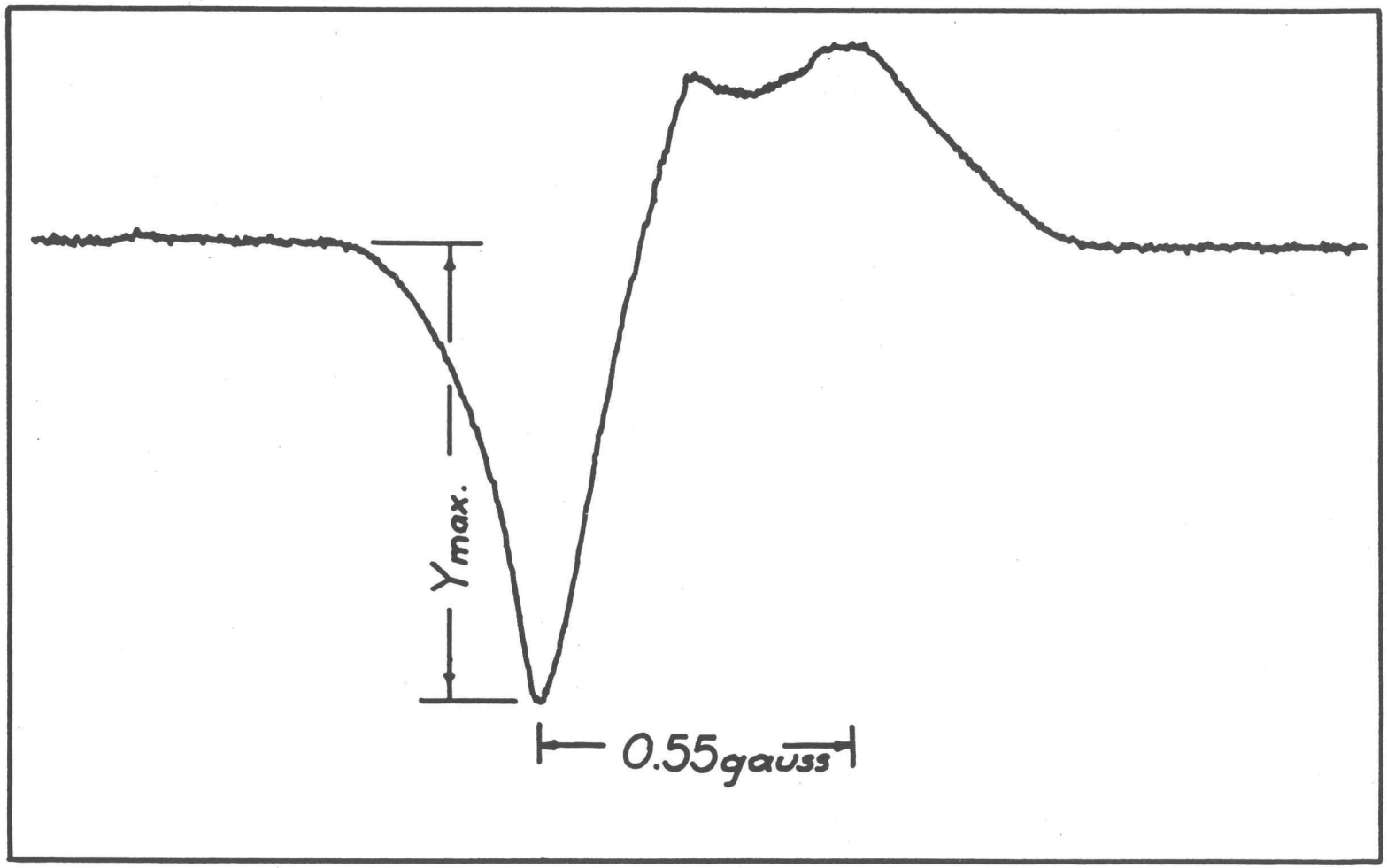

Figure 12. Atomic Nitrogen Epr Line Shape with Quartz Cavity

become very pronounced in this distorted and broadened line.

The increased signal width obtained in the quartz resonant cavity results in a corresponding decrease in signal height and hence a decrease in signal-to-noise ratio. However, this decrease was more than compensated for in the quartz cavity by three factors: 1) The Q in this quartz cavity was higher than in the Varian cavity. 2) The entire volume of the cavity was filled with sample while only about one-third of the Varian cavity was filled. 3) A 10 decibels increase in the microwave power level above that used in the Varian cavity was possible because saturation effects were decreased by the nearly uniform configuration of magnetic energy in this mode, and by the larger volume, both of which resulted in a maximum magnetic energy density less than that in the Varian cavity when both cavities were operated at the same microwave power levels.

Atomic oxygen. Atomic oxygen O^{16} has a $^3P_2$ ground state with $^3P_1$ and $^3P_0$ states lying a few hundredths of an electron volt above the ground state. O^{16} has no nuclear magnetic moment and hence no hyperfine splitting. The spectrum shown in Figure 13 exhibits 6 lines, one for each $\Delta M_J = \pm 1$ transition. The separation of these lines is due to a quadratic magnetic field displacement by the field of 4,400 gauss acting on the ^3P states (41). The widths of the atomic oxygen lines were much broader than those of atomic hydrogen or atomic nitrogen, and varied approximately

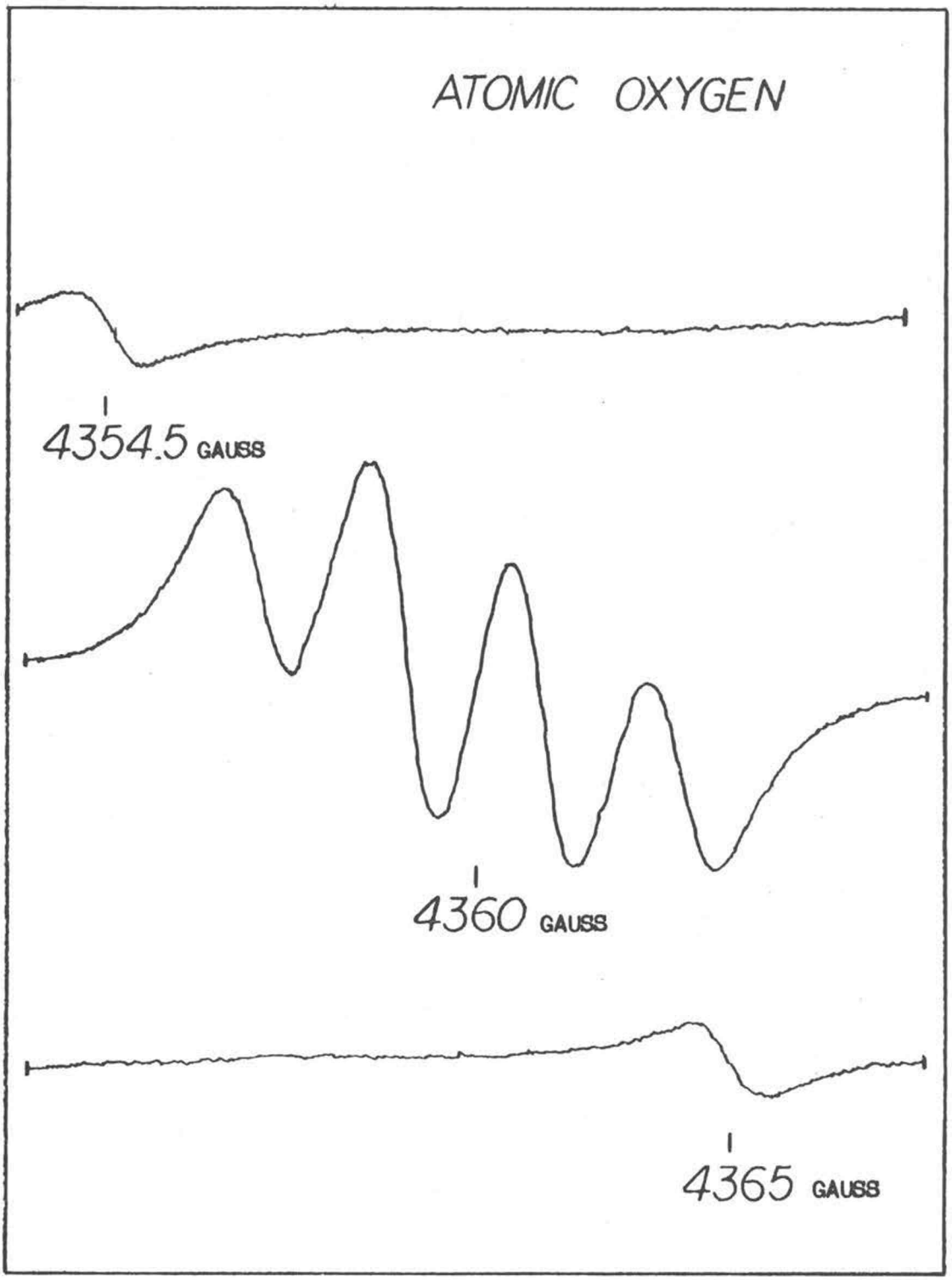

Figure 13. Atomic Oxygen Epr Spectrum

linearly with total pressure.

Molecular oxygen. The epr spectra of molecules are much more complex than those of atoms as can be seen from Figures 14 and 15. A total of 110 lines of molecular oxygen were observed between 1,850 and 6,100 gauss. The spectra were taken with the use of the quartz resonant cavity for which the sensitivity was about a factor of 5 greater than that of the Varian cavity. The number of lines observed in magnetic fields ranging from 1,850 to 6,100 gauss by other workers were 10 (6) and 48 (47, p. 958-959); thus a considerable increase in overall sensitivity was achieved in our measurements.

The molecular oxygen line used in calibrating the epr spectrometer is marked in Figure 14 and shown in greater detail in Figure 16. The asymmetry in this line is caused by the magnetic field inhomogeneity. The line widths were found to vary linearly with pressure at pressures which produced line widths greater than the inhomogeneity of the field. The line widths were about 10 gauss at a pressure of 7 torr.

Nitrogen dioxide. The epr spectrum of nitrogen dioxide is shown in Figure 17. Currently the theory of triatomic molecules is insufficiently advanced to explain this spectrum with a thoroughness comparable to the theory of the epr spectrum of molecular oxygen; however, it is known that the nitrogen dioxide epr spectrum

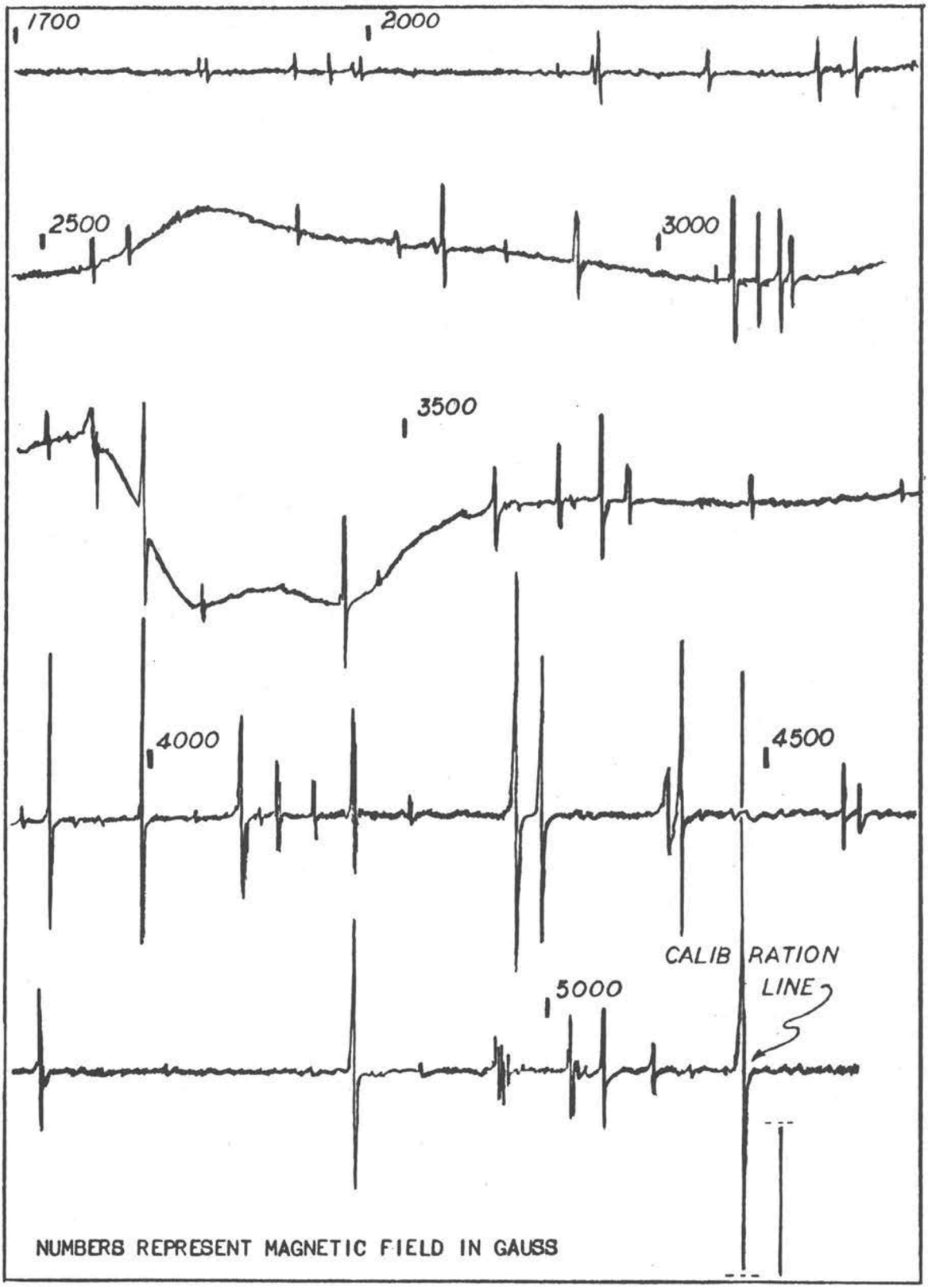

Figure 14. Molecular Oxygen Epr Spectrum, Part I

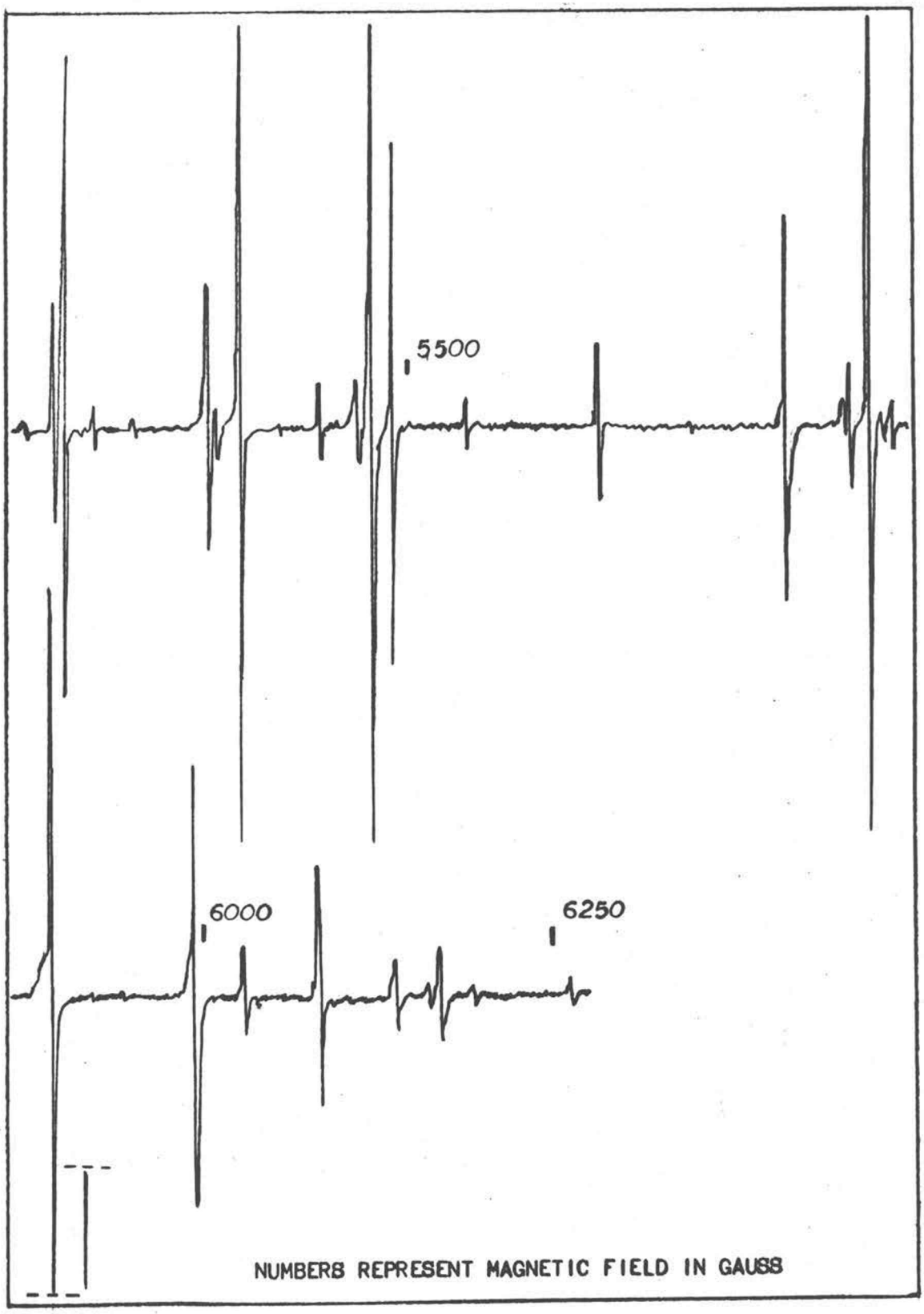

Figure 15. Molecular Oxygen Epr Spectrum, Part 2

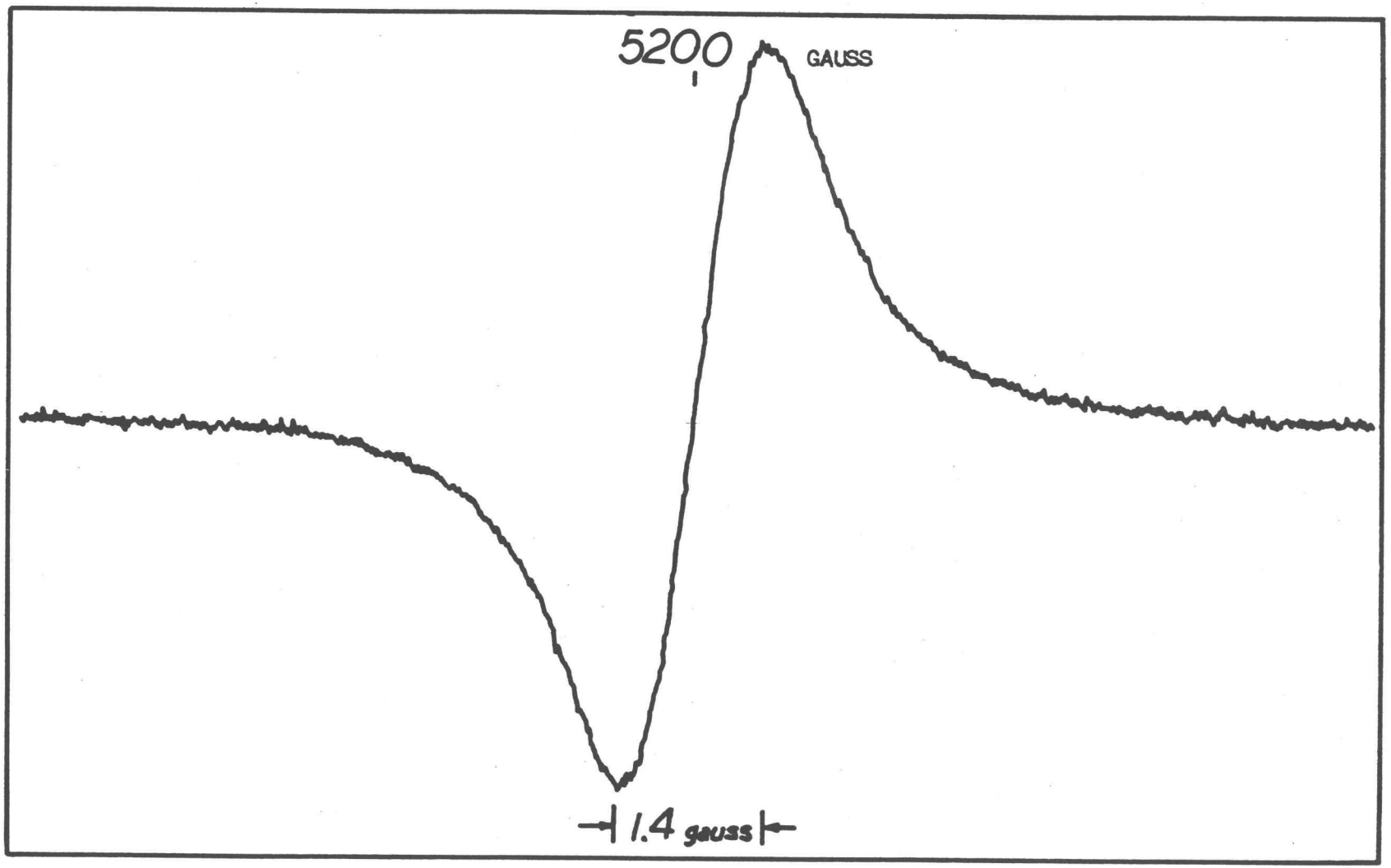

Figure 16. Molecular Oxygen Calibration Line

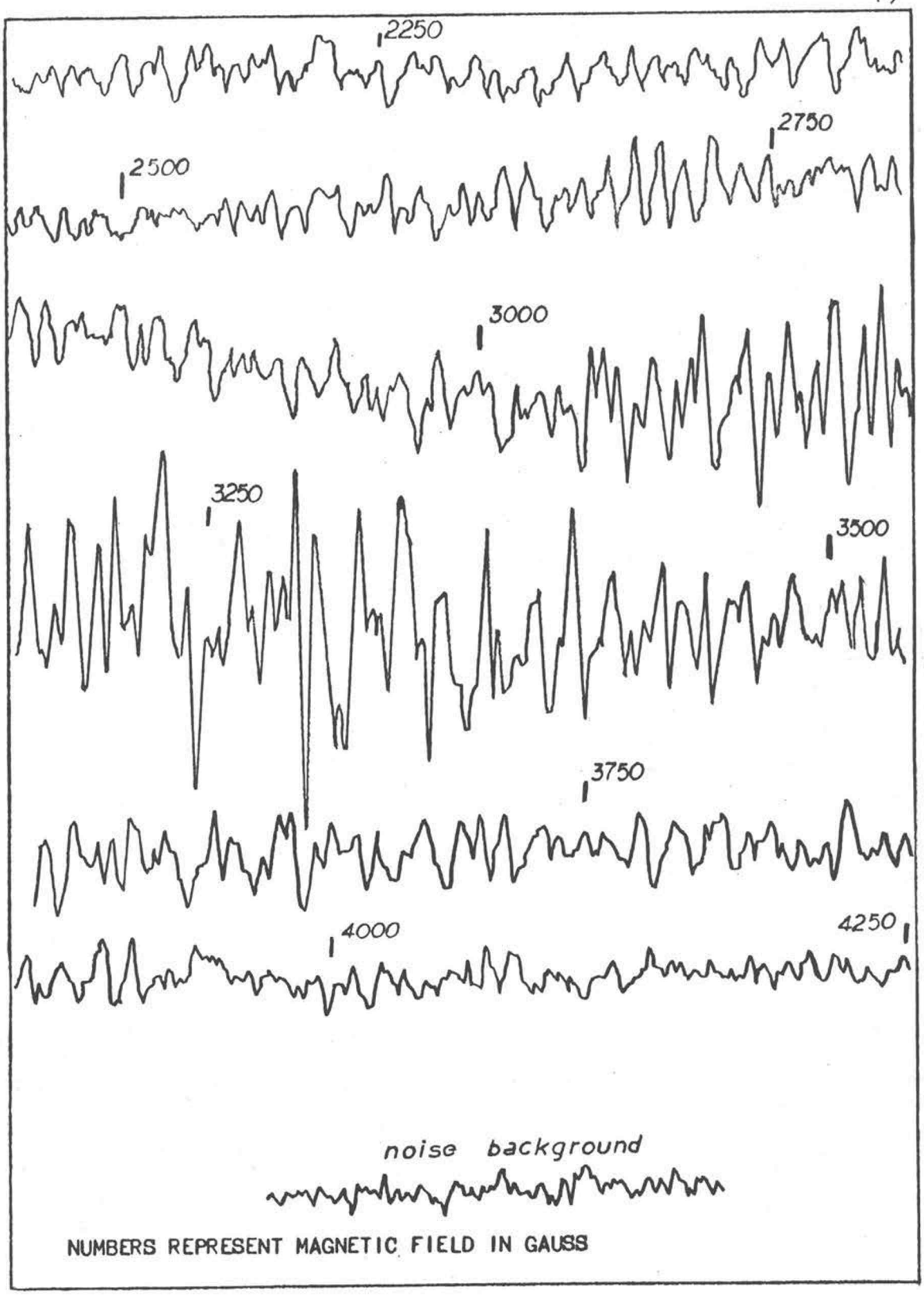

Figure 17. Nitrogen Dioxide Epr Spectrum

is due to a nearly free magnetic moment of its odd electron coupled to the nuclear spin of N^{14}. This coupling produces three main sets of lines which are further split by the rotational levels. The spectrum of nitrogen dioxide was found to be composed of about 125 lines while 17 lines were previously observed by Castle and Beringer (12). If the more sensitive quartz cavity and a lower pressure (which decreases the line width and hence increases the resolution) had been used, a spectrum of even greater complexity would probably have been observed.

The five gases observed with the use of the epr spectrometer have shown increasingly complicated spectra, from the rather simple cases of atomic hydrogen and atomic nitrogen, to the somewhat more complex spectrum of atomic oxygen, to the detailed spectrum of molecular oxygen and the complicated and poorly understood spectrum of nitrogen dioxide.

The Recombination of Atomic Nitrogen Measured in a Quartz Flow Tube

Qualitative measurements. Several preliminary measurements of the three-body volume recombination coefficient of atomic nitrogen were performed using the quartz flow tube and Airco water-pumped nitrogen which was analyzed by means of a mass spectrograph and found to contain as impurities 0.65% molecular oxygen, 0.04% argon, and 0.02% hydrogen, and negligible water and

hydrocarbons. These volume recombination measurements were reproducible from day to day and the atomic nitrogen epr signal was constant after about one minute each time the discharge cavity was moved to a new location on the flow tube. Flow velocities of several hundred centimeters per second and pressures between 5 and 10 torr were utilized to obtain values of about 1×10^{-32} cc.^{2} sec.$^{-1}$ for k_1.

After successful initial experiments, the flow system was cleansed by evacuation to about 10^{-6} torr and Matheson prepurified nitrogen, passed through the hot titanium-zirconium oxygen getter to remove oxygen impurities, was substituted for the Airco nitrogen. The nitrogen which passed through the getter was termed "extra pure" nitrogen. The same pressures and velocities were used with this "extra pure" nitrogen as with the Airco nitrogen. Mass spectrographic analysis of the prepurified nitrogen (directly from the tank) before and after it flowed through the oxygen getter yielded the following concentrations of impurities, respectively: molecular oxygen, 20 ppm. and less than 10 ppm. (10 ppm was the minimum detectable concentration); argon, 0.02% and 0.02; hydrogen, 0.04% and 0.02%; and negligible amounts of other impurities.

An atomic nitrogen signal comparable with those observed with the use of Airco nitrogen was observed when the discharge, positioned at the top of the flow tube, was first ignited. However, it was found to have completely disappeared after 12 hours; the

afterglow was also greatly diminished. The flow tube was removed, cleansed with hydrofluoric acid, rinsed in distilled water, remounted, and re-evacuated; however, the same results were again observed. With the tube in this condition extinguishing the discharge for 5 or 10 minutes did not result in a return of the nitrogen signal; however, twenty-four hours later, during which time the system was at fore-pump pressure, the initial ignition of the discharge produced a signal as strong as before with the afterglow again as bright. The signal and afterglow were again found to be gradually decreasing in intensity. Moving the discharge cavity down the flow tube to a position which had not yet been "discharged" greatly enhanced the afterglow and the nitrogen signal. When the cavity was returned to the original position, however, the nitrogen signal and the afterglow had diminished in comparison with their prior intensities. The movement of the ignited discharge cavity down the entire flow tube in about five minutes and then its placement back to the original position at the top of the flow tube resulted in the complete loss of the nitrogen signal and a greatly diminished afterglow. The process of moving the discharge up and down the flow tube to produce a stable situation was called conditioning the walls with the discharge.

Qualitative observations were then made to determine the effects of adding various gaseous impurities up to about 10% to the flowing nitrogen prior to its passage through the discharge region.

These observations are summarized below.

1) Water vapor. Water vapor resulting from the evaporation of water in a small flask was cleansed of dissolved gases by evacuation until about 50% of the water remained. The use of this "pure" water vapor produced no increase in the nitrogen signal and afterglow intensity.

2) Molecular oxygen. A very large increase in the atomic nitrogen concentration was noted upon the addition of a few parts per million oxygen to the flowing nitrogen. The addition of about one percent of oxygen caused the afterglow to become bluish; however, the atomic nitrogen signal continued to increase up to about 1.5% of added oxygen. The addition of still more oxygen decreased the nitrogen signal, and the afterglow became bright green, quite different from the usual yellow-green color. These color changes have been previously reported by Kaufman (27) as due to the reactions of NO. The addition of molecular oxygen directly to the afterglow by means of a special tube produced very little change in the afterglow or the signal, thus indicating that the oxygen effect was dependent upon its passage through the discharge region.

3) Water vapor plus molecular oxygen. The addition of this combination produced the same effect as molecular

oxygen alone.

4) Helium or argon. A very slight increase in the atomic nitrogen signal and the afterglow intensity was noted upon the addition of either of these two gases.

5) Molecular hydrogen. The addition of hydrogen produced a violet color in the discharge and decreased the atomic nitrogen signal.

6) Nitrogen dioxide, nitric oxide, or nitrous oxide. Each of these gases when added to the flowing nitrogen produced the same general effect as the addition of molecular oxygen.

7) Carbon dioxide. This gas also produced the same effect as that of oxygen.

8) Ammonia. The afterglow disappeared but the nitrogen signal increased slightly for small additions of ammonia to the flowing nitrogen.

From these observations it was concluded that all gases added which contained oxygen in their molecules, except water vapor, increased the nitrogen signal and the afterglow intensity. Of these gases tested which produced this effect, molecular oxygen is the most likely impurity found in commercial nitrogen gas; it was,for this reason,decided to measure and observe the quantitative effects due to the addition of only molecular oxygen as an impurity.

Observations were made on the effects of the addition of about 0.3 ppm. of oxygen to the flowing nitrogen before it entered the discharge cavity when the latter was located at the top of the flow tube. The afterglow front was seen to gradually extend down the flow tube and to reach the epr cavity 80 cm. away in about one-half hour, at which time, the atomic nitrogen signal rapidly increased to a constant level. The discharge was then extinguished for one-half hour while the gas mixture was allowed to flow continuously; upon re-ignition of the discharge the afterglow and the signal were only slightly decreased, apparently indicating that the effects of this wall conditioning did not rapidly disappear. Increasingly larger percentages of added oxygen resulted in correspondingly faster movements of the afterglow front down the tube; with 1% oxygen the flow almost instantaneously filled the entire flow tube.

The foregoing observations may be explained as follows (although other more complicated explanations are also possible).

1) The increase of the nitrogen signal and afterglow intensity are associated with the addition of some substance, resulting from the discharged oxygen-nitrogen mixture, which forms on the walls of the vessel.

2) This substance was adsorbed on the walls at a considerably higher rate from the discharged oxygen-nitrogen mixture than from either molecular oxygen or air.

3) Possibly the detachment of this substance from the walls into the discharge volume enhanced the formation of atomic nitrogen as was indicated by the immediately brighter afterglow when the discharge cavity was moved to a fresh section of the flow tube.

4) Since the unknown substance remains on the walls in the absence of the discharge for periods of more than one-half hour, it is apparently a relatively stable material.

These observations, agreeing with those of Lord Rayleigh (42, p. 123-139), seem to indicate a greatly decreased wall recombination when slight amounts of oxygen are present.

Quantitative measurements of oxygen's possible effect upon the atomic nitrogen recombination rates. Quantitative measurements were made to determine any possible effects of added oxygen upon the three-body volume and wall recombination coefficients of atomic nitrogen. The three-body volume recombination coefficient k_1 in a flowing gas was obtained from the linear sections of graphs of $1/n$ versus $\frac{z[M]}{\bar{v}}$. The previously derived expression (2-14) relating k_1 to the parameters in a flowing gas with k_2, k_3, and k_4 equal to zero is:

$$\frac{\Delta\left(\frac{1}{n}\right)}{\Delta\left(\frac{z[M]}{\bar{v}}\right)} = k_1 \qquad (4-2)$$

The quantity $\frac{\Delta\left(\frac{1}{n}\right)}{\Delta\frac{z[M]}{\bar{v}}}$ is the straight line slope of the reciprocal

of the atomic nitrogen concentration n (number of atoms per cc.) determined on the epr spectrometer plotted against the distance z (cm.) between the discharge and the epr cavity times the third body concentration [M] (#/cc.) divided by the velocity of the gas. [M] was nearly equal to the pressure in the flow tube since the atomic species was less than 1% of the total gas concentration. The velocity $\bar{v}$ (cm./sec.) of gas at pressure P_2 in the flow tube of cross-sectional area A was determined by measuring the quantity W (cc./sec.) of gas at pressure P_1 flowing through the flowmeter. Since the quantity of gas flowing through the flow tube must equal the quantity of gas through the flowmeter in the same time interval, and assuming constant temperature, then

$$\bar{v} A P_2 = W P_1 \tag{4-3}$$

or

$$v = \frac{WP_1}{AP_2} \tag{4-4}$$

The slope of the graph obtained using these mentioned values will yield the value of k_1 in units of $cc.^2 sec.^{-1}$. Atom concentrations used in determining recombination coefficients were taken at several distances, z, between the discharge, and the epr cavity, the discharge cavity always being moved towards the epr cavity to eliminate effects due to the heating and conditioning of the quartz tube by the discharge. The discharge cavity was generally moved about 3 to 7 cm. before each measurement and the atomic nitrogen signal

was allowed to stabilize for a minute or so before the next measurement was taken.

A set of four curves of $\frac{1}{n}$ versus $\frac{P(z)}{v}$ is shown in Figure 18. Values of k_1 which varied from 0.8 to 2.4 x 10^{-32} cc.^{2} sec.$^{-1}$ were obtained from the three experiments in which oxygen was added as an impurity to "extra pure" nitrogen. The curve representing no added oxygen had no straight line portion and hence yielded no value of k_1.

A summary of all of the measured values of k_1 using the quartz tube, plotted as a function of added oxygen, is shown in Figure 19. These values were all taken with flow velocities between 200 and 450 cm./sec. and pressures between 9 and 35 torr. The accuracy of such measurements of k_1 depends upon the accuracy in the measurements of z, v, n, and [M], the constancy of the production of atomic nitrogen atoms, and the extent of wall recombination present. These data show a trend for the k_1 values to decrease at about 20 to 50 ppm. of added oxygen; however, since the spread in values of k_1 lies outside of the bars representing the ranges of accuracy of the experiment, a rather innaccurate value, about 1.5 x 10^{-32} ± 70% cc.^{2} sec.$^{-1}$, of k_1 was obtained from these measurements. The data were insufficiently accurate to determine $k_2 + k_3$.

The assumptions which were made in deriving the expression used in calculating k_1 were justified for the quartz flow tube

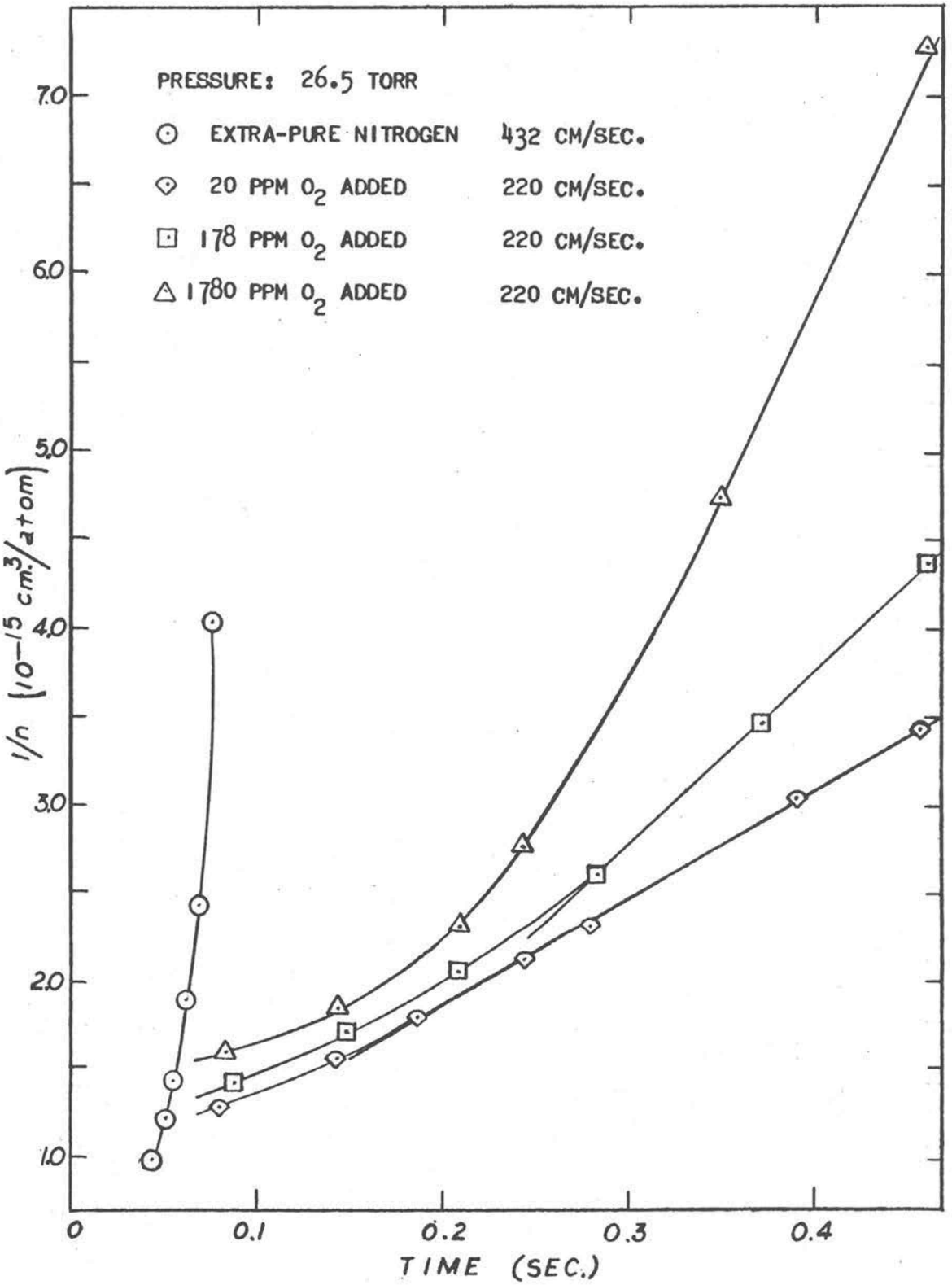

Figure 18. Three-Body Recombination Curves for Quartz Flow Tube

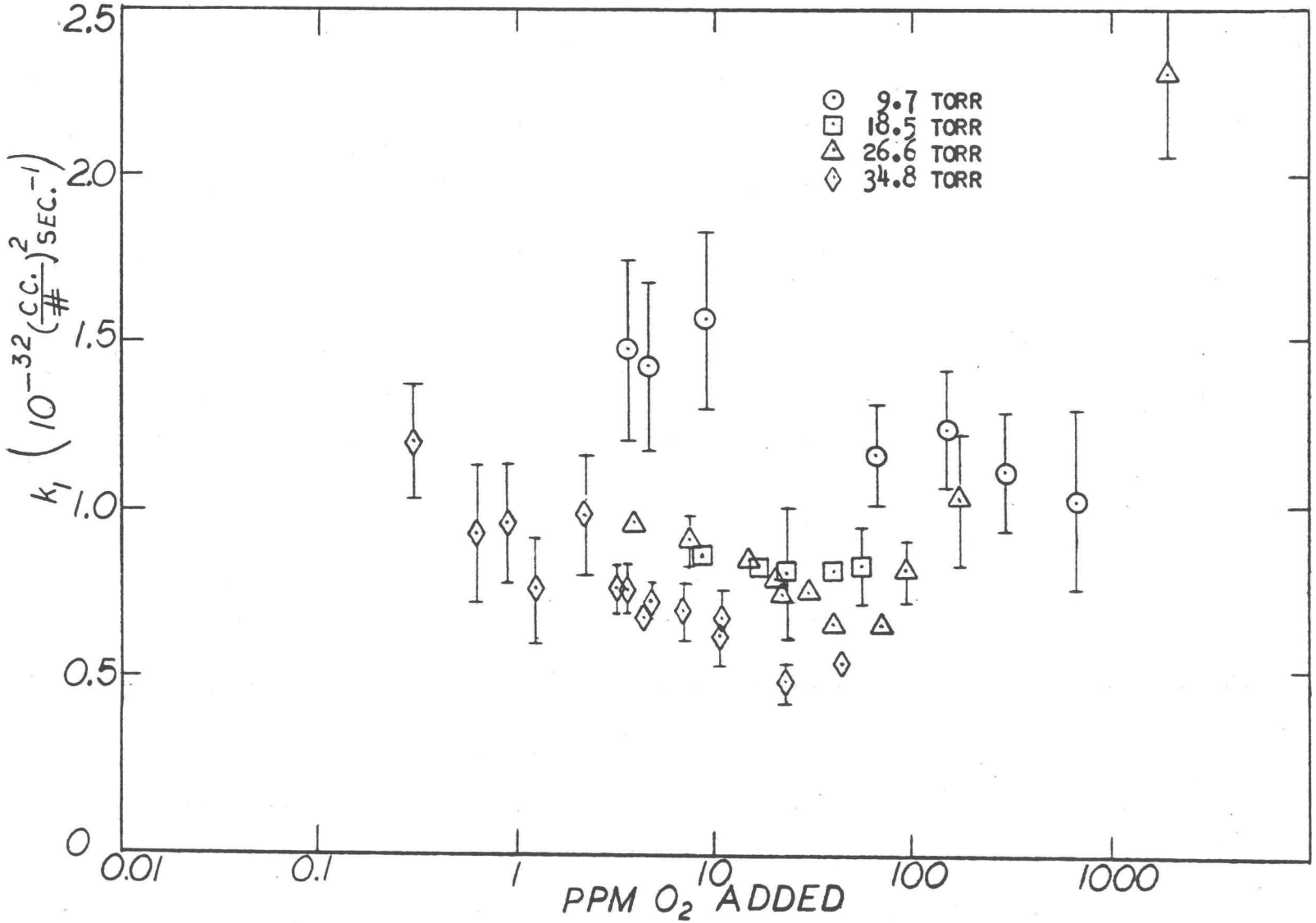

Figure 19. Three-Body Recombination Coefficient as a Function of Oxygen Added for Quartz Flow Tube

experiments; these assumptions are:

1) The gas flow is laminar. This assumption is valid since Reynold's numbers were less than 2, 200 for all gas velocities and pressures used, the value 2, 200 being the critical value for onset of turbidity (25, p. 216).

2) Gradients across the epr cavity were assumed to be small for all cases. By examination of the n versus z curves, it was determined that these gradients were small for all cases from which k_1 values were calculated.

3) The criterion for a radially uniform density was satisfied, again in all cases from which values of k_1 resulted.

4) Pressure gradients in the flow tube were small in all cases. This was verified by the use of a formula given by Kaufman (26, p. 11).

5) Axial diffusional velocities were small with respect to the flow velocities used in the experiments (26, p. 12).

6) Since the walls of the quartz flow tube were at room temperature, the temperature in the flowing gas was assumed to be nearly constant.

The data obtained using extra-pure nitrogen, plotted on a logarithmic scale in Figure 20, were used to calculate the atomic nitrogen wall recombination coefficient in the case of "extra-pure" nitrogen. The nearly identical straight line slopes at intermediate

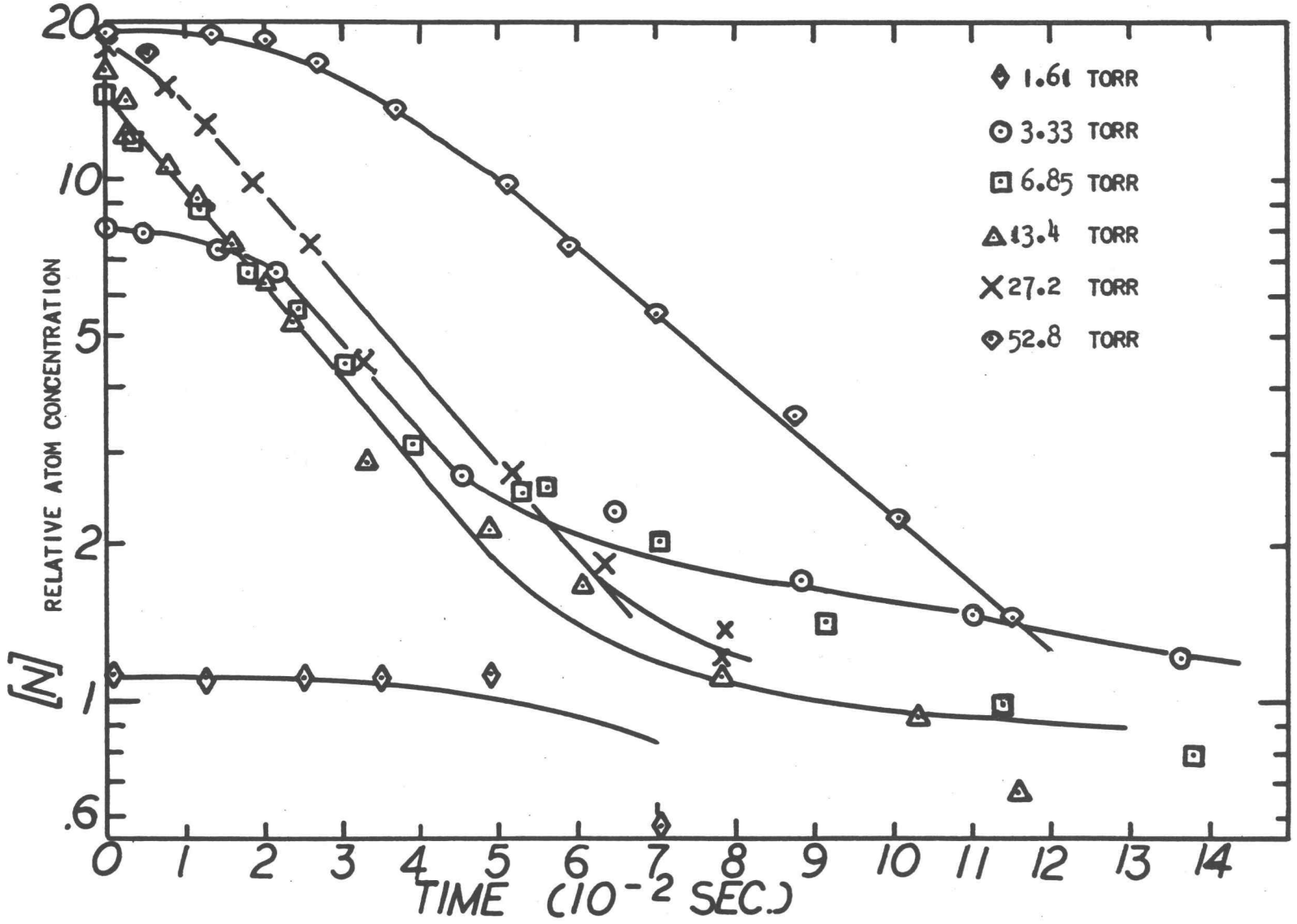

Figure 20. Wall Recombination Curves for Extra Pure Nitrogen in Quartz Flow Tube

values of $z/\bar{v}$ for each curve of Figure 20 were assumed to represent wall recombination almost exclusively. The average value of γ for these slopes was 63×10^{-5}. The shallow slopes at low concentrations were possibly due to a non-constant density of atoms attached to the wall due to the low atom concentration. The shallow initial portions of the slope of the 52.8 torr curve may be due to the slow diffusion rate to the walls at this high pressure. The shallow initial portion in the 3.33 torr curve might be due to a non-constant impurity level.

To measure the wall recombination rate in the presence of relatively large amounts of oxygen, Airco tank nitrogen was utilized in a non-flowing gas system. An atom concentration gradient which resulted from diffusional flow of nitrogen atoms in non-flowing molecular nitrogen was analyzed to yield a value of the wall recombination coefficient. For the steady state, $\frac{dn}{dt} = 0$ and assuming only wall recombination, $D\frac{d^2n}{dz^2} = k_4 n$, which can be integrated, yielding

$$\ln \frac{n_o}{n} = \left(\frac{k_4}{D}\right)^{\frac{1}{2}} z . \qquad (4\text{-}5)$$

In the non-steady state condition, analysis of the increase in atomic nitrogen concentration with time resulted in values of the diffusional coefficient, D, of $\frac{300 \pm 100}{P}$ cm.^{2} sec.$^{-1}$ where P is measured in torr. This value of D agrees with that of Schiff (43) which is $D = \frac{221 \pm 3}{P}$ cm.^{2} sec.$^{-1}$ torr.

By substituting Schiff's value of D into the above equation (4-5) the slope ℓ of a plot of $\ln \frac{n_o}{n}$ versus z is given by the expression

$$\ell = \frac{\ln n_1 - \ln n_2}{\Delta z} = \left(\frac{k_4 P}{221} \right)^{\frac{1}{2}} \qquad (4\text{-}6)$$

Then, k_4 may be determined from the slope of a plot of ℓ^2 versus P,

$$k_4 = 221 \ \frac{\Delta (\ell^2)}{\Delta P}, \qquad (4\text{-}7)$$

and γ is given by Equation (2-12):

$$\gamma = \frac{k_4^2 r_o}{\bar{c}} .$$

Figure 21 shows the logarithm of the atomic nitrogen concentration plotted versus z for four different gas pressures. The value of γ obtained from the slope of the graph of ℓ^2 versus P was found to be 0.7×10^{-5}.

Experiments Using a Quartz Flow Tube with Teflon Liner

The intensities of the atomic nitrogen signal and the afterglow obtainable with the use of the teflon tube liner were two or three times greater than those in the case of the unlined quartz tube. Also the signal and afterglow seemed to be nearly independent of the oxygen content of the gas sample. The increased signal and afterglow intensities plus the presence of a visible afterglow at much lower pressures indicated a possible reduced wall recombination coefficient by the use of the teflon liner.

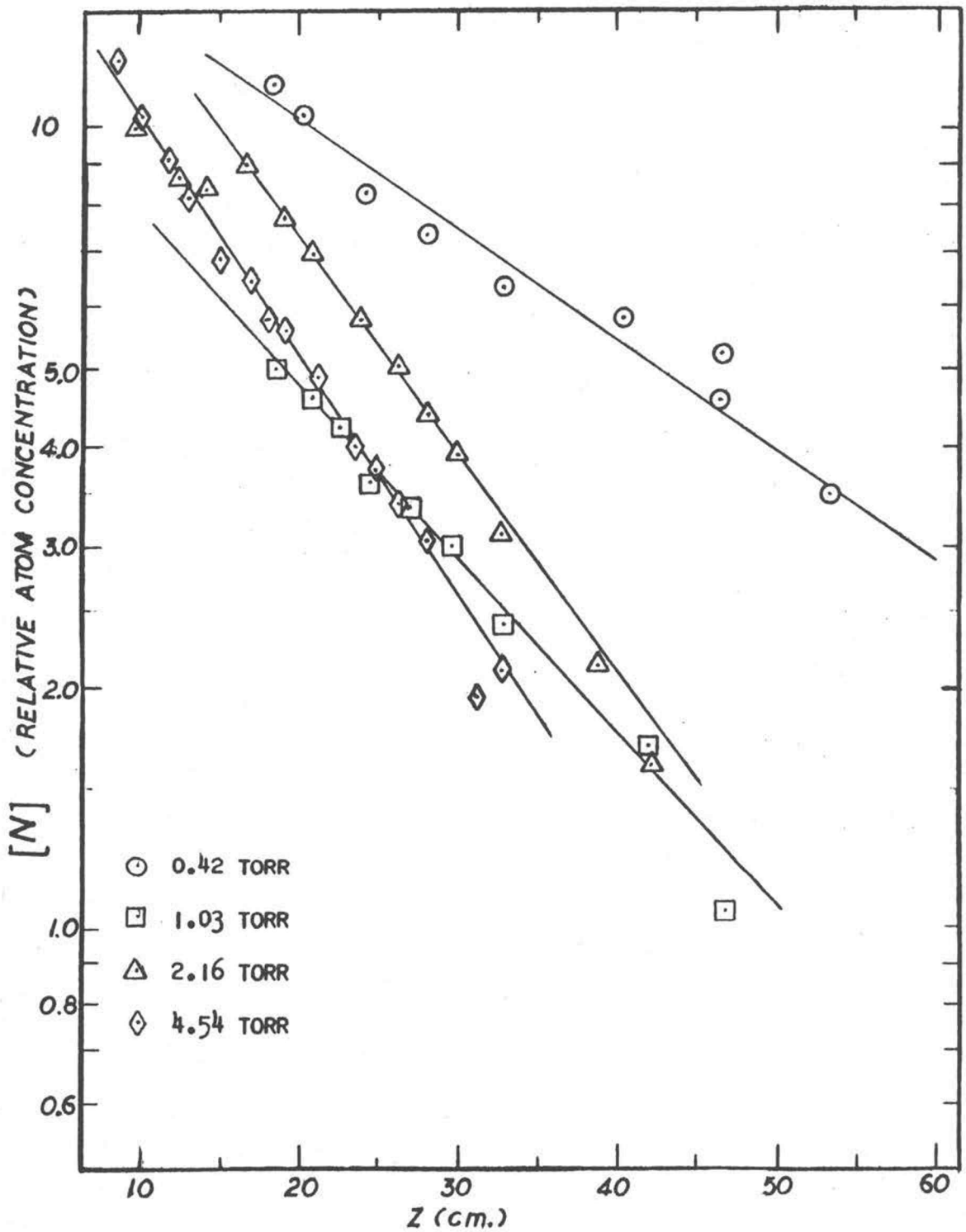

Figure 21. Wall Recombination Curves for Airco Nitrogen Flowing by Diffusion in Quartz Tube

When the discharge was operated above approximately 5 percent of full power, the afterglow became a whitish-green color, indicating a possible interaction between the hot gases of the discharge and the teflon wall. To minimize this wall reaction, the discharge was always operated below one percent of full power. At these power levels, the nitrogen signal and afterglow intensities were no greater than those noted in the use of the unlined quartz tube at the higher power levels.

Many of the values of $\frac{1}{n}$ versus $\frac{z}{\bar{v}} = t$, when plotted, were scattered more than in the case of the quartz flow tube. This scattering of points was considerably reduced by conditioning the teflon walls by slowly moving the operating discharge cavity down the flow tube, the entire procedure taking about two hours. The results of such a conditioning using "extra pure" nitrogen are indicated in Figure 22; the circled points were taken prior to the conditioning and the remaining points were taken subsequent to the conditioning procedure. Even after the conditioning, there was more scattering of the points than in the case of the unlined quartz flow tube. The lower wall recombination and high concentrations permitted the use of lower pressures and lower flow velocities than in the case of the quartz flow tube. Pressures from 3 to 12 torr and velocities from 15 to 100 cm./sec. were utilized. The value of the slope in Figure 22 was 7.3×10^{-15} cc. sec.$^{-1}$.

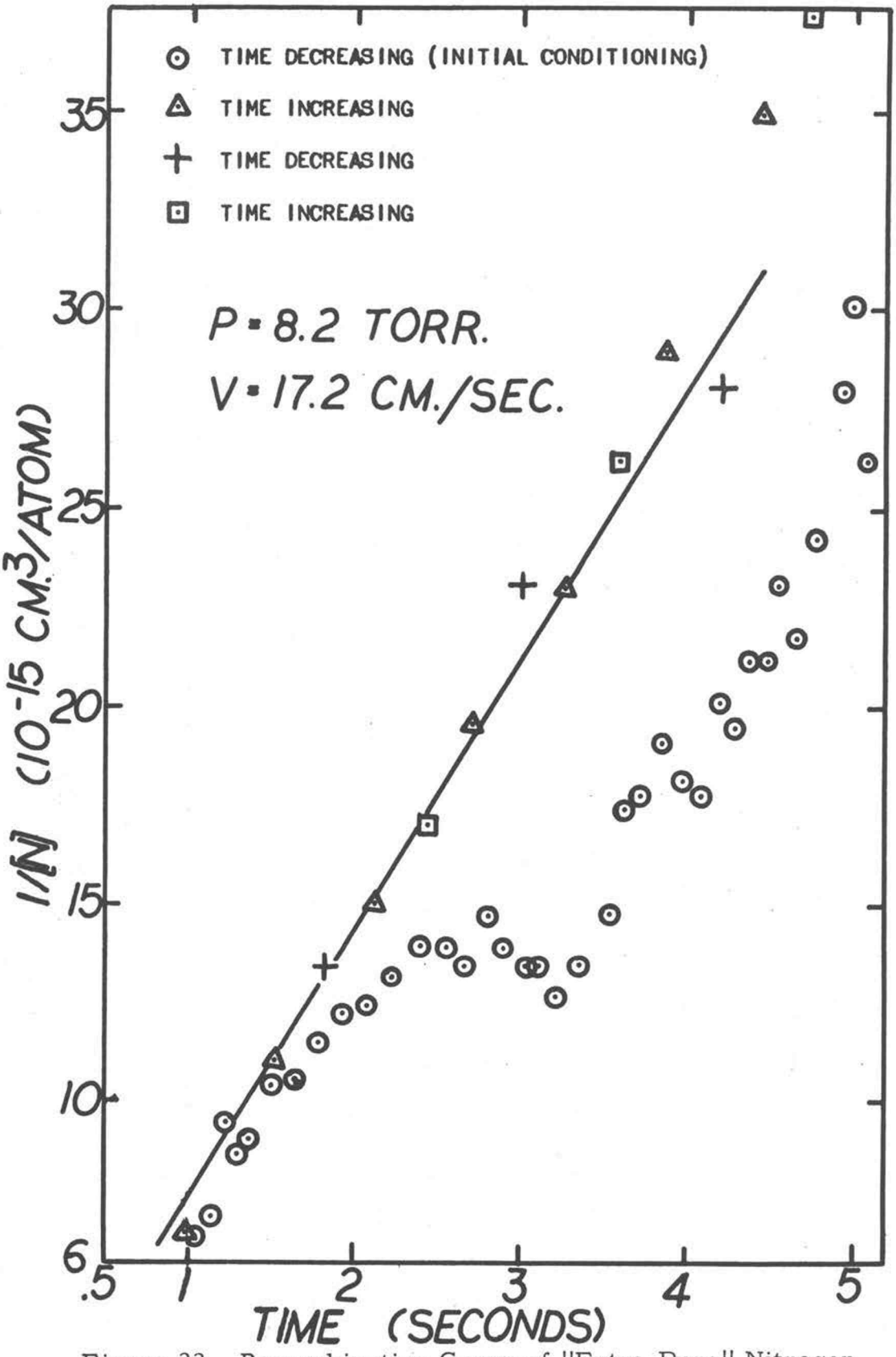

Figure 22. Recombination Curve of "Extra Pure" Nitrogen Nitrogen in Teflon-Lined Flow Tube

An experiment differing only by the use of Airco water-pumped nitrogen produced the curve in Figure 23. In this case the initial scattering of points was less and consequently the wall conditioning did not show such a pronounced effect. The value of the slope obtained from the steeper portions of the plot shown in Figure 23 was 6.7×10^{-15} cc. sec.$^{-1}$, which is in agreement with the value obtained from the slope of the line in Figure 22. The shallow initial part of the curve in Figure 23 approximated a straight line; this initial portion will be discussed later.

Values of the slopes, which should be equal to $k_1 [M] + k_2 + k_3$, obtained from the final straight line portions of the five experiments using the teflon liner with preliminary wall conditioning were plotted (Figure 24) versus the pressure to determine k_1. The slope of this curve equals k_1 and $(k_2 + k_3)$ is eliminated. Four of the points were nearly colinear yielding $k_1 = 2.2 \times 10^{-32}$ cc.^{2} sec.$^{-1}$ with a deviation of about 10%. This deviation plus the accuracy of the calibration (8%) yielded an overall accuracy of 13% for this value of k_1.

In the experiments employing the flow tube with the teflon liner, the wall recombination coefficient was again found to be variable, increasing with added oxygen rather than decreasing as in the case of the unlined quartz tube. When oxygen was present the wall recombination increased for a time as long as the discharge was in operation, approaching a constant value after about two hours. Values

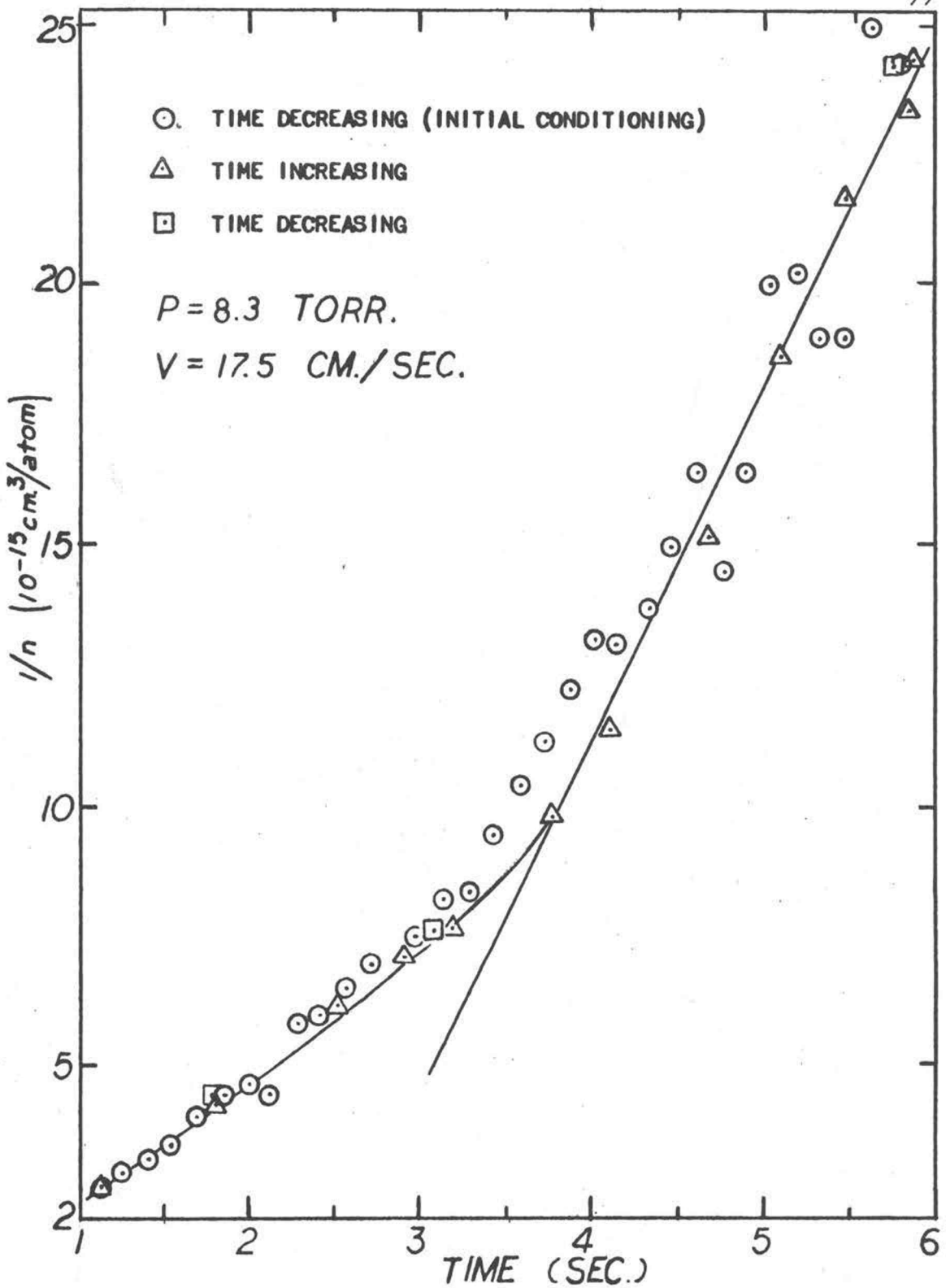

Figure 23. Recombination Curve of Airco Nitrogen In Teflon-Lined Flow Tube

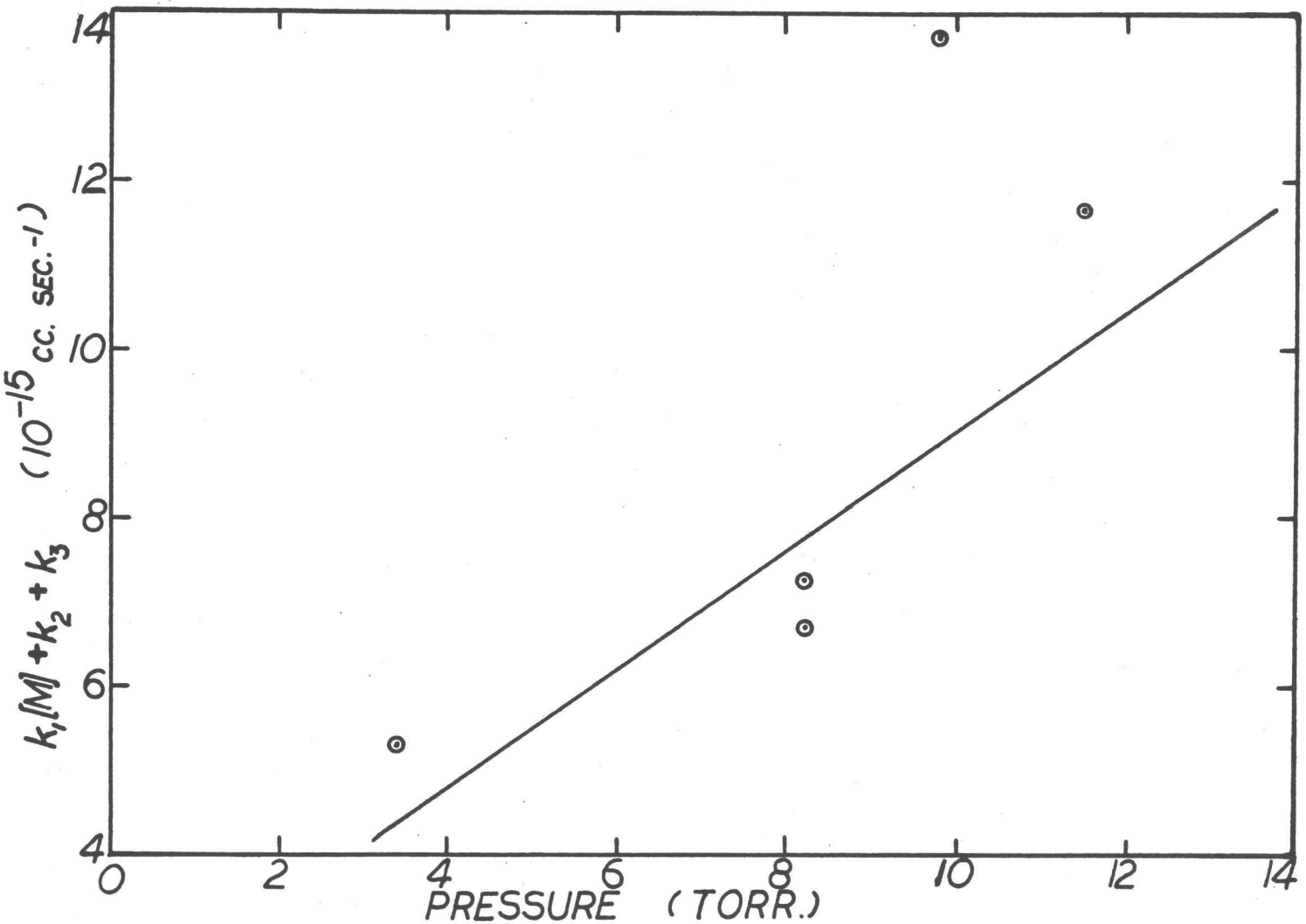

Figure 24. Slopes of Recombination Curves ($k_1[M] + k_2 + k_3$) vs. Pressure for Teflon-Lined Flow Tube Data

for γ , obtained by the diffusional method, were 4.5×10^{-6} using prepurified nitrogen discharged for two hours, and 0.5×10^{-6} in the case of "extra pure" nitrogen.

Assumptions used in deriving the flow equations and discussed in the previous section on the use of the unlined quartz flow tube were justified for all experiments employing the flow tube with a teflon liner.

Recombination Studied by the Use of the Quartz Resonant Cavity

To eliminate the time-consuming wall conditioning process and to minimize the scatter in the plots of the data apparently caused by the variable wall conditions at the discharge in the case of the teflon-lined flow tube, the three-body volume recombination coefficient was measured by the use of the quartz resonant cavity which could be sealed off from the nitrogen source.

The results of the experiments using this specially constructed cavity were indeed impressive. Straight line plots of $\frac{1}{n}$ versus t were obtained with time intervals up to 30 seconds and with $\frac{1}{n}$ varying by factors of up to 12. The nitrogen concentration was monitored continuously on a chart recorder and an oscilloscope equipped with a camera.

Three representative sets of data from the oscilloscope and the chart recorder are shown in Figure 25. The magnetic field was

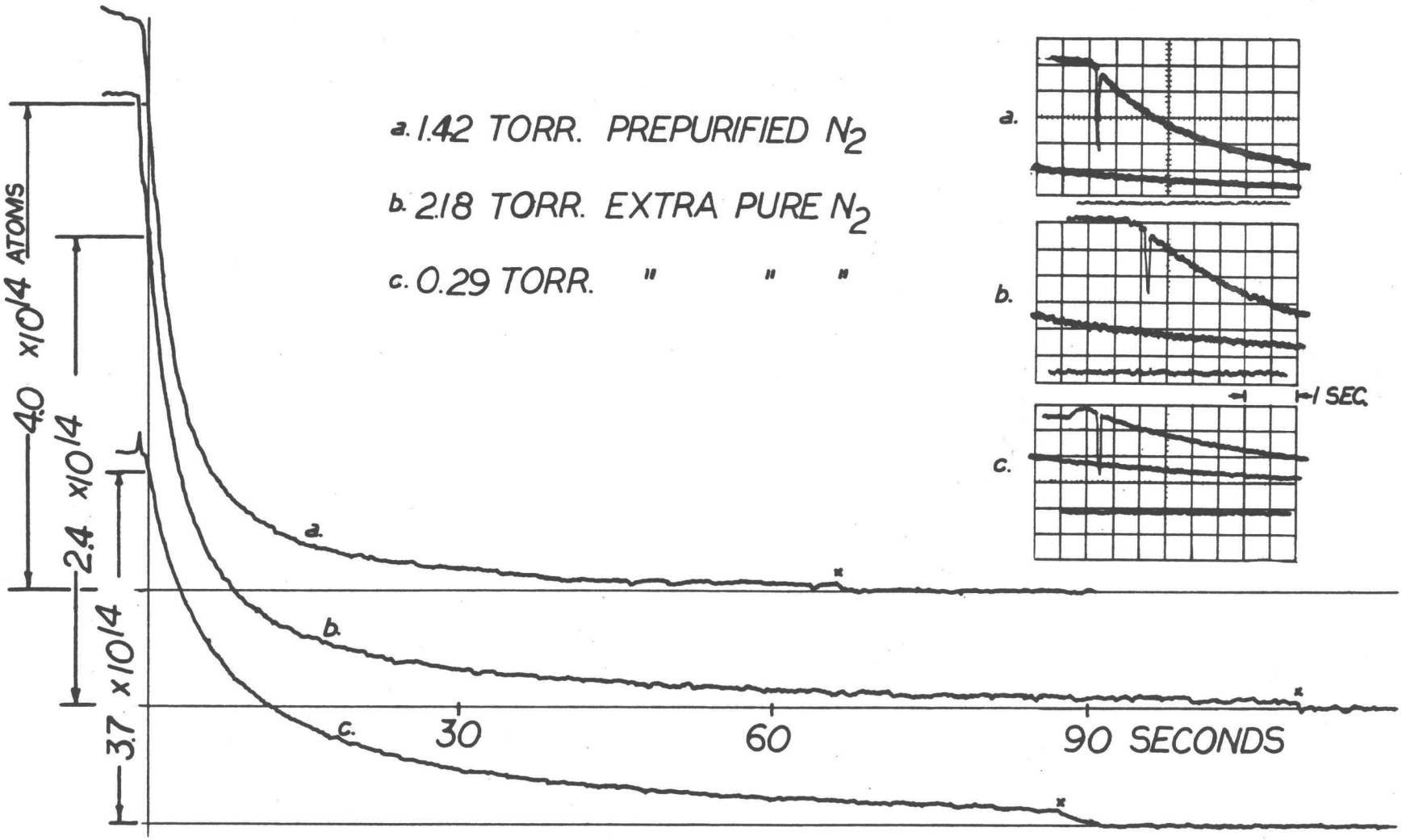

Figure 25. Quartz Cavity Data for Recorder at Bottom Left and Oscilloscope at Upper Right

adjusted to permit continuous monitoring of the peak signal height, $Y_{max.}$ (Y_{max} is illustrated in Figure 12). Activation of the dc solenoid caused the spike in the oscilloscope traces of the epr signal, signifying closure of the valve at the quartz resonant cavity. Graphs of the data shown in Figure 25 with n plotted on a reciprocal scale are illustrated in Figures 26 and 27. The accuracy of the oscilloscope data was not as great as that of the recorder data; however, because of the faster response times, more information on the initial portions of the recombination curve was available with the use of the oscilloscope.

As may be noted from an examination of Figures 26 and 27, the scatter of the data points is considerably less than in the case of either of the flow tube experiments.

A plot of the slopes from the straight line graphs of $\frac{1}{n}$ versus t resulting from a study of the recombination of "extra pure" nitrogen using chart recorded data is shown in Figure 28. The slope of the curve illustrated in Figure 28 yields a value of $(1.94 \pm 0.14) \times 10^{-32}$ cc.^{2} sec.$^{-1}$ for k_1 ; the intercept at zero pressure gives a value of 2.7×10^{-16} cc. sec.$^{-1}$ for $(k_2 + k_3)$. The point at 7.1 torr deviated considerably from the straight line determined from the remaining points because of a low signal-to-noise ratio at this high pressure and hence was not used in the determination of k_1. The slopes of the recombination curves of atomic nitrogen were independent of

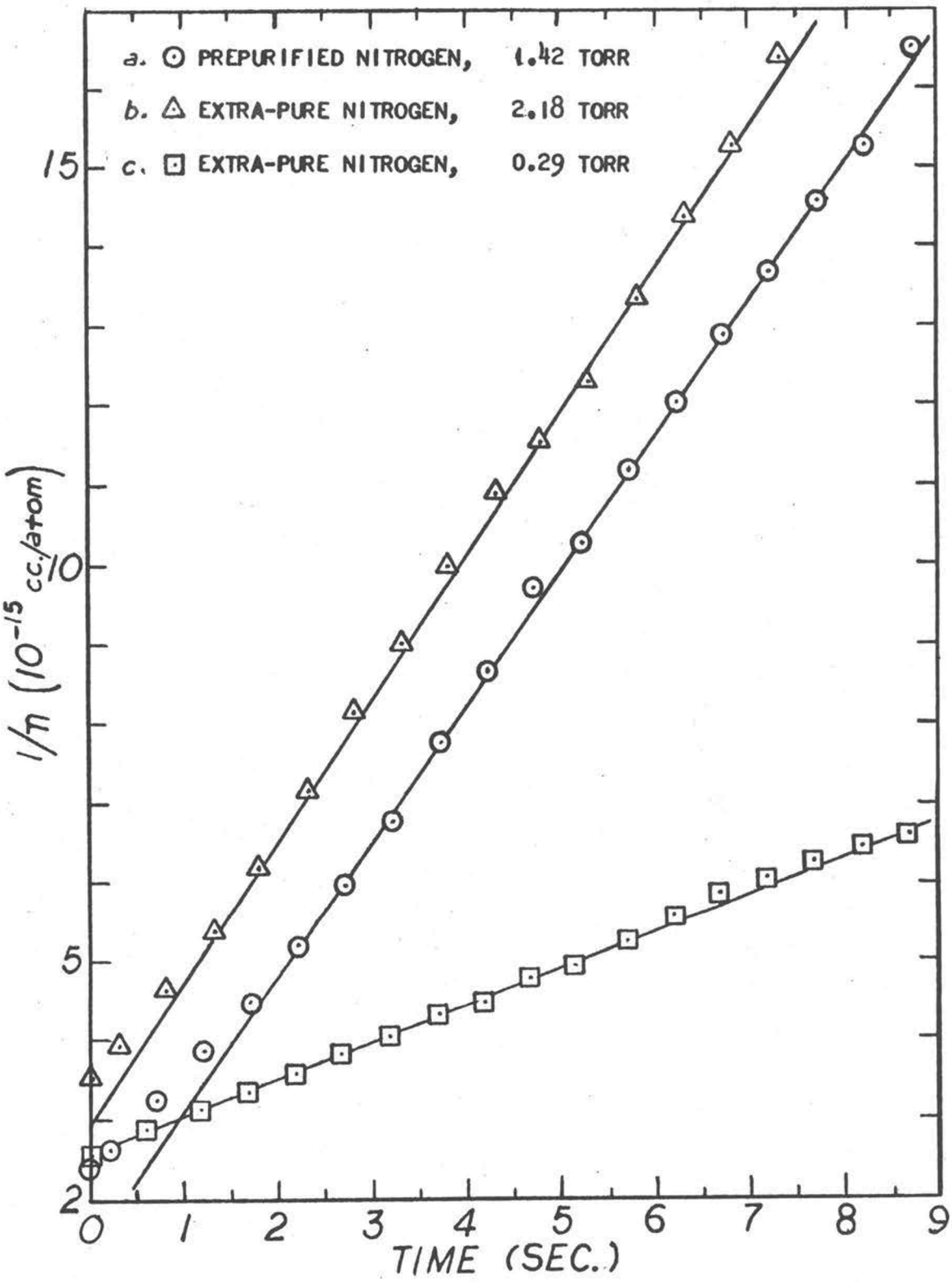

Figure 26. Recombination Curves for Oscilloscope Data of Figure 25

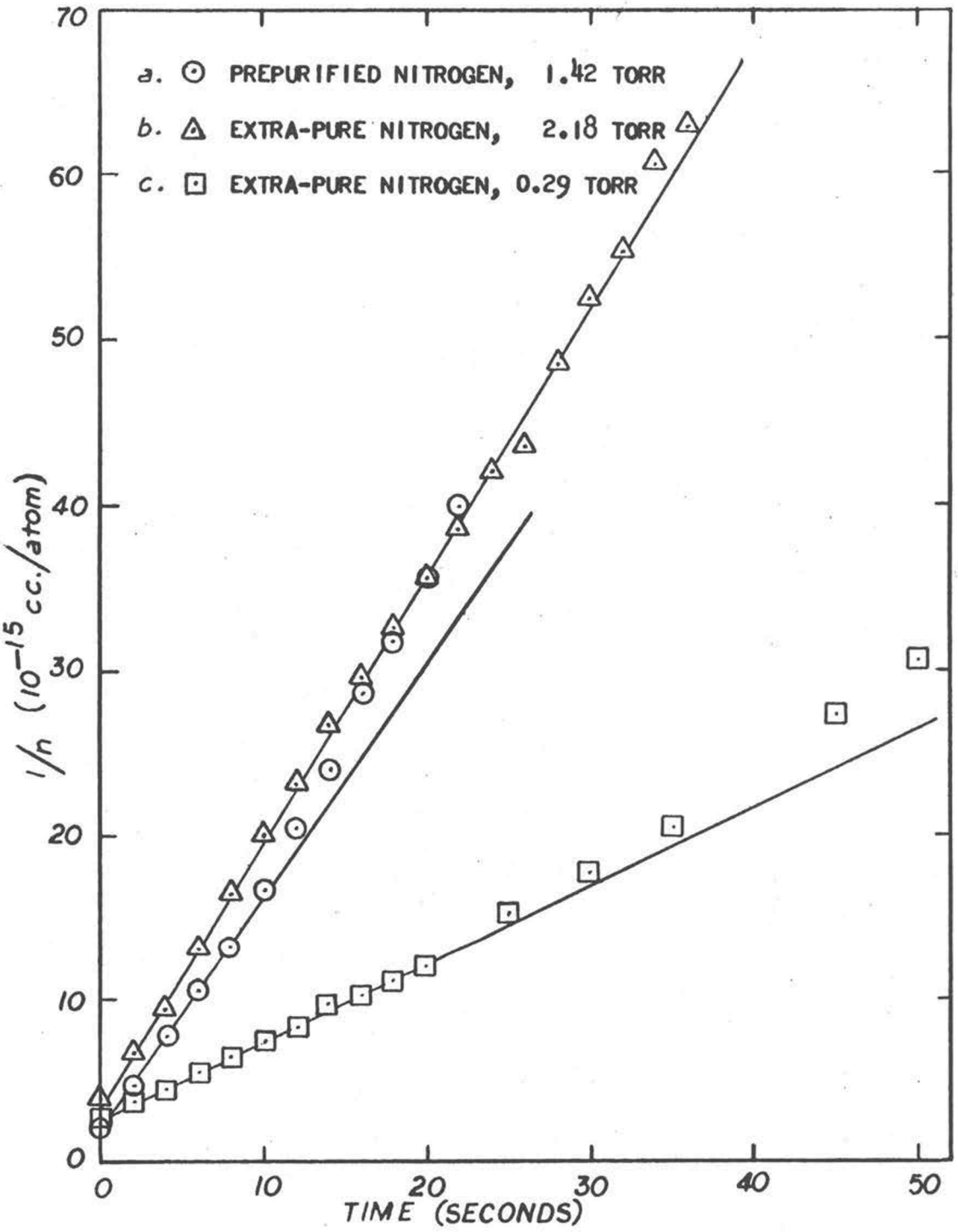

Figure 27. Recombination Curves for Recorder Data of Figure 25

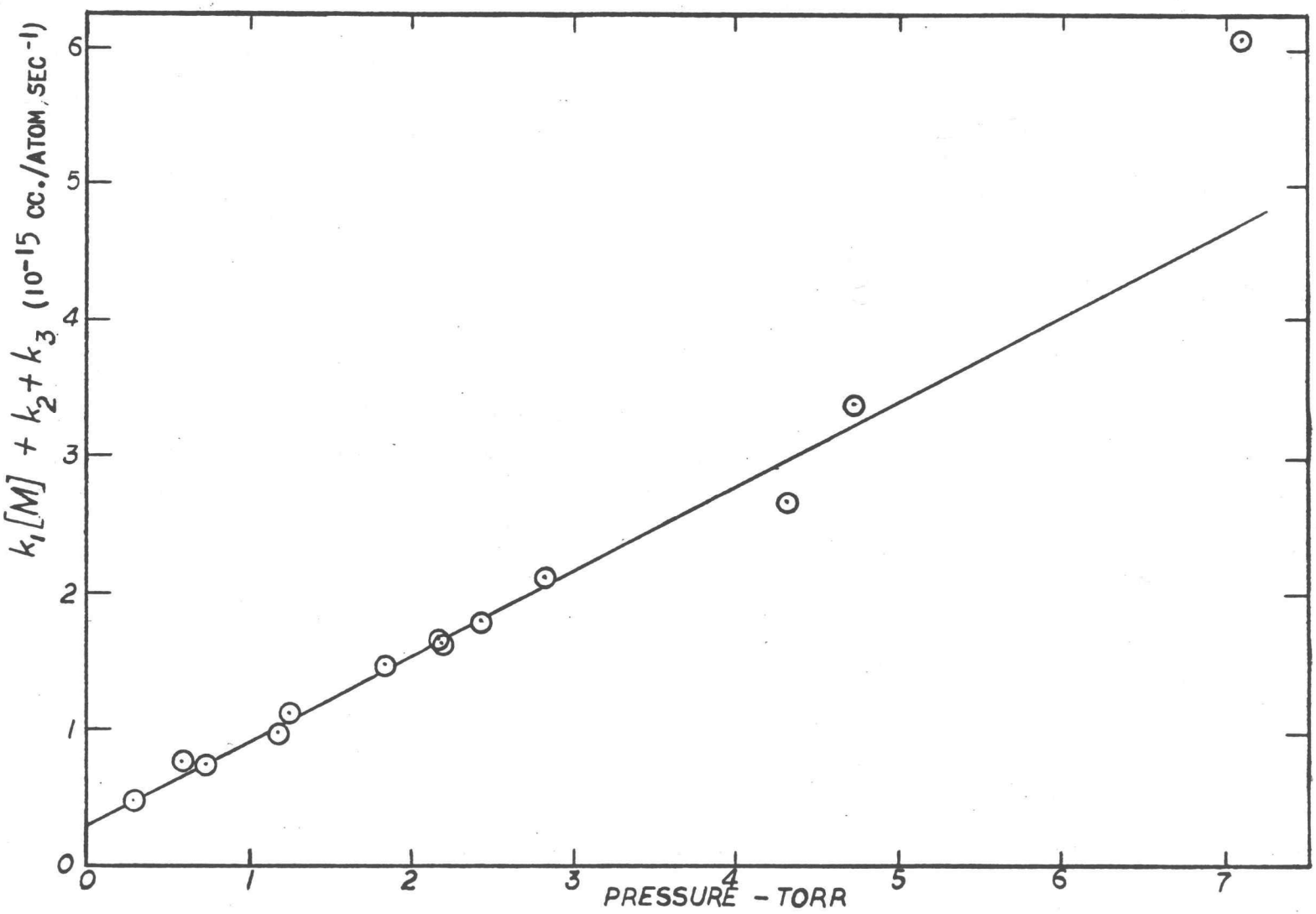

Figure 28. Slopes of Recombination Curves (k_1 [M] + k_2 + k_3) vs. Pressure for Quartz Cavity Data

varying amounts of added oxygen up to 0.24%, revealing no dependency of k_1 upon this amount of oxygen.

The data for "extra pure" nitrogen given in curve "c" of Figure 25 is shown in Figure 29, with the logarithm of n plotted versus t, to obtain the value of k_4 less than $\frac{1}{60}$ sec.$^{-1}$ for the teflon-lined quartz cavity. However, the straight line portion of $\frac{1}{n}$ versus t extending for times up to 30 seconds would indicate a value of k_4 of less than $\frac{1}{300}$ sec.$^{-1}$. Values of less than 0.4×10^{-6} and 0.08×10^{-6} for γ were calculated from k_4 by substituting the surface-to-volume ratio for the cavity into Equation (2-11A). A value of γ of about 25×10^{-6} was obtained in the experiment using Airco water-pumped nitrogen.

Four factors led to an increased accuracy in the value of k_1 as determined in the quartz cavity compared with the flow tube.

1) An increase in the volume-to-surface ratio as well as a somewhat lower value of the wall recombination probability resulted in linear plots of $\frac{1}{n}$ versus time to much larger value of $\frac{n_o}{n}$.

2) Because of the greater inhomogeneity in the magnetic field, the same modulation setting was used with both O_2 and N; this factor thus did not appear in the calibration formula.

3) The time was measured directly, rather than by measuring $\frac{z}{v}$, and hence was much more accurately determined.

4) Possible effects due to the repositioning of the discharge

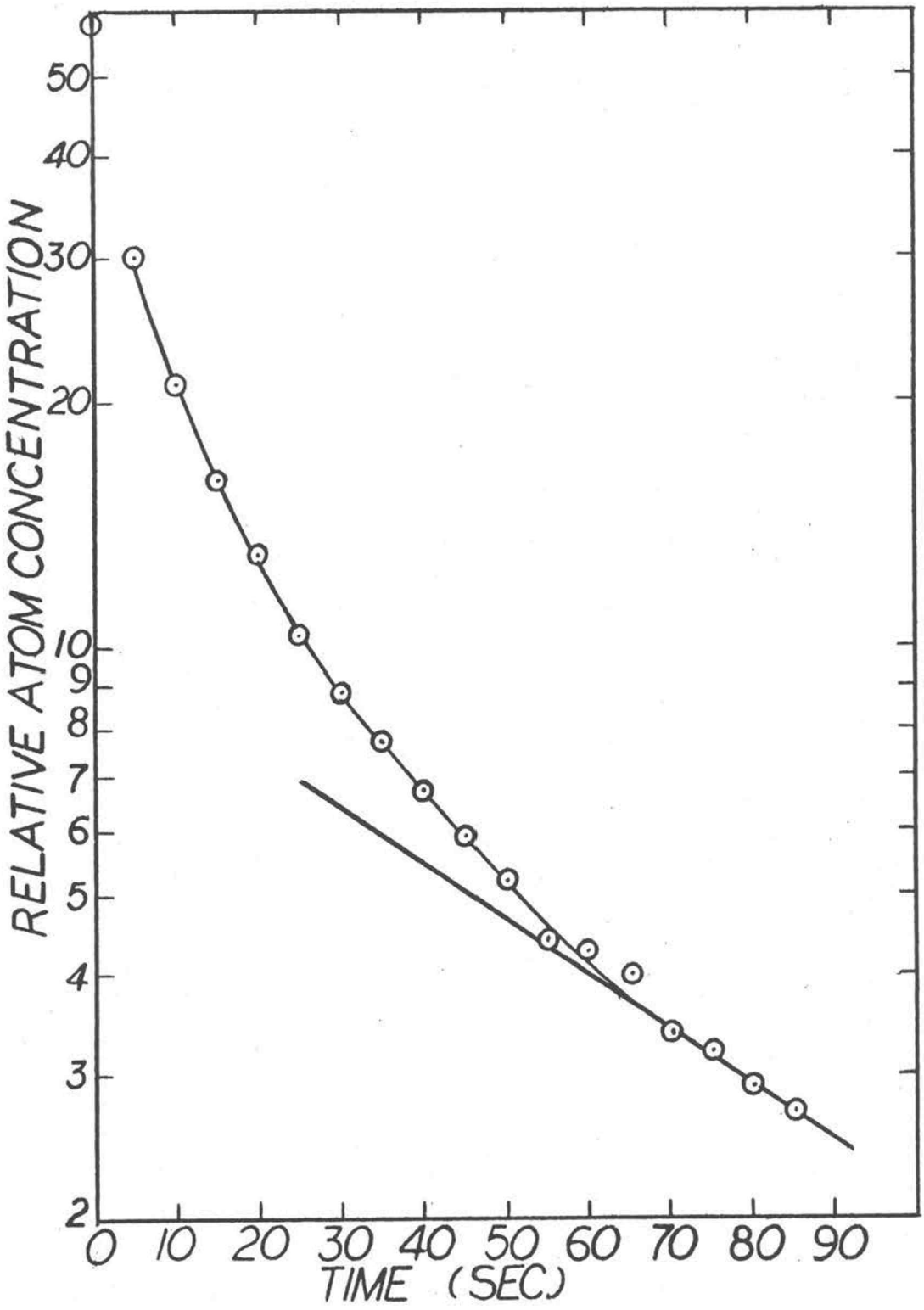

Figure 29. Wall Recombination Curve for "Extra Pure" Nitrogen in Quartz Cavity

on the flow tube were eliminated. The net result was an overall accuracy of about 7% in the measured value of k_1 with the quartz cavity.

The only assumption made in determining k_1 by the use of the quartz cavity is that the concentration be spatially uniform. Since the shape of the epr signal is dependent upon spatial distribution of the sample in the inhomogeneous magnetic field, different distributions of atomic nitrogen in the cavity would produce correspondingly different shapes of the epr signal. No variations in the signal shape taken under steady-state conditions with the trap door open were observed, even though the pressure and the discharge power were varied over their widest limits; it was therefore concluded that no appreciable atom gradients existed in the cavity under the experimental conditions used.

Comparison of the Atomic Nitrogen Recombination Coefficients Measured by the Use of the Three Experimental Arrangements

A summary of the three-body recombination coefficients, which were determined for atomic nitrogen using the two types of flow tubes and the quartz resonant cavity, is given in Table 2 along with corresponding values reported by other workers. No experimental or theoretical values of either k_2 or k_3 have been reported with which to compare our measured values of $2.5 \pm 0.4 \times 10^{-16}$

Table 2

Summary of Atomic Nitrogen Three-Body Recombination Coefficients

k_1 (10^{-32} cc.^{2} sec.$^{-1}$)	Percent accuracy	P torr	Time after discharge seconds	$n_{max.}$ #/cc.	$\frac{n_{max.}}{n_{min.}}$	Method used	Source
In these experiments							
0.5 to 2.4	30	9 to 35	0.1 to 0.5	10^{15}	2	unlined quartz flow tube	
2.2 ± 0.3	13	3 to 12	0.5 to 6	10^{15}	3 to 4	quartz tube with teflon liner	
1.94 ± 0.14 (best value)	7	0.3 to 5	1 to 40	5×10^{14}	10	quartz resonant cavity	
By other workers							
3.3	25	0.1 to 1	< 2	--	--	non-flowing gas platinum wire thermometer	(50)
3.44	10	0.5 to 1.3	< 1	10^{15}	2	flow system NO titration	(15)
1.57	14	3 to 8	0.2	--	2 to 3	flow system NO titration	(18)
1.5 (corrected to 4.5)	20	2 to 10	0.5	8×10^{15}	7	flow system epr	(34)
3.0	16	2.5 to 4	0.1	--	--	flow system NO titration	(35)
2.56 (average of other workers values)							

cc. sec.$^{-1}$ for $(k_2 + k_3)$ of teflon.

A comparison of the results of the three different methods used in the present experiments reveals an apparently lower value of k_1 for measurements taken at distances corresponding to short times after the discharge. This apparent decrease in the recombination rate may be seen in the shallow initial portions of the curves in Figures 18, 23, and 26. The data representative of all three curves may be combined in a hypothetical three-body recombination curve of the type shown in Figure 30. The approximate intervals for which the data were taken by the three methods are shown on the time scale. The initial time for the sealed cavity measurements was taken as the approximate time required for diffusion of the atomic nitrogen into the cavity.

Since no single experiment covered the entire time scale shown in Figure 30, a final experiment was performed using prepurified nitrogen in the quartz flow tube at much slower velocities to obtain measurements covering the entire time scale. Although the effects of wall recombination became pronounced after about eight seconds, the curve of $\frac{1}{n}$ versus time up to that point was nearly identical to the hypothetical curve. Thus, it is concluded that the hypothetical curve is representative of the combined data taken with all three experimental arrangements. An explanation must now be found for the shape of this curve. Since the three-body recombination

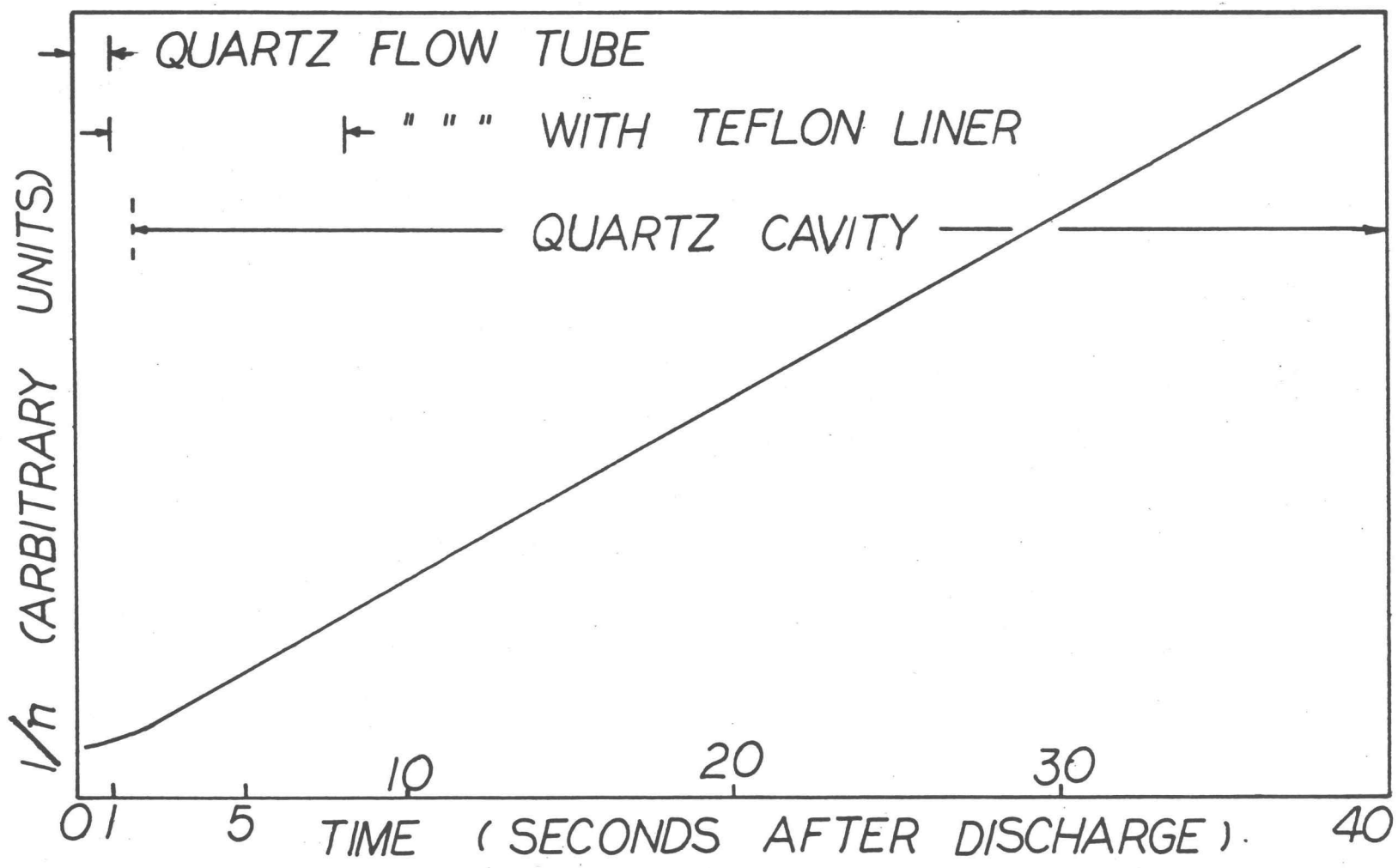

Figure 30. Hypothetical Recombination Curve Summarizing Results of all Three Experimental Arrangements

curves for the quartz cavity data have linear portions over approximately an order of magnitude change in the nitrogen atom concentration and exhibit little scatter, the value of k_1, $(1.94 \pm 0.14) \times 10^{-32}$ cc.^{2} sec.$^{-1}$, calculated from these curves was accepted as representing the most accurate value of k_1. This value is in reasonable agreement with those obtained using both quartz and teflon-lined flow tube. Thus the final linear portion of the hypothetical curve represents a process in which nitrogen atoms are disappearing by three-body plus radiative and two-body wall recombination processes with negligible first order wall recombination. The shallow inital portions were dependent upon the amount of oxygen impurity as was evidenced by the varying values of k_1 measured with the quartz flow tube.

There are at least three possible explanations of the shallow initial portions of these recombination curves: 1) in the immediate proximity of the discharge the gas was sufficiently hot either a) to decrease the third body concentration or b) to decrease the value of k_1, 2) the diffusional flow of the nitrogen atoms was appreciable, or 3) some process was in operation which produced nitrogen atoms in the afterglow.

These three possibilities will now be examined: 1a) and 1b) the recombining gas could be hot either because it had not cooled after passing through the discharge or because energy was being added by the recombination process. A study of the steady-state

solution of the heat-flow equation in the case of energy addition by three-body recombination at a constant rate twice as large as the greatest we observed experimentally, assuming the walls were at room temperature, yielded a temperature difference across the radius of the flow tube of only one-fourth of a degree centigrade. A temperature difference of several hundred degrees would be required in order to explain the low recombination by excessive heating of the gas, causing a decrease in the third-body concentration. The intensity of the afterglow, which has been shown to be proportional to the rate of atom recombination, has a temperature dependence of $T^{-0.64}$ (24, p. 117); using this value a temperature of 900° C would be necessary to explain the shallow portion of the recombination curves. Similar considerations show that the hot discharge gases were cooled within a few hundredths of a second, far too rapidly to account for the low recombination coefficients. 2) The rapid diffusional flow of atomic nitrogen is not a satisfactory explanation of the shallow portion of the curves for two reasons: a) the shallow portions were dependent upon the additions of very small amounts of oxygen and b) they were present at the high pressures where diffusional flow should be smaller. 3) The only remaining possibility is that there is some mechanism providing continuous formation of atomic nitrogen outside the discharge region. A simple hypothesis which could account for the addition of atoms to the afterglow is that there is a

constituent X which is present in the early afterglow and which may be altered to yield nitrogen atoms in the ground state. If this hypothetical particle were disappearing to yield nitrogen atoms at a rate proportional to its own concentration, then, with $\frac{1}{t_o}$ as the proportionality constant,

$$\frac{d[X]}{dt} = -\frac{[X]}{t_o}, \tag{5-1}$$

which may be integrated,

$$[X] = [X_o]\ e^{-\frac{t}{t_o}}. \tag{5-2}$$

The rate of increase of nitrogen atoms would be proportional to $\frac{d[X]}{dt}$, and for a qualitative discussion will be considered equal to $\frac{d[X]}{dt}$. The equation governing the nitrogen concentration, assuming only three-body recombination and the atom-producing process are in operation, may then be written:

$$\frac{dn}{dt} = -k_1 [M]\ n^2 + \frac{[X_o]\ e^{-\frac{t}{t_o}}}{t_o} \tag{5-3}$$

or

$$[X_o]\ e^{-\frac{t}{t_o}} = \left(\frac{dn}{dt} + k_1 [M]\ n^2\right) t_o . \tag{5-4}$$

Thus, a plot of the logarithm of $\frac{dn}{dt} + k_1 [M]\ n^2$ versus time should be a straight line. The results of such plots using the data from three of the curves in Figures 23 and 26 which represent recombination of prepurified nitrogen are shown in Figure 31. All three plots yielded straight lines with nearly identical time constants of about

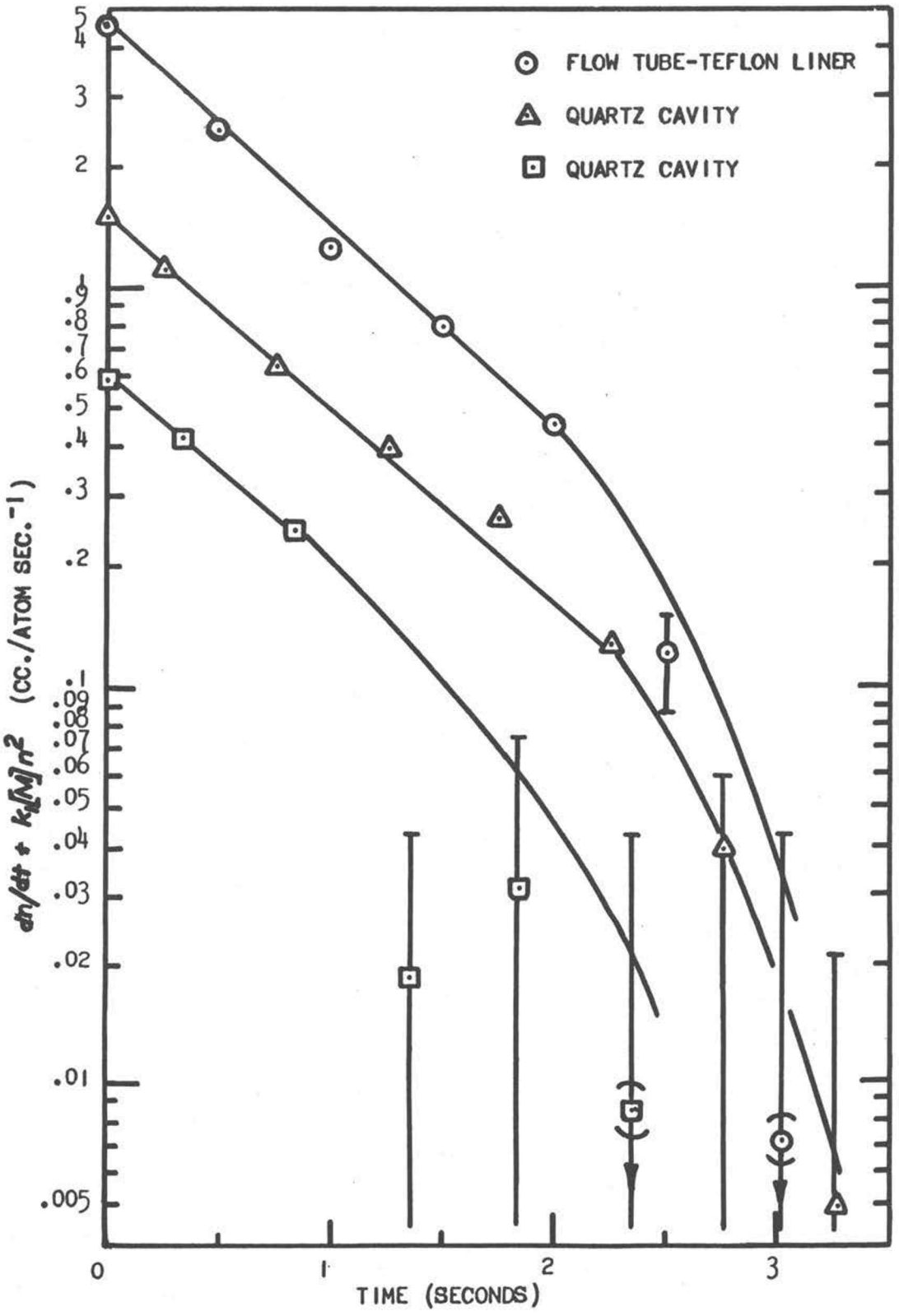

Figure 31. Decay of Particle X (Nitrogen-Atom-Forming Particle)

0.9 seconds, thus adding considerably to the evidence for the existence of a particle decaying in the postulated fashion. It should be noted however, that all the points corresponding to times greater than about two seconds fell appreciably below the straight line portions of the curve. This would seem to indicate that this simple mechanism is not a complete explanation for the entire decay mechanism, but only an indication of a more complex process which may be occurring in the nitrogen afterglow. A similar plot for the curve in Figure 18 showing the addition of 1780 ppm. of oxygen had a time constant of 0.075 seconds; however, the large amount of added oxygen may have considerably shortened the life of particle X. The maximum concentration obtained for X was between 1×10^{14} and 4×10^{14} particles/cc. Other workers (2, p. 882-884; 10, p. 3-5) have reported deviations from straight lines in plots of the reciprocal of the square root of the optical intensity of the afterglow plotted versus time; however, it is not firmly established that the intensity of the afterglow is proportional to the square of the nitrogen atom concentration, especially in cases of extreme purity of the gas (1, p. 887-899), so that no exact comparison of their results and ours is possible.

The strength of the magnetic field was scanned near values where the $^2P_{3/2}$ and $^2D_{5/2}$ epr spectral lines should occur, to determine if hypothetical X might actually be atomic nitrogen in

either of these states. No indication of the presence of either state was found; the limit of detectability of the concentration of atoms in either of these states, assuming that each of their spectra is of the same character as that of the ^4S ground state of atomic nitrogen, was 2×10^{12} atoms/cc.

The existence of some high energy substance, which has been postulated for some time to be in the nitrogen afterglow, is indicated by the short-lived, pink, auroral afterglow (4; 9; 53;). The maximum intensity of the pink afterglow and the maximum value of the hypothetical particle postulated here both occur when nitrogen with small amounts of oxygen, approximately the amount found in Matheson's prepurified nitrogen, is used in the discharge.

It has been suggested by Innes and Oldenburg (23) that the ^6S state of atomic nitrogen might be the energy carrier for the pink afterglow. In the present study the epr spectrometer was used to attempt to detect the presence of the ^6S state. It was assumed that the nuclear splitting of the epr spectral lines for the ^6S state would be different from that of the ^4S, and the line width would be roughly the same. No evidence was found in either the pink afterglow or the normal afterglow and an upper limit of 2×10^{12} particles/cc. for atoms in this state was set in the same manner as in the case of the $^2P_{3/2}$ and $^2D_{5/2}$ states.

The foregoing discussion cannot be interpreted as positive

evidence for the existence of a hypothetical particle which forms nitrogen atoms; however, it can explain some of the low values of k_1 obtained. At any rate, the evidence indicates that accurate measurements of k_1 should be made using time intervals of several seconds. The fact that none of the measurements of k_1 reported in the literature have been made using such long time intervals may explain the variation noted among values of k_1 cited, although inaccuracies in the different methods of atom concentration measurement should also be considered in this regard.

Marshall (33), the only other worker reporting values of k_1 using epr techniques identical to ours and employing a quartz flow tube, reported a value of 1.5×10^{-32} cc.^{2} sec.$^{-1}$ for k_1; however, he claims to have made an arithmetical correction of Krongelb and Strandberg's calibration formula. A check of the arithmetic in the calibration formula and the performance of the calibration test convinced us that Marshall was in error. Marshall also calculated an average velocity by integrating over the radius rather than the area of the flow tube, thus adding an additional error to the determination of k_1. Correction of both of Marshall's errors would change his listed value of k_1 to 4.5×10^{-32} cc.^{2} sec.$^{-1}$. This value would probably be reduced if Marshall had evaluated the integral $\int \Delta x\, Y\, dx$ of the nitrogen line rather than used the width squared times height as a measure of $\int \chi''\, dH$. The method Marshall employed to

determine $\int \chi'' dH$ would have been satisfactory only if both the oxygen and nitrogen lines had identical shapes; his reported width of 200 milligauss for the atomic nitrogen lines, which was five times greater than the value determined in the present investigation, could have been caused by either magnetic field inhomogeneity or modulation broadening. It is highly unlikely that a Lorenzian line for atomic nitrogen would result under these conditions.

Our measured values of the wall recombination probability γ are listed in Table 3 along with the values measured by other workers. Our value of γ for quartz determined by the use of the "extra pure" nitrogen agrees well with that of Marshall (34) who also used a carefully cleansed system. Besides that of Marshall, all values of γ reported for silica-containing materials have been for pyrex which may be expected to have γ values similar to those of quartz. The three values of γ for pyrex listed in Table 4 apparently were obtained using no special effort to condition the walls or to use "extra pure" nitrogen; these values agree quite closely with our reported value of γ for quartz using Airco water-pumped nitrogen.

Young's (52) value of γ for teflon is somewhat higher than any of ours; however, slightly different baking techniques used in applying the teflon finish can result in finishes differing markedly in appearance. It is thus likely that values of γ for teflon may vary considerably.

Table 3

Summary of Wall Recombination Probabilities

defined by: $\frac{dn}{dt} = -k_4 n$

with: $\gamma = \frac{(k_4)(4)}{\bar{c}} \frac{(\text{volume})}{(\text{area})}$

Wall Material	Grade of Nitrogen	γ	Method used	Source
In these experiments				
quartz	"extra pure"	630×10^{-6}	quartz flow tube	
quartz	Airco water-pumped	9.1×10^{-6}	quartz flow tube	
teflon tube	"extra pure"	0.67×10^{-6}	quartz flow tube with teflon liner	
teflon tube	Matheson prepurified	5.7×10^{-6}	quartz flow tube with teflon liner	
teflon finish	"extra pure"	0.1×10^{-6}	quartz resonant cavity	
teflon finish	Airco water-pumped	25×10^{-6}	quartz resonant cavity	
By other workers				
quartz	Matheson prepurified	800×10^{-6}	flow system, epr	(34)
pyrex	super-dry	15×10^{-6}	flow system, NO titration	(18)
pyrex	?	30×10^{-6}	non-flow, platinum wire	(50)
pyrex	99.9%	75×10^{-6}	flow system, NO titration	(35)
pyrex	mass spectroscopically pure	17×10^{-6}	flow system, afterglow intensity measurements	(52)
teflon finish	mass spectroscopically pure	29×10^{-6}	flow system, afterglow intensity measurements	(52)

SUMMARY

This investigation of the recombination of atomic nitrogen utilized both a flowing gas, passing through either an unlined quartz tube or a quartz tube with a teflon liner, and a non-flowing gas sealed in a specially constructed quartz resonant cavity. Atomic nitrogen concentrations were measured by employing a Varian epr spectrometer. The results of experiments culminating in the accurate measurement of k_1 by the use of the quartz resonant cavity are summarized as follows:

1. The epr spectra of molecular oxygen and nitrogen dioxide have been observed with greater resolution than has been reported in the literature.
2. The natural width of the nitrogen line was found to be less than 49 milligauss, approximately one-half the previously reported values.
3. Molecular oxygen was shown to be an excellent calibration substance for the measurement of gas concentrations with an epr spectrometer. The calibration formula of Krongelb and Strandberg (30, p. 1199) was experimentally verified by comparison of the oxygen sensitivity with that of two other commonly used calibration standards.
4. The value for the three-body recombination coefficient of

atomic nitrogen, k_1, which was independent of oxygen concentrations up to 0.25%, was found to be $(1.94 \pm 0.14) \times 10^{-32}$ $cc.^2$ $sec.^{-1}$ in the experiments utilizing the quartz resonant cavity.

5. The value of the wall recombination probability γ for quartz varies from 9.1×10^{-6} to 630×10^{-6}, increasing with nitrogen purity. The smaller values may be caused by the adsorption of some substance present when oxygen or several gases containing oxygen in their molecules are present in the nitrogen passing through the discharge.

6. The wall recombination probability γ for teflon has a value of less than approximately 0.1×10^{-6} to 25×10^{-6}, increasing with oxygen content.

7. The sum of the two-body radiative recombination coefficient and the two-body wall recombination coefficient $(k_2 + k_3)$ was found to have an average value of $(2.5 \pm 0.4) \times 10^{-16}$ $cc.^2 sec.^{-1}$ in the case of the teflon surfaces.

8. If the $^2P_{3/2}$, $^2D_{5/2}$, and ^6S states of atomic nitrogen have spectral lines of approximately the same width as those of the ^4S state, then these states are present in the nitrogen afterglow in amounts less than 2×10^{12} atoms/cc.

9. Evidence was presented for the possible presence of some particle which produces atomic nitrogen in the afterglow

by some unknown process. From a hypothesized decay scheme for this particle, experimental evidence led to the estimation of its lifetime to be 0.9 seconds and its concentration about 2×10^{14} particles/cc. Its existence and lifetime are apparently very dependent upon oxygen impurity.

BIBLIOGRAPHY

1. Anderson, J. M. The nature of active nitrogen. Proceedings of the Physical Society (London) A 70:887-899. 1957.

2. Anderson, J. M., A. D. Kavadas, and R. W. McKay. The decay of the nitrogen afterglow. Proceedings of the Physical Society (London) A 70:877-886. 1957.

3. Bauer, Ernest. Three-body recombination of oxygen atoms. The Journal of Chemical Physics 33:1202-1208. 1960.

4. Beale, G. E., Jr. and H. P. Broida. Spectral study of a visible, short-duration afterglow in nitrogen. The Journal of Chemical Physics 31:1030-1034. 1959.

5. Benson, Sidney W. and Takayuki Fueno. Mechanism of atom recombination by consecutive vibrational deactivations. The Journal of Chemical Physics 36:1597-1607. 1962.

6. Beringer, Robert and J. G. Castle, Jr. Microwave magnetic resonance absorption in oxygen. The Physical Review 75: 1963. 1949.

7. Beringer, Robert and Mark Heald. Electron spin magnetic moment in atomic hydrogen. The Physical Review 95:1474-1481. 1954.

8. Berkowitz, Joseph, William A. Chupka, and G. P. Kistiakowsky. Mass spectrometric study of the kinetics of nitrogen afterglow. The Journal of Chemical Physics 25:457-466. 1956.

9. Broida, H. P. and Ikuzo Tanaka. Double probe measurements of ionization in active nitrogen. The Journal of Chemical Physics 36:236-238. 1962.

10. Brömer, Herbert Heinrich. Untersuchung des "Auroral Afterglow" und seiner Präparationstadien. II. Das Abklingen des Nachleuchtens in Airglow --, NO --, und Lewis-Rayleigh-Stadium. Zeitshrift für Physik 158:1-11. 1960.

11. Bunker, Don L. Mechanics of atomic recombination reactions. The Journal of Chemical Physics 32:1001-1005. 1960.

12. Castle, J. G. and Robert Beringer. Microwave magnetic resonance absorption in nitrogen dioxide. The Physical Review 80:114. 1950.

13. Gaydon, A. G. Dissociation energies and spectra of diatomic molecules. New York, Dover, 1950. 239 p.

14. Halbach, K. Modulation-effect corrections for moments of magnetic resonance line shapes. The Physical Review 19: 1230-1233. 1960.

15. Harteck, Paul, Robert R. Reeves, and Gene Mannella. Rate of recombination of nitrogen atoms. The Journal of Chemical Physics 29:608-610. 1958.

16. Heald, Mark A. and Robert Beringer. Hyperfine structure of nitrogen. The Physical Review 96:645-648. 1954.

17. Heisenberg, W. and P. Jordan. Anwendung der Quantenmechanik auf das Problem der anomale Zeemaneffecte. Zeitschrift für Physik 38: 263-277. 1926.

18. Herron, John T., et al. Kinetics of nitrogen atom recombination. The Journal of Chemical Physics 30:879-885. 1959.

19. Hildebrandt, A. F., F. B. Booth, and C. A. Barth. Paramagnetic line widths in gaseous atomic hydrogen. The Journal of Chemical Physics 31:273. 1959.

20. Holloway, W. W., Jr., E. Lüscher, and R. Novick. Hyperfine structure of atomic nitrogen. The Physical Review 126:2109-2115. 1962.

21. Hopfield, J. J. Capillary valves for gases. Journal of the Optical Society of America 12:391-392. 1926.

22. Ingram, David John Edward. Spectroscopy at radio and microwave frequencies. London, Butterworth Scientific Publications, 1955. 332 p.

23. Innes, F. R. and O. Oldenberg. Metastable atoms and the auroral afterglow of nitrogen. The Journal of Chemical Physics 37:2427-2428. 1962.

24. Jennings, K. R. and J. W. Linnett. Active nitrogen. Quarterly Reviews, Chemical Society, London 12:116-132. 1958.

25. Joos, George. Theoretical physics. 3d. ed. New York, Hafner, 1958. 885 p.

26. Kaufman, Frederick. Reactions of oxygen atoms. In: Progress in Reaction Kinetics, vol. 1. New York, Pergamon, 1961. pp. 1-39.

27. Kaufman, F. The air afterglow and its use in the study of some reactions of atomic oxygen. Proceedings of the Royal Society (London) A 247:123-139. 1958.

28. Keck, James C. Statistical theory of chemical reaction rates. The Journal of Chemical Physics 29:410-415. 1958.

29. Keck, James C. Variational theory of chemical reaction rates applied to three-body recombinations. The Journal of Chemical Physics 32:1035-1050. 1960.

30. Krongelb, S. and M. W. P. Strandberg. Use of paramagnetic-resonance techniques in the study of atomic oxygen recombinations. The Journal of Chemical Physics 31:1196-1210. 1959.

31. Kurzweg, U. H. and H. P. Broida. Vibrational intensity distributions in the nitrogen afterglow. Journal of Molecular Spectroscopy 3:388-404. 1959.

32. Lewis, Percival. Some new fluorescence and afterglow phenomena in vacuum tubes containing nitrogen. The Astrophysical Journal 12:8-15. 1900.

33. Marshall, Thomas. Studies of atomic recombination of nitrogen, hydrogen, and oxygen by paramagnetic resonance. The Physics of Fluids 5:743-753. 1962.

34. Marshall, Thomas. Surface recombination of nitrogen atoms upon quartz. The Journal of Chemical Physics 37:2501-2502. 1962.

35. Mavroyannis, C. and C. A. Winkler. The reaction of nitrogen atoms with oxygen atoms in the absence of oxygen molecules. The Canadian Journal of Chemistry 39:1601-1607. 1961.

36. Miller, Lewis E. The chemistry and vertical distribution of atomic nitrogen in the upper atmosphere. U. S. Air Force. Cambridge Research Center. Geophysical Research Directorate. Geophysical Research Paper no. 71. Cambridge, 1960. 466 p.

37. Mitra, S. K. Active nitrogen--a new theory. Calcutta, J. N. Bose, 1945. 73 p.

38. Pake, George E. Paramagnetic resonance. New York, W. A. Benjamin, 1962. 205 p.

39. Panofsky, Wolfgang, K. H. and Melba Phillips. Classical electricity and magnetism. Reading, Addison-Wesley, 1955. 400 p.

40. Primas, H. Ein Modulationsverfahren für die Kernresonanzspektroskopie mit höher Auflösung. Helvetica Physica Acta 31:17-24. 1958.

41. Radford, H. E. and V. W. Hughes. Microwave Zeeman spectrum of atomic oxygen. The Physical Review 114:1274-1279. 1959.

42. Rayleigh, Lord. Further studies on active nitrogen. III. Experiments to show that traces of oxygen or other impurity affect primarily the walls of the vessel and not the phenomena in the gas space. Proceedings of the Royal Society (London) 180:123-139. 1942.

43. Schiff, H. I. Measurements of diffusion coefficients in various gases. Paper read before a seminar at the National Center for Atmospheric Research, Boulder, Colorado, Sept. 10, 1963.

44. Strong, John. Procedures in experimental physics. New York, Prentice Hall, 1938. 642 p.

45. Strutt, R. J. A chemically active modification of nitrogen, produced by the electric discharge. Proceedings of the Royal Society (London) 85:219-229. 1911.

46. Tanaka, Y., A. Jursa, and F. Leblanc. Vacuum ultraviolet spectra of the afterglows of pure N_2 and a mixture of N_2 and O_2. In: Proceedings of the Conference on Chemical Aeronomy, Cambridge, Mass., 1956, ed. by M. Zelikoff. New York, Pergamon, 1957. p. 89-93.

47. Tinkham, M. and M. W. P. Strandberg. Interaction of molecular oxygen with a magnetic field. The Physical Review 97:951-966. 1955.

48. Tinkham, M. and M. W. P. Strandberg. Theory of the fine structure of the molecular oxygen ground state. The Physical Review 97:937-950. 1955.

49. Tolman, Richard C. Statistical mechanics with applications to physics and chemistry. New York, Chemical Catalog Company, 1927. 334 p.

50. Wentink, Tunis, Jr., John O. Sullivan, and Kurt L. Wray. Nitrogen atomic recombination at room temperature. The Journal of Chemical Physics 29:231-232. 1958.

51. Wigner, E. Calculation of the rate of elementary association reactions. The Journal of Chemical Physics 5:720-729. 1937.

52. Young, Robert A. Measurements of the diffusion coefficient of atomic nitrogen in molecular nitrogen and the catalytic efficiency of silver and copper oxide surfaces. The Journal of Chemical Physics 34:1295-1301. 1961.

53. Young, Robert A. Observations on the pink nitrogen afterglow. The Journal of Chemical Physics 11:2854-2857. 1962.

54. Zavoisky, E. K. Spin magnetic resonance in paramagnetic substances. The Journal of Physics (U.S.S.R.) 9:245. 1945. (Abstracted in Chemical Abstracts 40:1072. 1946.)